UNIVERSITY OF
KWAZULU-NATAL

CHEBYSHEV SPECTRAL PERTUTRBATION BASED METHOD FOR SOLVING NONLINEAR FLUID FLOW PROBLEMS

A DISSERTATION SUBMITTED IN FULFILLMENT OF THE ACADEMIC REQUIREMENTS FOR THE DEGREE OF MASTER OF SCIENCE IN THE COLLEGE OF AGRICULTURE, ENGINEERING AND SCIENCE

By

Titilayo Morenike Agbaje

School of Mathematical Sciences

University of KwaZulu Natal, Pietermaritzburg

October 2014

Dedication

I DEDICATE THIS WORK TO MY LOVELY PARENTS MR AND MRS AGBAJE, MY DEAREST FIANCEE AYODEJI EMMANUEL ADEDOYIN, MY LOVELY SISTERS MRS OLUWABUKOLA AGBAJE ODAGI AND MOYINOLUWA AGBAJE.

Acknowledgment

I am most grateful to the Almighty God for his Grace and Mercy bestowed upon me, and for giving me a good and sound health, guidance and protection to complete this dissertation. I heartily express my profound gratitude to my supervisor, Professor Sandile S. Motsa, for his invaluable guidance, advise, encouragement, understanding and continued support throughout the duration of my studies. I will always be indebted to him for introducing me to new numerical methods of solving complex nonlinear boundary value problems and thereby creating my interest in this area of Applied Mathematics and shaping my future.

I am indebted to my lovely parents Mr and Mrs C.U Agbaje, who funded my academic career up to this level. Without their financial support, prayers and encouragement, it would have been impossible to complete this desertation and i appreciate them for their unflinching support and love.

I also would like to thank my fiancee and best friend Ayodeji Emmanuel Adedoyin for his continuous love, unequivocal support, prayers and best wishes.

Special thanks to Dr Zodwa G. Makukula, for her academic support, understanding, love, encouragement and personal attention, thereby providing good and smooth basis for this dissertation. There are many others who assisted me also, but I would like to thank my colleagues in the office who helped me with LATEX.

I am grateful for the facilities made available to me by the School of Mathematics, Statistics and Computer Science of the University of Kwazulu-Natal (UKZN), Pietermaritzburg. I am also grateful for the financial support that I have received from UKZN.

Finally my unalloyed gratitude goes to my sisters Mrs Oluwabukola Agbaje Odagi, and Moyinoluwa Agbaje and my cousin Ayoola Adedipe for helping me get through this tedious period in the most positive way.

Declaration

I hereby declare that this thesis presents my original work and effort. It was carried out in the School of Mathematics, Statistics and Computer Science, University of KwaZulu-Natal Pietermaritzburg, from February 2013 to July 2014 under the supervision of Professor Sandile S. Motsa.

It has not been submitted in any form to any University or institution for any degree or diploma. Due acknowledgement has been made of the work of others in this dissertation.

October, 2014.

Student: _____ _____

Titilayo Morenike Agbaje Date

Supervisor: _____ _____

Prof. S. Sandile Motsa Date

Abstract

In this dissertation, a modification of the classical perturbation techniques for solving nonlinear ordinary differential equation (ODEs) and nonlinear partial differential equations (PDEs) is presented. The method, called the Spectral perturbation method (SPM) is a series expansion based technique which extends the use of the standard perturbation scheme when combined with the Chebyshev spectral method. The SPM solves a sequence of equations generated by the perturbation series approximation using the Chebyshev spectral methods. This dissertation aims to demonstrate that, in contrast to the conclusions earlier drawn by researchers about perturbation techniques, a perturbation approach can be effectively used to generate accurate solutions which are defined under the Williams and Rhyne (1980) transformation. A quasi-linearisation technique, called the spectral quasilinearisation method (SQLM) is used for validation purpose. The SQLM employs the quasi-linearisation approach to linearise nonlinear differential equations and the resulting equations are solved using the spectral methods. Furthermore, a spectral relaxation method (SRM) which is a Chebyshev spectral collocation based method that decouples and rearrange a system of equations in a Gauss - Seidel manner is also presented. In the SRM, the differential equations are decoupled, rearranged and the resulting sequence of equations are numerically integrated using the Chebyshev spectral collocation method. The techniques were used to solve mathematical models in fluid dynamics. This study consists of an introductory chapter which gives the description of the methods and a brief overview of the techniques used in developing the SPM, SQLM and the SRM. In Chapter 2, the SPM is used to solve the equations that model magnetohydrodynamics (MHD) stagnation point flow and heat transfer problem from a stretching sheet in the presence of heat source/sink and suction/injection in porous media. Using similarity transformations, the governing partial differential equations are transformed into ordinary differential equations. Series solutions for small velocity ratio and asymptotic solutions for large velocity ratio were generated and the results were also validated against those obtained using the SQLM. In Chapter 3, the SPM was used to solve

the momentum, heat and mass transfer equations describing the unsteady MHD mixed convection flow over an impulsively stretched vertical surface in the presence of chemical reaction effect. The governing partial differential equations are reduced into a set of coupled non similar equations and then solved numerically using the SPM. In order to demonstrate the accuracy and efficiency of the SPM, the SPM numerical results are compared with numerical results generated using the SRM and a good agreement between the two methods was observed up to eight decimal digits which is a reasonable level of accuracy. Several simulation are conducted to ascertain the accuracy of the SPM and the SRM. The computational speed of the SPM is demonstrated by comparing the SPM computational time with the SRM computational time. A residual error analysis is also conducted for the SPM and the SRM, in order to further assess the accuracy of the SPM. In Chapter 4, the SPM was used to solve the equations modelling the unsteady three-dimensional MHD flow and mass transfer in a porous space previously reported in literature. Efficiency and accuracy of the SPM is shown by validating the SPM results against the results obtained using the SRM and the results were found to be in good agreement. The computational speed of the SPM is demonstrated by comparing the SPM and the SRM computational time. In order to further assess the accuracy of the SPM, a residual error analysis is conducted for the SPM and the SRM. In Chapter 2, we show that the SPM can be used as an alternative to the standard perturbation methods to get numerical solutions for strongly nonlinear boundary value problems. Also, it is demonstrated in Chapter 2 that the SPM is efficient even in the case where the perturbation parameter is large, as the convergence rate is seen to improve with increase in the large parameter value. In Chapters 3 and 4, the study shows that SPM is more efficient in terms of computational speed when compared with the SRM. The study also highlighted that the SPM can be used as an efficient and reliable tool for solving strongly nonlinear partial differential equations defined under the Williams and Rhyne (1980) transformation. In addition, the study shows that accurate results can be obtained using the perturbation method and thus, the conclusions earlier drawn by researchers regarding the accuracy of the perturbation method is corrected.

Contents

List of Tables

List of Figures

1

Introduction

Investigations such as that carried out by Hale (2006) have shown that a large number of natural phenomena problems such as oceanography, meteorology, planets motion, nonlinear optics, physics and engineering are fluid flow problems. Hale (2006) revealed that these problems are often modeled and analyzed using ordinary differential equations (ODEs) or partial differential equations (PDEs) due to their complexity. In addition, Hale (2006) noted that finding solutions of the differential equations (ODEs and PDEs) play an important role in understanding the behavior of the problems. As pointed out by Liao (2003a), most equations modeling real life problems are complicated, nonlinear and cannot be solved analytically in some cases. Numerical methods have to be used for cases where the equations cannot be solved analytically Liao (2003a).

Many researchers have employed various analytical and numerical methods in solving nonlinear ODEs and PDEs problems that arise in science and engineering (Motsa et al., 2013). These methods include finite differences (Asaithambi, 2004), finite element methods, Keller-box method (Keller and Cebeci, 1971; Cebeci and Bradshaw, 1984), Runge-Kutta with shooting methods (Prasad et al., 2000; Alam et al., 2007), spectral collocation methods (Elbarbary and Elgazery, 2004a,b; Elgazery, 2009) amongst others are being employed in solving nonlinear differential equations arising from fluid mechanics and other engineering applications. Liao (2003a), noted that these methods have their own advantages and limitations such as when dealing with problems with singularities or problems with multiple solutions. Therefore, as a result of these limitations, it was suggested by Motsa et al. (2013) numerical methods need to be improved.

This dissertation aim to present a Chebyshev spectral perturbation based method namely spectral perturbation method (SPM). The SPM can be used as an alternative numerical approach in the

solution of nonlinear ODEs and PDEs that arise in fluid mechanics and other engineering applications. The SPM is a series expansion based technique which extends the use of the standard perturbation scheme when combined with the Chebyshev spectral method. The SPM solves a sequence of equations generated by the perturbation series approximation. Also, this dissertation aim at highlighting the advantages of the SPM over the standard analytical perturbation based methods of solving ODEs and PDEs. In order to ascertain the accuracy of the SPM, we compare and validate using the spectral quasilinearisation method (SQLM) and the spectral relaxation method (SRM). The SQLM was introduced by Motsa and Sibanda (2013b) for solving nonlinear BVPs. The SQLM employs the principles of the quasilinearisation technique developed by Bellman and Kalaba (1965) to linearize nonlinear differential equations and solves the resulting equations using the spectral method (Dlamini et al., 2013). The SRM on the other hand was introduced by Motsa and Makukula (2013) for the solution of the nonlinear ODE model of von Karman flow a Reiner - Rivlin fluid. The SRM is based on simple decoupling and rearrangement of the governing nonlinear equations and numerically integrating the resulting equations using the Chebyshev spectral collocation method (Motsa et al., 2012). For the applicability of these numerical methods, three fluid flow problems were considered in this dissertation. In Chapter 2, magnetohydrodynamics (MHD) stagnation point flow and heat transfer towards a stretching sheet in the presence of heat source/sink and suction/injection in porous media is examined and solved numerically using the SPM and SQLM. The equations modeling this problem in Chapter 2 are characterized by systems of nonlinear ODEs. The model equations solved in Chapter 2, are a combination of the work of Ishak et al. (2009) who used the Keller-box numerical scheme to investigate the steady two-dimensional MHD stagnation point flow towards a stretching sheet, Yian et al. (2011) who studied MHD stagnation-point flow towards a shrinking sheet using the Keller-box method and Al-sudais (2012) who carried out a numerical study using the shooting method to investigate the thermal radiation effect on MHD fluid flow near stagnation point of linear stretching sheet with variable thermal conductivity. In Chapter 3, the problem of unsteady heat and mass transfer of MHD mixed convection flow over an impulsively stretched vertical surface with chemical reaction effect was considered. Numerical solutions were generated using the SPM and SRM. The equations describing the problem considered in Chapter 3 are characterized by systems of nonlinear PDEs. The problem extends the analysis of EL-Kabeir and Rashad (2012) by introducing a chemical reaction parameter. EL-Kabeir and Rashad (2012) previously used the implicit finite difference based Keller-box method to solve the equations describing the melting effect on unsteady

heat and mass transfer by MHD mixed convection flow over an impulsively stretched vertical surface in a quiescent fluid in the absence of chemical reaction. In Chapter 4, the unsteady three dimensional MHD flow and mass transfer in a porous space previously reported in literature by Hayat et al. (2010) is revisited. The Homotopy analysis method (HAM) was earlier utilized by Hayat et al. (2010) in solving this problem, but in this work, the SPM and SRM are applied. The SPM and the SQLM numerical results are compared in terms of the accuracy when solving ODEs in Chapter 2. In Chapters 3 and 4, the performance of the SPM and SRM are being compared in terms of accuracy and computational speed when solving nonlinear PDEs. A residual error analysis is also conducted in Chapters 3 and 4 in order to further assess the accuracy of the SPM and SRM. In developing the numerical schemes for the SPM, SQLM, and SRM, the following techniques are used,

- Spectral Methods (On the SPM, SQLM and SRM),
- Perturbation Methods (On the SPM),
  (i) Regular Perturbation,
- Gauss-Seidel Methods (On the SRM),
- Newton-Raphson based quasilinearisation (On the SQLM),
- Finite Difference Method (On the SRM),
  (i) Implicit Finite Difference Method,
  (ii) Crank-Nicholson Method.

The techniques listed above will be discussed briefly in this chapter before we give a brief description of the SRM, SQLM and SPM.

Definitions 1.1 : Linearisation of a function

Suppose for a function $f(y)$ that is sufficiently smooth, we assume that the function is linearly approximated using Taylor series expansion to first order about an evaluation point $y = a$ if;

$$f(y) \approx f(a) + f'(a)(y - a). \tag{1.1}$$

Definitions 1.2: Linearisation of a multi-variable function

For a function $f(u, v, w)$ at a point (a, b, c), the equation for the linearisation of the function is given

as;

$$f(u,v,w) \approx f(a,b,c) + \left.\frac{\partial f}{\partial u}\right|_{a,b,c}(u-a) + \left.\frac{\partial f}{\partial v}\right|_{a,b,c}(v-b) + \left.\frac{\partial f}{\partial w}\right|_{a,b,c}(w-c) \tag{1.2}$$

Therefore in terms of the notation used in this work to describe the methods of solution, a general nonlinear function of m variables $N\left(y_1, y_{2,\cdots}, y_m\right)$ can be linearised about $\left(y_{1,r}, y_{2,r,\cdots}, y_m\right)$ as follows:

$$N\left(y_1, y_{2,\cdots}, y_m\right) \approx f\left(y_{1,r}, y_{2,r,\cdots}, y_{m,r}\right) + \sum_{j=1}^{m} \left.\frac{\partial N}{\partial y_j}\right|_{[\cdots]} \left(y_j - y_{j,r}\right) \tag{1.3}$$

where $[\cdots]$ is defined as

$$[\cdots] = \left[y_{1,r}, y_{2,r,\cdots}, y_{m,r}\right] \tag{1.4}$$

1.1. Spectral Methods

According to Gheorghiu (2007), spectral methods involve approximating the unknown functions using truncated series of orthogonal functions or polynomials. The Fourier series for periodic problems, as well as Chebyshev or Legendre polynomials for non-periodic problems, are examples of such classical orthogonal functions, Gheorghiu (2007). Mantzaris et al. (2001) noted that the polynomials are defined over the entire spatial interval of a specific problem. A number of studies have noted that spectral method can further be considered as an improvement of the method of weighted residuals (MWR) of Finlayson and Scriven (1966), a class of discretization scheme used to find approximate solutions to differential equations (Mantzaris et al., 2001; Babolian et al., 2007; Ogundare, 2009). In the MWR, the major elements are refereed to as trial functions or the expansion or approximating functions. Several studies have revealed that the trial functions form a basis function for a certain space of global, smooth functions and truncated series expansion of the solution, such that when substituted into the differential equation, it yields the residual (Hussaini et al., 1984; Babolian et al., 2007).

Investigations such as those by Babolian et al. (2007); Ogundare (2009), highlighted that the three most commonly used spectral methods namely, Galerkin method, tau method, collocation or pseudo-spectral method are classified according to the choice of the test or trial functions. Gheorghiu (2007) pointed out that the choice of the category of method rely basically on the application. Previous studies have shown that the Tau method is a modification of the Galerkin method which is suitable for problems with nonlinear periodic boundary conditions (Babolian et al., 2007; Saravi

et al., 2009). The major difference between these methods is that the Tau and Galerkin methods are implemented in terms of the coefficients expansions, while collocation method are implemented in terms of physical space values of unknown function (Babolian et al., 2007; Ogundare, 2009; Saravi et al., 2009). (Gheorghiu, 2007) noted that the collocation methods are suitable to nonlinear problems or problems having complex coefficients whereas, the Galerkin methods have an advantage of a more appropriate analysis and optimal error estimates. The Tau approach is appropriate in the case of complex nonlinear boundary conditions where the Galerkin method cannot be utilized and the collocation method would be very tedious(Gheorghiu, 2007). One major drawback of the Tau and Galerkin approach is that substantial central processing unit (CPU) time is essential when dealing with higher dimensional approximations (Mantzaris et al., 2001).

Detailed examination of spectral methods by Bruno (2004) reported that the essential idea behind the method is to approximate the unknown solution in the whole computational interval by interpolating higher order polynomials at the collocation points. In addition, some authors (e.g Babolian et al. (2007); Ogundare (2009); Saravi et al. (2009)) have noted that the fundamental idea of spectral methods to solve differential equations is to expand the solution function as a finite series of a very smooth function as;

$$y_N(x) = \sum_{k=0}^{N} a_k \phi_k(x), \tag{1.5}$$

where ϕ_k represents Chebyshev or Legendre polynomials. Spectral methods have been used in various areas of science, engineering and physics because of their capability to give accurate solutions to differential equations. Examples of these areas include the fluid flow (Hussaini and Zang, 1987; Grandclément and Novak, 2009), wave and electrodynamics (Belgacem and Grundmann, 1998), meteorology, weather prediction models, geophysics (Bourke, 1988; Segami et al., 1989; Canuto et al., 2007; Grandclément and Novak, 2009), quantum mechanics (Canuto et al., 2007; Hesthaven et al., 2007), and in magnetodynamics (Shan et al., 1991; Shan and Montgomery, 1994). Spectral methods are known to give very accurate results (Gheorghiu, 2007). Trefethen and Trummer (1987) showed that spectral methods attained accuracy within only few grid points when compared to finite element or finite differences. Investigation by Mantzaris et al. (2001) revealed that spectral method, requires no additional numerical boundary conditions for the mathematical formulation of a problem. Furthermore, a number of studies have found that spectral methods converge significantly faster to the solution of a problem than any finite power of $1/N$, where N is the dimension of the reduced

order model (Juang and Kanamitsu, 1994; Mantzaris et al., 2001). Juang and Kanamitsu (1994) noted that the methods are efficient when used, and there is absence of truncation error in linear terms.

Regardless of the advantages mentioned above, spectral methods have a number of well known limitations which include being inferior to finite methods in handling complicated geometries and severe nonlinearities (Mantzaris et al., 2001). Furthermore, (Cueto-Felgueroso and Juanes, 2009) showed that spectral methods work under a specific domain known as the spectral domains (that is $[-1, 1]$) which makes the methods often unable to solve some problems in their elementary domain unless it is transformed into the spectral domain. Also, convergence of spectral methods reduces for problems that have singularities in the complex plane close to spectral domain (Cueto-Felgueroso and Juanes, 2009). According to Trefethen and Trummer (1987), the stability of spectral methods for initial boundary value problems and the general theory behind the spectral method is not proven.

Recent developments have emerged in order to address some of the limitations of spectral methods. Amongst these, we can name the domain decomposition techniques where the geometry divided into quadrangle sub domains (Macaraeg and Streett, 1986; Demaret and Deville, 1991). The spectral element method which was established by Patera (1984) to address problems in fluid dynamics and handle problems with complex geometries. According to Patera (1984), the SEM evolution was the outcome of combining the accuracy and accelerated convergence of the pseudo-spectral methods with the geometrical flexibility of the finite element method. In addition, the direct spectral domain decomposition technique was presented by Raspo (2003) to regain an excellent accuracy in the case of a problem with crystal growth demonstrating a singular solution as well to show that the multi-domain approach is appropriate for the effective extension of spectral approximations from the square geometry to non-rectangular geometries including re-entrant corners. Korostyshevskiy and Wanner (2007) introduced a Hermite spectral method for the computation of homoclinic orbits and associated functionals. (Korostyshevskiy and Wanner, 2007) showed that the methods provide spectral accuracy and can be used to approximate nonlinear functionals of the homoclinic in a direct way. In recent years, there have been more improvements and applications made to spectral methods.

1.2. Perturbation Methods

Perturbation methods are used as alternative approach to numerical methods for obtaining analytic approximate solutions to nonlinear differential equations that cannot be solved exactly (Simmonds and Mann, 1985). According to Simmonds and Mann (1985), the analytic approximations of nonlinear problems produced by perturbation methods often reveal the important dependence of the exact solution on a parameter in a more satisfactory way. Previous studies have reported that perturbation methods in general are based on the existence of a dimensionless small or large parameter called the perturbation quantities or parameter (Simmonds and Mann, 1985; Liao, 2003a). Several investigations have shown that the perturbation quantity may either be in the governing differential equation, boundary conditions or both (Nayfeh, 1973; Kevorkian and Cole, 1981; Liao, 2003a). It was noted by Kevorkian and Cole (1981) that in perturbation methods, when the perturbation parameter equals zero, the solution of the differential equation should be known. A number of studies have shown that the perturbation approximate solutions are expressed in series of perturbation parameter using asymptotic expansion (Bellman, 1966; Kevorkian and Cole, 1981). It has been noted that the smaller the perturbation parameter, the more accurate the approximate solution will be (Simmonds and Mann, 1985; Nayfeh, 1973). Liao (2003a) noted that the presence of the perturbation parameter in a differential equation is a keystone of the perturbation methods. A study of perturbation methods by Liao (2003a) reported that based on small physical parameters contained in a nonlinear problem, perturbation approximation usually give clearer physical meanings of the problem. However, one major draw back of this approach highlighted by Liao (2003a) is the fact that the perturbation techniques depends on the existence of a small perturbation quantity in an equation and not every nonlinear problem has such type of perturbation parameter. This view was supported by Liao (2003b) who argued that, even if it is possible that there exist a small parameter in each nonlinear problem, perturbation methods might have no solution for the sub-problems, or might even be so difficult to solve only few sub-problems. For example, it was shown by Liao (2002) that a satisfactory theoretical drag formula of a sphere in a uniform stream could not be obtained by using both direct and singular perturbation methods. To corroborate this, Kevorkian and Cole (1981) have shown that the perturbation method may fail to work for the entire computational region of some problems. Thus, it has been shown that perturbation approximations are guaranteed only for nonlinear problems with weak nonlinearity (Liao, 2003a). Furthermore, surveys such as

that conducted by Nayfeh (1973) have revealed that if the highest derivative term is multiplied by the perturbation parameter, the solutions might not be correct. According to Nayfeh (1973), this is due to the fact that a lower order equation will govern the first approximation which may not satisfy all the initial boundary conditions given. Therefore, it is not guaranteed that one can always obtain a perturbation approximation for any given nonlinear problem. A large volume of published literature and book now exist describing perturbation methods (for example, Kato (1958); Cole and Cole (1968); Keller and Kogelman (1970); Nayfeh (1973); Kevorkian and Cole (1981); Kato (1982); Smith (1985); Simmonds and Mann (1985); Kevorkian (1987); Hinch (1991); Holmes (1995); Kato (1995); Ostrovsky and Gorshkov (2000); Kahn and Zarmi (2004); Hu (2008); Witelski and Bowen (2009); Aksoy and Pakdemirli (2010); Skinner (2011); Nayfeh (2011)).

Definitions 1.3: Regular Perturbation

A regular perturbation problem as defined by Hunter (2004), is one for which the perturbed problem for small, non-zero values of the perturbation parameter is qualitatively the same as the unperturbed problem when the perturbation parameter equals zero. Hunter (2004) showed that in regular perturbation, an approximation can be obtained by simply setting the perturbation parameter to zero. Similarly, a convergent expansion of the solution with respect to the perturbation parameter, consisting of the unperturbed solution and higher order correction is obtained in regular perturbation.

1.3. Gauss-Seidel Method

The Gauss-Seidel iterative method is used to solve linear systems of algebraic equations. The Gauss-Seidel uses the new approximate values of x_i immediately as soon as they are known. That is, once the x_1 is known from the first equation, its value is then used in the second equation to determine the new x_2. Similarly, the x_1 and x_2 are utilized in the third equation to obtain the new x_3 and so on. The Gauss - Seidel method which uses the new values of $x_i^{(k+1)}$ as soon as they are known. To describe how the Gauss-Seidel method is used, we consider a set of algebraic equations of the form:

$$a_{11}x_1 + a_{12}x_2 + a_{13}x_3 + \cdots + a_{1n}x_n = b_1, \tag{1.6}$$

$$a_{21}x_1 + a_{22}x_2 + a_{23}x_3 + \cdots + a_{2n}x_n = b_2, \tag{1.7}$$

$$a_{31}x_1 + a_{32}x_2 + a_{33}x_3 + \cdots + a_{3n}x_n = b_3. \tag{1.8}$$

The unknown functions associated with the diagonal terms are solved as follows:

$$x_1^{(k+1)} = \frac{1}{a_{11}}\left[b_1 - a_{12}x_2^{(k)} - a_{13}x_3^{(k)} - \cdots - a_{1n}x_n^{(k)}\right], \tag{1.9}$$

$$x_2^{(k+1)} = \frac{1}{a_{22}}\left[b_2 - a_{21}x_1^{(k+1)} - a_{23}x_3^{(k)} - \cdots - a_{2n}x_n^{(k)}\right], \tag{1.10}$$

$$x_3^{(k+1)} = \frac{1}{a_{33}}\left[b_3 - a_{31}x_1^{(k+1)} - a_{32}x_2^{(k+1)} - a_{34}x_4^{(k)} - \cdots - a_{3n}x_n^{(k)}\right]. \tag{1.11}$$

In general, the Gauss - Seidel method for ith element of x is formally described using index notation as;

$$x_i^{(k+1)} = \frac{1}{a_{ii}}\left[b_i - \sum_{j=1}^{i=1} a_{ij}x_j^{(k+1)} - \sum_{j=i+1}^{n} a_{ij}x_j^{(k)}\right], \quad 1 \leq i \leq n, \quad k \geq 0. \tag{1.12}$$

Equation (1.12) can be rearranged as follows:

$$x_i^{(k+1)} = x_i^{(k)} + \left(\frac{\phi_i^{(k)}}{a_{ii}}\right), \tag{1.13}$$

where

$$\phi_i^{(k)} = \left[b_i - \sum_{j=1}^{i=1} a_{ij}x_j^{(k+1)} - \sum_{j=i+1}^{n} a_{ij}x_j^{(k)}\right]. \tag{1.14}$$

1.4. Newton-Raphson based quasilinearisation Method

The quasilinearisation method originally established by Bellman and Kalaba (1965) is a generalized Newton-Rapson method intended to solve non-linear two-point boundary value problems arising in science and engineering (Lee, 1966). The method provides lower and upper bound solutions of nonlinear differential equations (Motsa and Sibanda, 2013a). The quasilinearisation method was confirmed by Bellman and Kalaba (1965) to converge quadratically to a solution of the differential equation (El-Gebeily and ORegan, 2006; Motsa and Sibanda, 2013a). Motsa and Sibanda (2013a) noted that the initial proof of quadratic convergence was under restrictive conditions of small step size and convexity. According to Ahmad et al. (2001), the convexity assumption was relaxed and the method was generalized and extended in diverse directions to make it applicable to a wider class of nonlinear differential problems. These include the work of Mandelzweig (1999); Krivec and Mandelzweig (2001) who used the quailinearisation method to solve models in quantum mechanics, nonlinear ODEs (Mandelzweig and Tabakin, 2001), Lakshmikantham and his co-workers (Laksh-

mikantham, 1994; Lakshmikantham et al., 1995, 1996; Lakshmikantham, 1996). Other applications of the quasilinearisation method include application to Volterra integro-differential equations (Pandit, 1997; Ahmad, 2006; Ramos, 2007; Maleknejad and Najafi, 2011), mixed boundary value problems (Ahmad et al., 2002), nonlinear boundary value problems with integral boundary conditions (Suna et al., 2010), second order ordinary differential equation with Dirichlet boundary conditions (Nieto, 1997), second order nonlinear differential equations with nonlinear boundary conditions (El-Gebeily and ORegan, 2006), forced duffing equation (Ahmad et al., 2008), reaction diffusion equations (Jiang and Vatsala, 1998; Yang and Vatsala, 2005; Vatsala and Yang, 2006), amongst others.

1.5. Finite Difference Method

According to Moczo et al. (2004), the finite difference method belongs to the commonly named grid point methods whereby in the grid-point methods a computational domain is bounded by a space-time grid and each function is characterized by its values at grid points. A number of studies have shown that the finite difference method is based upon the application of a local Taylor series expansion to approximate the differential equations Tandjiria (1999); Peiró and Sherwin (2005). Several studies have showed that in the finite difference method, the governing differential equations are discretized and solved approximately at each of the nodal points of the grid (Kikani, 1989; Tandjiria, 1999). In another major investigation, Leveque (1998) observed that the finite difference method is accelerated by substituting the derivatives in the differential equations by finite difference approximations. Detailed examination by Leveque (1998) showed that the finite difference approximation dispense an extensive algebraic system of equations to be solved in place of the differential equation and this can be easily solved on a computer. Furthermore, it has been noted by Moczo et al. (2004), that the fundamental principle behind the use of the finite difference method on a specific differential equation includes developing a discrete finite difference model of the problem, evaluating the finite difference model and the numerical computations.

Surveys such as that conducted by Ampadu (2007), listed three different types of finite difference methods. These are the implicit finite difference method, the explicit finite difference method, and the Crank-Nicolson finite difference method. There are numerous applications of the finite difference method. For instance, in simulating the weather pattern on earth so as to have an accurate predictions over land than over the wide-open sea (Ampadu, 2007), in oil and geothermal industries (Kikani,

1989), several geotechnical engineering problems (Tandjiria, 1999), in seismic wave propagation and seismic wave modeling (Moczo, 1998; Moczo et al., 2004), in earthquake ground motion modeling (Moczo et al., 2004), in geophysics (Durran, 1999), in financial engineering (Duffy, 2006), financial mathematics (Ekström and Tysk, 2011), groundwater modeling (Wang and Anderson, 1995), the dynamics of HIV transmission(Ampadu, 2007). Tandjiria (1999) noted that the method has been proven accurate enough in as much as the model meets the basic conditions. In addition, (Moczo et al., 2004) pointed out that the finite difference method is computationally efficient, relatively accurate and comparatively easy to encode. However, the finite difference method has a number of limitations. Moczo et al. (2004), for example, pointed out that the major limitation of the approach is that the boundary conditions are difficult to implement and its application to complicated nonlinear equations requires much more expansion. Another disadvantage of this method is that the conservation is not invoked except distinctive care is taken and the constraint to simple geometries is a cogent draw back in complex flows (Ferziger and Perić, 1996). In spite of all the disadvantages, (Kikani, 1989) highlighted that finite difference methods are the most powerful general method available for solving complex nonlinear problems.

In this work, the implicit finite difference scheme and the Crank-Nicholson scheme are used in the derivation of the SRM scheme. Therefore, there is need to state what is meant by implicit, explicit and Crank-Nicholson finite difference scheme.

Definitions 1.4: Implicit Finite Difference

Consider the general heat equation in one dimension

$$U_t = U_{xx}. \tag{1.15}$$

One approach of solving (1.15) numerically is to approximate all the derivatives using the finite difference method. The domain in space is partitioned using a mesh $x_0, \cdots, x_J$ and in time using a mesh $t_0, \cdots, t_N$. A uniform partition in space and in time is assumed, so that the difference between two consecutive space points will be Δx and between two consecutive time points will be Δt. The numerical approximation of $u(x_j, t_n)$ will be represented by the points $u(x_j, t_n) = u_j^n$. Hence, using a backward difference at time t_{n+1} and a second order central difference for the space derivative at position x_j (The Backward Time, Centered Space Method) (BTCS), the implicit finite difference

scheme for solving the one dimensional heat equation is given as;

$$\frac{u_j^{n+1} - u_j^n}{\Delta t} = \frac{u_{j-1}^{n+1} - 2u_j^{n+1} + u_{j+1}^{n+1}}{(\Delta x)^2} \tag{1.16}$$

Definitions 1.5: Explicit Finite Difference

Using a forward difference at time t_n and a second order central difference for the space derivative at position x_j (The Forward Time, Centered Space Method) (FTCS), the explicit finite difference scheme for solving the one dimensional heat equation is given as;

$$\frac{u_j^{n+1} - u_j^n}{\Delta t} = \frac{u_{j-1}^{n} - 2u_j^{n} + u_{j+1}^{n}}{(\Delta x)^2}. \tag{1.17}$$

Definitions 1.6: Crank-Nicholson Finite Difference

Using the central difference at time $t_{n+1/2}$, and a second order central difference for the space derivative at position x_j (The Central Time, Centered Space Method) (CTCS). The Crank-Nicholson finite difference scheme for solving the one dimensional heat equation is the average of the explicit at (j, n) and the implicit at $(j, n+1)$ which is given as;

$$\frac{u_j^{n+1} - u_j^n}{\Delta t} = \frac{1}{2}\left[\frac{u_{j-1}^{n} - 2u_j^{n} + u_{j+1}^{n}}{(\Delta x)^2}\right] + \frac{1}{2}\left[\frac{u_{j-1}^{n+1} - 2u_j^{n+1} + u_{j+1}^{n+1}}{(\Delta x)^2}\right] \tag{1.18}$$

1.6. Description of the Methods of Solution

In this section a brief description of how the spectral relaxation method (SRM), spectral quasilinearisation method (SQLM) and spectral perturbation method (SPM) iterative methods of solution are derived is presented.

1.6.1 Spectral Relaxation Technique (SRM)

The development of the spectral relaxation method (SRM) to obtain solutions to differential equations would be discussed in this section. To develop the SRM iteration scheme, we use the Gauss-Seidel concept of decoupling the governing nonlinear systems of equation and linearizing them by rearranging them in the manner in which they are listed and solved consecutively. A sizeable body of literature now exist based on the use of the spectral relaxation method for the solution of fluid

mechanics problems. To mention a few, the method has been used in the solution of thermal dispersion and radiation effects in a nanofluid flow (Kameswaran et al., 2013, 2014), chaotic and hyper-chaotic systems (Motsa et al., 2012, 2013), steady von Karman flow of a Reiner-Rivlin fluid (Motsa and Makukula, 2013), nonlinear boundary layer flow systems (Motsa, 2014), Maxwell fluid (Shateyi, 2013), upper-convected Maxwell (UCM) fluid (Shateyi and Marewo, 2013), Hydromagnetic stagnation-point flow (Shateyi and Makinde, 2013), MHD laminar boundary layer flow and heat transfer of nanofluids (Shateyi and Prakash, 2014), synthesis of biodiesel (Makukula et al., 2014), unsteady boundary-layer flow and heat transfer of a nanofluid (Sibanda et al., 2014), unsteady boundary layer flow problems (Motsa et al., 2014). Thus, a summary of the SRM algorithm for any given nonlinear differential equation is given as follows:

- Classify the governing nonlinear partial differential equation in a specific order such that the equations with the least number of unknowns is placed at the top of the equations list.
- Allot the labels $Y_1, Y_2, Y_3, \cdots$, to the ordered equations in number 1 above. Here, each $Y_i (i = 1, 2, 3)$ is an unknown function which, in the ith equation, is recognized as the unknown function linked with the highest order derivative.
- From the decoupled equations, the iteration scheme for the first equation (Y_1), the iteration scheme is derived by presuming that at the current iteration denoted by $(r+1)$, only the linear terms in (Y_1) are to be evaluated and all other linear and nonlinear terms in $(Y_2), (Y_3), \cdots$ are presumed to be known from the previous iteration denoted by (r).
- Likewise, in the derivation of the second equation (Y_2) iteration scheme, only linear terms in (Y_2) are evaluated at the current iteration $(r + 1)$ while all other terms are evaluated at the previous iteration other than Y_1 which already is known from the solution of the first equation.
- The same iteration procedure is repeated in the ith equation where $(i = 1, 2, 3, \cdots)$ using the updated solutions for Y_{i-1} which are obtained from the previous $i - 1$ equations until convergence is reached.

The desired convergence can be determined by considering the error due to the decoupling and subsequent solution of the governing equations. This error (E_d) at the $(r + 1)$ iteration is given by

Motsa (2014) and defined as;

$$E_d = Max\left(\| y_{1,r+1} - y_{1,r} \|_\infty, \| y_{2,r+1} - y_{2,r} \|_{\infty,\cdots}, \| y_{m,r+1} - y_{m,r} \|_\infty\right). \tag{1.19}$$

Using the SRM algorithm described above results to a series of linear differential equations which are discretized and solve using the spectral collocation method. The Chebyshev spectral collocation method was chosen because of its high level of accuracy and its ease of use. Also, spectral methods are known to give good accuracy even with only few grid points compared to other numerical techniques such as finite differences and finite element methods. We remark that the solution to any given governing nonlinear differential is the initial approximation Y_0 chosen as a function that satisfies the given underlying boundary conditions. To apply the spectral methods, it is convenient to first transform the interval on which the governing equations are defined to the domain $[-1, 1]$ on which we can now implement the spectral methods. The transformation $\eta = \dfrac{(b-a)(\zeta+1)}{2}$ is used to map the domain $[a, b]$ to $[-1, 1]$. The Chebyshev region in $[-1, 1]$ is discretized using the Gauss-Lobatto collocation points given by Canuto et al. (1988); Trefethen (2000) and defined as;

$$\zeta_j = \cos\frac{\pi j}{N_x}, \tag{1.20}$$

where N_x is the number of collocation points used. In addition, the idea behind the Chebyshev spectral collocation method is the introduction of the differentiation matrix $\mathbf{D}$, which is used to approximate the derivatives of the unknown variables $Y_i(\eta)$ $(i = 1, 2, 3, \cdots,)$ at the collocation points as the matrix vector product:

$$\left.\frac{dY_i}{d\eta}\right|_{\eta=\eta j} = \sum_{k=0}^{N} \mathbf{D}_{jk} Y_i(\zeta_k) = \mathbf{D}\mathbf{Y}_i, \qquad j = 0, 1, \ldots, N_x, \tag{1.21}$$

where $\mathbf{D} = 2D/(b-a)$, and $\mathbf{Y}_i = [Y_i(\zeta_0), Y_i(\zeta_1), Y_i(\zeta_2), \cdots, Y_i(\zeta_{N_x})]^T$ is the vector function at the collocation points ζ_i. Higher order derivatives are obtained as powers of $\mathbf{D}$, that is,

$$Y_i^{(p)} = \mathbf{D}^p Y_i, \tag{1.22}$$

where p is the order of the derivative.

1.6.2 Spectral Quasi-linearisation Method (SQLM)

In this section, we describe the spectral quasi-linearisation method (SQLM). According to Motsa (2013), the SQLM is a generalization of the Newton-Raphson method. The SQLM combines the Chebyshev spectral method and the quasi-linearisation method (QLM) that was first proposed by Bellman and Kalaba (1965) for solving nonlinear boundary value problems (Dlamini et al., 2013; Motsa, 2013). In the SQLM, the nonlinear components of the differential equations are linearised using the Taylor series expansion for multiple variables and the resulting equations are solved using the Chebyshev spectral collocation method (Dlamini et al., 2013; Motsa, 2013). There has been some applications of the SQLM by researchers to solve a range of nonlinear fluid dynamics problems. These includes the work of Motsa and Sibanda (2013b), Dlamini et al. (2013), Motsa (2013), Motsa (2014), Motsa et al. (2014).

To illustrate the development of the SQLM iteration scheme, we consider a nonlinear ordinary differential equation of the form:

$$y''(\eta) - y(\eta) - y^2(\eta) = 0, \quad \eta \in [0,1], \tag{1.23}$$

subject to the boundary conditions

$$y'(0) = 0, \;\; y(1) = 0, \tag{1.24}$$

where $y(\eta)$ is an unknown function, η an independent variable, $[0,1]$ is the domain of the problem, and prime denotes differentiation with respect to η. Equation (1.23) contains linear and nonlinear components which are written as;

$$\mathcal{L}[y(\eta)] = y'' - y, \quad \mathcal{N}[y(\eta)] = -y^2 \tag{1.25}$$

where $\mathcal{L}$ and $\mathcal{N}$ are the linear and nonlinear operators respectively. The nonlinear term of (1.25) can be linearised using Taylor series expansion to first order with the assumption that the difference between the value of the unknown functions at the current iteration level (denoted by $(r+1)$) $y_{r+1}(\eta)$ and at the previous iteration level (denoted by r) $y_r(\eta)$ is small. Applying the Taylor series expansion on the nonlinear term gives:

$$-\left[y_r^2 + 2y_r\left(y_{r+1} - y_r\right)\right] = 0 \tag{1.26}$$

Substituting (1.26) into (1.23) and applying the QLM gives;

$$y''_{r+1} + a_{1,r} y_{r+1} = Q_r, \quad y_{r+1}(1) = 0,\ y'_{r+1}(0) = 0, \tag{1.27}$$

where

$$a_{1,r} = (-1 - 2y_r), \quad \text{and} \quad Q_r = -y_r^2. \tag{1.28}$$

In solving the now linear iteration scheme (1.27), we use the Chebyshev pseudo-spectral collocation method. Thus, due to this reason, the method is refereed to as spectral quasilinearisation method (SQLM) in this work. It should be noted that other numerical methods can be used to solve equations (1.26) - (1.28). Applying the spectral collation method to (1.27) gives;

$$\mathbf{A}\mathbf{Y}_{r+1} = \mathbf{Q}_r, \quad \text{with } \mathbf{A} = D^2 + \ \mathbf{a}_{1,r}, \tag{1.29}$$

where

$$\begin{aligned}
\mathbf{Y} &= [y(\eta_0), y(\eta_1), \cdots, y(\eta_{N_x})]^T, \\
\mathbf{Q}_r &= [Q_r(\eta_0), Q_r(\eta_1), \cdots, Q_r(\eta_{N_x})]^T, \\
\mathbf{a}_{1,r} &= diag\left([a_{1,r}(\eta_0), a_{1,r}(\eta_1), \cdots, a_{1,r}(\eta_{N_x})]^T\right).
\end{aligned} \tag{1.30}$$

In the above definitions, the superscript T denotes transpose and *diag* is a diagonal matrix of size $(N_x + 1) \times (N_x + 1)$. The boundary conditions become;

$$y_{r+1}(\eta_{N_x}) = 0, \quad \sum_{k=0}^{N_x} D_{N_x,k}\, y_{r+1}(\eta_k) = 0. \tag{1.31}$$

The boundary conditions (1.31) are imposed on the first and last row of (1.29) as follows;

$$\left[\begin{array}{c|ccc|c} 1 & 0 & \cdots & 0 & 0 \\ \hline & & & & \\ & & \mathbf{A} & & \\ & & & & \\ \hline \mathbf{D}_{N_x,0} & \mathbf{D}_{N_x,1} & \cdots & \mathbf{D}_{N_x,N_x-1} & \mathbf{D}_{N_x,N_x} \end{array}\right] \left[\begin{array}{c} y(\eta_0) \\ \hline y(\eta_1) \\ \vdots \\ y(\eta_{N_x-1}) \\ \hline y(\eta_{N_x}) \end{array}\right] = \left[\begin{array}{c} 0 \\ \hline Q_r(\eta_1) \\ \vdots \\ Q_r(\eta_{N_x-1}) \\ \hline 0 \end{array}\right]. \tag{1.32}$$

Starting from an appropriate initial approximation $y_0(\eta)$ which is chosen as a function that satisfies the boundary condition (1.24), the approximate SQLM solution $y(\eta)$ can be obtained by iteratively solving equation (1.32).

1.6.3 Spectral Perturbation Method (SPM)

The Spectral Perturbation method (SPM) extends the use of standard perturbation techniques to obtain solutions of both ordinary differential and partial differential equations. A spectral method based method is proposed to solve the governing sequence of any differential equations generated by the perturbation series approximation. Using a perturbation expansion procedure in terms of a small parameter or perturbation parameter (say ε), it is possible to solve any given differential equation provided there exist a small parameter in the differential equation. To illustrate the derivation of the SPM iteration scheme, we consider a nonlinear ordinary differential equation of the form:

$$y''(\eta) - y(\eta) - \varepsilon y^2(\eta) + 1 = 0, \tag{1.33}$$

subject to the boundary conditions

$$y'(0) = 0, \quad y(1) = 0. \tag{1.34}$$

where $y(\eta)$ is an unknown function, η is an independent variable and prime denotes the differentiation with respect to η. The algorithm for the method is then summarized as follows:

- We regard ε as a small parameter to look for a regular perturbation expansion for $y(\eta)$ in powers of ε, one can expand $y(\eta)$ as follows

$$y(\eta) = y_0(\eta) + y_1(\eta)\varepsilon + y_2(\eta)\varepsilon^2 + \cdots + y_n(\eta)\varepsilon^m. \tag{1.35}$$

  In general, the kth order solution $y(\eta)$ can be approximated by:

$$y(\eta) = \sum_{k=0}^{+\infty} y_k(\eta)\varepsilon^k. \tag{1.36}$$

  From (1.35), $y_0(\eta), y_1(\eta), y_2(\eta), \cdots, y_n(\eta)$ are unknown functions that are determined from

higher order deformation equations.

- Substituting equation (1.36) into the governing equation (1.33) and equating the coefficients of like power of ε, one has an infinite number of linear differential equations:

$$y_0''(\eta) - y_0(\eta) + 1 = 0, \quad y_0(1) = 0, \quad y_0'(0) = 0, \tag{1.37}$$

$$y_k''(\eta) - y_k(\eta) = \sum_{n=0}^{k-1} y_{k-1-n} y_n, \quad y_k(1) = 0, \quad y_k'(0) = 0. \tag{1.38}$$

We remark that the initial approximation at $\varepsilon = 0$ for equation (1.33) is obtained as solution of the equation (1.37). Thus, starting from a suitable initial approximation $y_0(\eta)$, the solutions to the resulting equations (1.37 - 1.38) can be obtained in a direct way using any numerical method. In this work, the Chebyshev spectral collocation method earlier described in the previous section was used to integrate (1.37 - 1.38) since they are now a sequence of linear ordinary differential equations. It is for this reason the method is called SPM. The spectral method was used here because of its high level of accuracy as earlier highlighted.

1.7. Dissertation Outline

The rest of this dissertation is structured as follows:

- In Chapter 2, the SPM and the SQLM are used to solve the equations that describe magneto-hydrodynamics (MHD) stagnation point flow and heat transfer problem, towards a stretching sheet in the presence of heat source/sink and suction/injection in porous media,
- In Chapter 3, the SPM and the SRM are used to solve the equations that model unsteady heat and mass transfer by MHD mixed convection flow over an impulsively stretched vertical surface with chemical reaction effect,
- In Chapter 4, the SPM and the SRM are used to solve the equations that describe unsteady three dimensional MHD flow and mass transfer in a porous space,
- In Chapter 5, the conclusion of the dissertation is given. The dissertation ends with a list of references.

2

MHD Stagnation Point Flow and Heat Transfer Towards a Stretching Sheet in the Presence of Heat Source/Sink and suction/injection in Porous Media

2.1. Introduction

The study of flow around a stagnation point in a plane was pioneered by Hiemenz (1911). He considered a two-dimensional stagnation flow problem on a stationary plate and used similarity transformations to reduce the Navier-Stokes equations to non-linear ordinary differential equations (Salem and Fathy, 2012). Since then, many researchers have extended the idea to different aspects of the stagnation point flow problems. Stagnation point flow is still attracting many researchers' attention because of its various practical applications. These applications include cooling of electronic devices by fans, cooling of nuclear reactors during emergency shutdown, hydrodynamic processes in engineering applications (Ibrahim et al., 2013), MHD generators and cooling of infinite metallic plates in a bath (Salem and Fathy, 2012), metallurgical processes, such as drawing, annealing, and tinning of copper wires (Ali et al., 2011). Hydromagnetic stagnation point flow and heat transfer finds applications in boundary layers along material handling conveyers, in aerodynamic extrusion of plastic sheets and in blood flow problems (Ali and Ashraf, 2012).

Different aspects of the stagnation point flow have been considered by many researchers. Ishak et al. (2009) . The steady magnetohydrodynamic mixed convection stagnation point flow of an

incompressible, viscous, and electrically conducting fluid over a vertical flat plate was studied by Ali et al. (2011). In their study, numerical solutions were generated using an implicit finite-difference scheme. Ali et al. (2012) carried out a numerical investigation of the steady laminar two dimensional nonlinear MHD stagnation point flow and heat transfer of an incompressible viscous fluid towards a stretching sheet. In their study the induced magnetic field, viscous dissipation and radiation effects were taken into consideration. Numerical solutions were generated using the finite difference method. Al-sudais (2012) carried out a numerical study using the shooting method to investigate the effects of variable thermal conductivity and heat source/sink on MHD boundary-layer flow of a viscous fluid near a stagnation point on a non-conducting stretching sheet. The Runge-Kutta fourth order method with shooting technique was used by Ibrahim et al. (2013) to solve the equations that model MHD stagnation point flow and heat transfer due to nanofluid towards a stretching sheet. Mahapatra et al. (2010) used the shooting method to solve the equations that describe the effect of a uniform transverse magnetic field on two-dimensional stagnation point flow of an incompressible viscous electrically conducting fluid over a stretching surface. Numerical investigation of stagnation point flow over a stretching sheet with convective boundary conditions was carried out by Mohamed et al. (2013) using the shooting method. Nandy (2013) used the homotopy analysis method to generate analytical solutions of MHD stagnation point flow and heat transfer of Casson fluid over a stretching sheet with partial slip. Other stagnation point flow studies were carried out by Pop et al. (2004), Qi and Hong-Qing (2009), Sharma and Singh (2009), Yian et al. (2011), Rasekh et al. (2013), and Ramesh et al. (2014).

The current study serves to carry out a numerical investigation of a steady, two-dimensional flow and heat transfer of an incompressible electrically conducting fluid near a stagnation point. A spectral perturbation method (SPM) was used to generate the numerical solutions of the skin friction coefficient, heat transfer rate, velocity and temperature profiles. Series solutions for small perturbation parameter and asymptotic solutions for large perturbation parameter were generated to study the behavior of the solution for the two cases. The SPM is a recent development that improve the performance of analytical based ordinary perturbation methods. In general, perturbation approaches use small quantities, called perturbation parameters, to transform a nonlinear problem into a infinite number of linear sub-problems. The solution of the nonlinear problem is then approximated by the sum of solutions of the first several sub-problems. However, the dependence of perturbation methods on the perturbation quantity brings perturbation methods to serious limita-

tions. Firstly, not all nonlinear problems have such quantities. Secondly, the resulting solutions are usually complicated making it more difficult to get higher-order perturbation approximations. Also, if the perturbation parameter multiplies the highest derivative term, the results may be erroneous due to the first approximation being governed by a lower order equation which may not satisfy all the given initial boundary conditions. Nonetheless, the problem under study is suitable to solve using perturbation methods when the velocity ratio parameter (ϵ) is sufficiently small because of the following reasons. Firstly, the perturbation parameter exists in the problem, both in the equations and boundary conditions. Secondly, it does not multiply the highest derivative term, hence when $\epsilon = 0$, the first approximation will be a true representation of the solution. The SPM then solves the resulting equations numerically using the Chebyshev spectral method. This makes it possible to get higher-order perturbation approximations even for complicated equations. The Chebyshev spectral method was chosen because spectral methods are well known for their high accuracy levels. The SPM approximate solutions were then validated using the spectral quasi-linearisation method (SQLM), a generalized Newton-Raphson Method that also uses the Chebyshev spectral method to solve the resulting equations.

2.2. Problem Formulation

A steady two-dimensional flow and heat transfer of an incompressible electrically conducting fluid near the stagnation point on a heated stretching surface with free stream $U_\infty(x)$ and uniform ambient temperature T_∞ were considered. The free stream velocity $U_\infty(x)$ and the stretching velocity $U_w(x)$ are assumed to be varying proportionally to x, the distance from the stagnation point, i.e. $U_\infty(x) = bx$ and $U_w(x) = ax$. The constants a and b are such that $a > 0$ and $b \geq 0$. The mass flux velocity is $V_w(x)$ and will be defined in detail later. The surface of the sheet is assumed to be subjected to a set temperature $T_w(x) = T_\infty + cx^n$, where c and n are constants with $c > 0$ at the heated surface. A uniform magnetic field of strength B_0 was assumed to be applied in the positive $y-$direction normal to the stretching sheet. The magnetic Reynolds number was assumed to be small, and thus the induced magnetic field is negligible. The flow model is shown in Figure 2.1.

Under the above assumptions, the simplified two-dimensional boundary layer equations governing the flow and heat transfer were derived from Al-sudais (2012); Ishak et al. (2009); Yian et al. (2011) as;

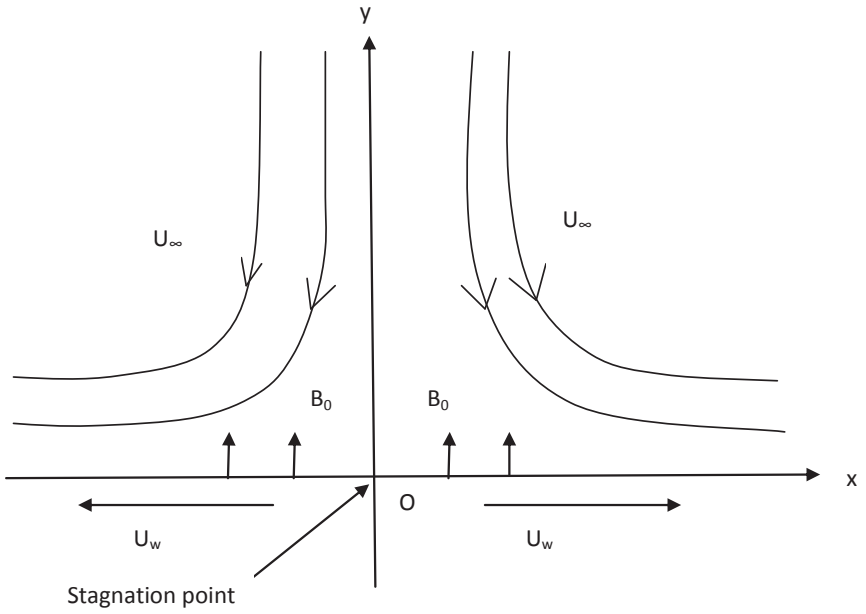

Figure 2.1: *Physical model of the flow.*

$$\frac{\partial u}{\partial x} + \frac{\partial v}{\partial y} = 0, \tag{2.1}$$

$$u\frac{\partial u}{\partial x} + v\frac{\partial u}{\partial y} = U_\infty \frac{dU_\infty}{dx} + \nu\frac{\partial^2 u}{\partial y^2} + \frac{\sigma B_0^2}{\rho}\left(U_\infty - u\right) - \frac{\nu}{K}u, \tag{2.2}$$

$$u\frac{\partial T}{\partial x} + v\frac{\partial T}{\partial y} = \alpha\frac{\partial^2 T}{\partial y^2} + \frac{Q}{\rho c_p}(T - T_\infty), \tag{2.3}$$

subject to the boundary conditions

$$u = U_w(x), \quad v = V_w(x), \quad T = T_w(x), \quad \text{at} \quad y = 0, \tag{2.4}$$

$$u \to U_\infty(x), \quad T \to T_\infty \quad \text{as} \quad y \to \infty. \tag{2.5}$$

In the above equations, u and v are the velocity components along the $x-$ and $y-$axes respectively, ν is the kinematic viscosity, ρ is the fluid density, α is the thermal diffusivity, K is the constant permeability of the porous medium, c_p is the specific heat capacity at constant pressure, Q represents the temperature-dependent heat source/sink (source when $Q > 0$ and sink when $Q < 0$) and σ is the electrical conductivity.

Equations (2.2) and (2.3) can be transformed into the corresponding ordinary differential equations

(2.10 - 2.11) by the following transformation:

$$\eta = \left(\frac{a}{\nu}\right)^{\frac{1}{2}} y, \quad f(\eta) = \frac{\psi}{(a\nu)^{\frac{1}{2}} x}, \quad \theta(\eta) = \frac{T - T_\infty}{T_w - T_\infty}, \tag{2.6}$$

where ψ is the stream function defined in the usual way as

$$u = \frac{\partial \psi}{\partial y}, \quad v = -\frac{\partial \psi}{\partial x}. \tag{2.7}$$

The velocity components are given as;

$$u = axf'(\eta), \quad v = -(a\nu)^{\frac{1}{2}} f(\eta), \tag{2.8}$$

and

$$V_w(x) = -(a\nu)^{\frac{1}{2}} s, \tag{2.9}$$

where prime denotes differentiation with respect to η, $s = f(0)$ is the constant mass flux with $s > 0$ for suction and $s < 0$ for injection. The transformed ordinary differential equations are derived from Al-sudais (2012); Ishak et al. (2009); Yian et al. (2011) as;

$$f''' + ff'' - f'^2 + \epsilon^2 + M(\epsilon - f') - \Omega f' = 0, \tag{2.10}$$

$$\frac{1}{Pr}\theta'' + f\theta' - nf'\theta + \gamma\theta = 0 \tag{2.11}$$

subject to

$$f(0) = s, \quad f'(0) = 1, \quad f'(\infty) = \epsilon, \tag{2.12}$$

$$\theta(0) = 1, \quad \theta(\infty) = 0. \tag{2.13}$$

In the above,

$M = \dfrac{\sigma B_0^2}{a\rho}$ is the magnetic parameter,

$\epsilon = \dfrac{b}{a}$ is the velocity ratio parameter,

$\Omega = \dfrac{\nu}{aK}$ is the permeability parameter,

$Pr = \dfrac{\nu}{\alpha}$ is the Prandtl number,

$\gamma = \dfrac{Q}{a\rho c_p}$ is the dimensionless heat generation/absorption coefficient.

The physical quantities of main interest are the skin friction coefficient C_f, and the local Nusselt number Nu_x, which are defined as;

$$C_f = \frac{\tau_w}{gU_w^2}, \quad Nu_x = \frac{h_x x}{k},$$

where

$\tau_w = \mu \left(\dfrac{\partial u}{\partial y}\right)_{y=0}$ is the wall shear stress,

$h_x = \dfrac{q_w}{T_w - T_\infty}$ is the local heat transfer coefficient,

$q_w = -k \left(\dfrac{\partial T}{\partial y}\right)_{y=0}$ is the local heat flux,

μ is the dynamic viscosity, and k is the thermal conductivity. It can be readily shown that

$$Re_x^{\frac{1}{2}} C_f = f''(0), \quad Re_x^{-\frac{1}{2}} Nu_x = -\theta'(0), \tag{2.14}$$

with

$$Re_x = \frac{U_w(x)x}{\nu}, \quad \text{being the local Reynolds number.}$$

2.3. Method of solution

In this section we present the spectral perturbation method (SPM) for solving equations (2.10) - (2.13). Perturbation techniques in general construct the solution for a problem by generating asymptotic expansions of the perturbation parameter. Usually the resulting solutions are compli-

cated, making it difficult to get higher-order perturbation approximations (see for example Nazar et al. (2004a,b) and Seshadri et al. (2002)) which leads to less accurate results.

2.3.1 Spectral Perturbation Method (SPM)

In the spectral perturbation method, the way the series equations are generated in the same way as with perturbation methods and then solved numerically using the Chebyshev spectral method, a method well documented for its accuracy. It becomes possible to get higher order approximate solutions which are more accurate than the analytic approach. The SPM can be efficiently used to find approximate solutions for equations (2.10) - (2.13) for sufficiently small values of the velocity ratio parameter (ϵ).

Equations (2.10) and (2.11) are decoupled, once the solution for $f(\eta)$ has been found, equation (2.11) becomes linear. Following Seshadri et al. (2002); Nazar et al. (2004a); Liao (2006a), a series expansion will be constructed to approximate the solution for $f(\eta)$ by taking ϵ as the small parameter and approximate

$$f(\eta) = \sum_{m=0}^{+\infty} \epsilon^m f_m(\eta). \tag{2.15}$$

Substituting (2.15) in equation (2.10) with corresponding boundary conditions (2.12) and balancing terms of equal order of ϵ gives

$$f_0''' + f_0 f_0'' - f_0'^2 - (M+\Omega) f_0' = 0, \quad f_0(0) = s, \quad f_0'(0) = 1, \quad f_0'(\infty) = 0, \tag{2.16}$$

$$f_1''' + f_0 f_1'' - (2f_0' + M + \Omega) f_1' + f_0'' f_1 = -M, \quad f_1(0) = 0, \quad f_1'(0) = 0, \quad f_1'(\infty) = 1, \tag{2.17}$$

$$f_2''' + f_0 f_2'' - (2f_0' + M + \Omega) f_2' + f_0'' f_2 = f_1'^2 - f_1 f_1'' - 1, \tag{2.18}$$

$$f_2(0) = 0, \quad f_2'(0) = 0, \quad f_2'(\infty) = 0,$$

$$f_m''' + f_0 f_m'' - (2f_0' + M + \Omega) f_m' + f_0'' f_m = \sum_{i=1}^{m-1} \left(f_i' f_{m-1-i}' - f_i f_{m-1-i}'' \right), \tag{2.19}$$

$$f_m(0) = 0, \quad f_m'(0) = 0, \quad f_m'(\infty) = 0, \quad m \geq 3.$$

The exact solution for equation (2.16) was found to be

$$f_0 = s + \frac{1}{a}(1 - e^{-a\eta}), \quad a = \frac{s + \sqrt{s^2 + 4(1 + M + \Omega)}}{2}. \tag{2.20}$$

The left hand sides of equations (2.17), (2.18) and (2.19) are linear and the right hand sides are known from previous estimations. These equations therefore may be solved using any numerical method. In this study, the Chebyshev spectral collocation method are used to integrate equations (2.17), (2.18) and (2.19). The spectral method has been found not only to be very accurate but also easy to use and more computationally efficient than other numerical methods because it requires only a few grid points in the discretization process to give very accurate solutions. The method is based on the Chebyshev polynomials defined on the interval $[-1, 1]$ by

$$T_k(x) = \cos[l \cos^{-1}(x)]. \tag{2.21}$$

The physical region $[0, \infty)$ was first transformed into the region $[-1, 1]$ using the domain truncation technique. The problem was solved in the interval $[0, L]$ instead of $[0, \infty)$. This leads to the following algebraic mapping

$$x = \frac{2\eta}{L} - 1, \quad x \in [-1, 1], \tag{2.22}$$

where L is the scaling parameter used to invoke the boundary condition at infinity. The Chebyshev nodes in $[-1, 1]$ are defined by the Gauss-Lobatto collocation points (Canuto et al., 1988; Trefethen, 2000) given by

$$x_j = \cos \frac{\pi j}{N}, \tag{2.23}$$

where $N+1$ is the number of collocation points. The basic idea behind the spectral collocation method is the introduction of a differentiation matrix $\mathcal{D}$ which was used to approximate the derivatives of the unknown variable $f_m(\eta)$, at the collocation points (grid points) as the matrix vector product

$$\left.\frac{dF_m}{d\eta}\right|_{\eta=\eta j} = \sum_{k=0}^{N} \mathbf{D}_{jk} f_m(x_k) = \mathbf{D}F_m, \qquad j = 0, 1, \ldots, N \tag{2.24}$$

where $\mathbf{D} = 2\mathcal{D}/L$ and

$$F_m = [f_m(x_0), f_m(x_1), \ldots, f_m(x_N)]^T$$

are the vector function at the collocation points. Higher order derivatives are obtained as powers of $\mathbf{D}$, that is

$$F_m{}^{(p)} = \mathbf{D}^p F_m, \tag{2.25}$$

where p is the order of the derivative. The entries of the differentiation matrix are given in Trefethen (2000); Canuto et al. (2007); Hesthaven et al. (2007) as;

$$\mathcal{D}_{kj} = \begin{cases} \frac{c_j}{c_k}\frac{(-1)^{j+k}}{x_j - x_k}, & j \neq k, \\ -\frac{x_k}{2(1-x_k^2)}, & 1 \leq j = k \leq N-1, \\ \frac{2N^2+1}{6}, & j = k = 0, \\ -\frac{2N^2+1}{6}, & j = k = N, \end{cases}$$

where

$$c_j = \begin{cases} 2, & j = 0, N, \\ 1, & 1, 2, \ldots, N-1. \end{cases}$$

Substituting equations (2.24) - (2.25) in (2.17), (2.18) and (2.19), respectively, gives rise to the following matrix equations

$$\mathbf{A}_1\mathbf{F}_1 = \mathbf{B}_1, \quad \sum_{k=0}^{N} \mathbf{D}_{0k} f_1(x_k) = 1, \quad \sum_{k=0}^{N} \mathbf{D}_{Nk} f_1(x_k) = 0, \; f_1(x_N) = 0, \tag{2.26}$$

$$\mathbf{A}_2\mathbf{F}_2 = \mathbf{B}_2, \quad \sum_{k=0}^{N} \mathbf{D}_{0k} f_2(x_k) = 0, \quad \sum_{k=0}^{N} \mathbf{D}_{Nk} f_2(x_k) = 0, \; f_2(x_N) = 0, \tag{2.27}$$

$$\mathbf{A}_m\mathbf{F}_m = \mathbf{B}_m, \quad \sum_{k=0}^{N} \mathbf{D}_{0k} f_m(x_k) = 0, \quad \sum_{k=0}^{N} \mathbf{D}_{Nk} f_m(x_k) = 0, \; f_m(x_N) = 0, \tag{2.28}$$

where

$$\mathbf{A}_1 = \mathbf{A}_2 = \mathbf{A}_m \tag{2.29}$$

$$= \mathbf{D}^3 + \mathrm{diag}(f_0)\mathbf{D}^2 - \mathrm{diag}(2f_0')\mathbf{D} - (M+\Omega)\mathbf{D} + \mathrm{diag}(f_0''), \tag{2.30}$$

$$\mathbf{B}_1 = -M(\mathrm{ones}(N+1,1)), \quad \mathbf{B}_2 = f_1^2 - f_1 f_1'' - 1, \tag{2.31}$$

$$\mathbf{B}_m = \mathrm{Sum}\mathbf{F} = \sum_{i=1}^{m-1} \left[(\mathbf{D}\mathbf{F}_i)\,(\mathbf{D}\mathbf{F}_{m-1-i}) - \mathbf{F}_i\left(\mathbf{D}^2\mathbf{F}_{m-1-i}\right) \right]. \tag{2.32}$$

In the equations above, diag() represents a diagonal matrix of size $(N+1)\times(N+1)$. The vectors $\mathbf{B}_m$ was generated by evaluating the right hand side of equation (2.19) at the collocation points with the derivatives replaced by spectral differentiation matrices. Thus, starting from F_0 the solutions F_m for $m \geq 1$ can be obtained from

$$\mathbf{F}_m = \mathbf{A}_{1,m}^{-1}\mathbf{B}_{1,m}. \tag{2.33}$$

Once the solution for equation (2.33) has been obtained, equation (2.11) with corresponding boundary conditions (2.13) is then solved using Chebyshev spectral method which yields the following equation

$$\left[(1/Pr)\mathbf{D}^2 + \mathrm{diag}(f_m)\mathbf{D} + \gamma\mathbf{I} - \mathrm{diag}(\mathbf{D}f_m)\right]\boldsymbol{\Theta} = \mathbf{0}, \quad \theta(x_0) = 1, \quad \theta(x_N) = 0, \tag{2.34}$$

with

$$\boldsymbol{\Theta} = [\theta(x_0), \theta(x_1), \ldots, \theta(x_N)]^T$$

and $\mathbf{I}$ is an $(N+1)\times(N+1)$ identity matrix.

2.3.2 Asymptotic Solution for large Perturbation Parameter (M)

The behavior of the solution to the governing equation (2.10) when the magnetic parameter M is large will be considered in this section. From equation (2.10), the order of magnitude analysis of the various terms in the equation shows that the largest terms are f''', Mf', and $M\epsilon$. As a result, these terms have to be balanced, that is $f''' \sim Mf' \sim M\epsilon$. Balancing these terms can only be done

by assuming that η is small thus derivatives with respect to η are large. An appropriate scaling parameter from for f and η need to be sought. On balancing f''', Mf' and $M\epsilon$, we note that

$$\eta = \frac{1}{\sqrt{M}} \quad \text{and} \quad f = \frac{\epsilon}{\sqrt{M}}.$$

The following transformations are introduced

$$f = \frac{\epsilon}{\sqrt{M}} F(\epsilon, \bar{\eta}), \quad \eta = \frac{1}{\sqrt{M}} \bar{\eta}. \tag{2.35}$$

Substituting the transformations in (2.35) into (2.10) and dividing all through by ϵM gives

$$F''' + \lambda \epsilon F F'' - \lambda \epsilon F'^2 + \lambda \epsilon + 1 - F' - \Omega \lambda F', \tag{2.36}$$

subject to the boundary conditions

$$F(0) = 0, \quad F'(0) = \frac{1}{\epsilon}, \quad F'(\infty) = 1, \tag{2.37}$$

where $\lambda = \dfrac{1}{M}$ and the prime now denote derivatives with respect to $\bar{\eta}$.

Therefore, for sufficiently large M, perturbation expansion is done in powers of λ. We search for a perturbation approximation in the format

$$F(\bar{\eta}) = \sum_{m=0}^{+\infty} \lambda^m F_m(\bar{\eta}). \tag{2.38}$$

Substituting equation (2.38) in (2.36) and balancing terms of equal magnitude yields

$$F_0''' - F_0' + 1 = 0, \quad F_0(0) = 0, \quad F_0'(0) = \frac{1}{\epsilon}, \quad F_0'(\infty) = 1, \tag{2.39}$$

$$F_1''' - F_1' = \epsilon F_0'^2 - \epsilon F_0 F_0'' + \Omega F_0' - \epsilon, \quad F_1(0) = 0, \quad F_1'(0) = 0, \quad F_1'(\infty) = 0, \tag{2.40}$$

$$F_m''' - F_m' = \Omega F_{m-1}' + \sum_{i=1}^{m-1} \epsilon \left(F_i' F_{m-1-i}' - F_i F_{m-1-i}'' \right), \tag{2.41}$$

$$F_m(0) = 0, \quad F_m'(0) = 0, \quad F_m'(\infty) = 0, \quad m \geq 2,$$

$$\frac{1}{Pr} \Theta'' + F_m \Theta' - n F_m' \Theta + \gamma \Theta = 0, \tag{2.42}$$

$$\Theta(0) = 1, \quad \Theta_(\infty) = 0.$$

We note that the left hand side of the higher order perturbation equation (2.41) is linear and the right hand side is known from previous estimations for $m \geq 2$. Therefore we apply the Chebyshev spectral collocation method described above to integrate equation (2.41). It is worth mentioning that when $\lambda = 0$ there exists a closed form solution of the form

$$F_0 = e^{-\eta} - 1 + \frac{1}{\epsilon}\left(1 - e^{-\eta}\right) + \eta.$$

2.3.3 Spectral Quasilinearisation Method (SQLM)

The quasilinearisation method (QLM) is basically a generalized Newton-Raphson Method that was originally proposed and used by Bellman and Kalaba (1965) for solving functional equations. The QLM scheme is derived by linearizing the nonlinear component of the governing equations using Taylor series expansion with the assumption that the difference between the value of the unknown functions at the current iteration level (denoted by $m+1$) and the value at the previous iteration level (denoted by m) is small. Applying the QLM on equations (2.10) - (2.11) gives,

$$f'''_{m+1} + f_m f''_{m+1} - (2f'_m + M + \Omega)f'_{m+1} + f''_m f_{m+1} = f_m f''_m - (f')^2_m - \epsilon^2 - M\epsilon, \quad (2.43)$$

$$f_m(0) = s, \quad f'_m(0) = 1, \quad f'_m(\infty) = \epsilon,$$

$$(1/Pr)\theta''_{m+1} + f_{m+1}\theta'_{m+1} + (\gamma - nf'_{m+1})\theta_{m+1} = 0, \quad (2.44)$$

$$\theta_{m+1}(0) = 1, \quad \theta_{m+1}(\infty) = 0, \quad m \geq 1.$$

Equations (2.43) and (2.44) are solved using the Chebyshev spectral method as discussed above, hence the method here is referred to as the spectral quasilinearisation method. The appropriate initial approximations $f_0(\eta)$ and $\theta_0(\eta)$ required to start the SQLM algorithm was chosen to be a function that satisfies the underlying boundary conditions (2.12) and (2.13). The initial approximate solutions considered suitable for the governing equations (2.10) and (2.11) are

$$f_0(\eta) = \epsilon\eta + e^{-\epsilon\eta} - e^{-\eta} + s, \text{ and } \theta_0(\eta) = e^{-\eta}. \quad (2.45)$$

2.4. Results and discussion

The spectral perturbation method was used to solve the governing equations (2.10) - (2.13) and the results are presented in this section. Numerical solutions of the skin friction coefficient and the heat transfer rate are presented. For all simulations, unless stated otherwise, we used $L = 30$, which was found to give accurate results through numerical experimentation. Increasing the value of L did not change the results to a significant extent. The number of collocation points used in the spectral method discretization was $N = 100$, unless indicated otherwise. To validate the SPM results, comparisons were made with those results obtained using the spectral quasilinearisation method for the same values of L and N.

Table 2.1 shows a comparison of the SPM and SQLM approximate solutions of the skin friction coefficient $f''(0)$ at different values of the magnetic parameter (M), the suction parameter ($s > 0$) and the permeability parameter (Ω). Comparing the SPM and SQLM results, it can be seen that they are in good agreement for the set level of accuracy. As can be seen from Table 2.1, the effect of the magnetic parameter is to reduce the skin friction coefficient when $\epsilon = 0.1$. The physical reasoning behind this result is that the presence of transverse magnetic field sets in Lorentz force. The Lorentz force in turn resulted in a retarding force on the velocity field and thus as M increases, the retarding force also increased and hence the momentum boundary layer thickness decreased consequently decreasing the shear stress at the sheet. These results are consistent with those of other analogous studies carried out by Qi and Hong-Qing (2009) and Sharma and Singh (2009). The suction parameter and Ω were both seen to decrease $f''(0)$ for fixed values of the magnetic parameter.

Table 2.1: *Comparison of the SPM and SQLM approximate solutions of* $f''(0)$ *at different values of* M, s *and* Ω *for* $\epsilon = 0.1$.

M	s	Ω	SPM	SQLM
0	0.5	0.5	-1.48367118	-1.48367118
1	0.5	0.5	-1.75363323	-1.75363323
5	0.5	0.5	-2.58041185	-2.58041185
2	0.1	1.0	-1.93458858	-1.93458858
2	0.5	1.0	-2.13541374	-2.13541374
2	1.0	1.0	-2.41148887	-2.41148887
2	0.5	0	-1.84065471	-1.84065471
2	0.5	1	-2.13541374	-2.13541374
2	0.5	5	-3.00509001	-3.00509001

A comparison of the SPM and SQLM approximate solutions of the Nusselt number for varying

Prandtl number Pr, the constant n and heat source γ parameters is shown in Table 2.2. The comparison of the two results reveals a good agreement for eight decimal places. The effect of the Pr was seen to reduce the heat transfer rate. Similarly, the constant n reduces the heat transfer rate while the heat source parameter was seen to increase the heat transfer rate. The heat transfer rate was reduced by an increase in Pr and n due to the decreasing manner of the thermal boundary layer thickness with increase in these parameters.

Table 2.2: *Comparison of the SPM and SQLM approximate solutions of* $-\theta'(0)$ *at different values of* Pr, n *and* γ *for* $M = 1,\ s = -0.5,\ \Omega = 1,\ \epsilon = 0.1$.

Pr	n	γ	SPM	SQLM
0.7	0.5	0.5	0.09204405	0.09204405
1	0.5	0.5	0.04705260	0.04705260
3	0.5	0.5	-3.22465634	-3.22465634
0.7	0.1	0.5	0.31124149	0.31124149
0.7	0.5	0.5	0.09204405	0.09204405
0.7	1	0.5	-1.57584749	-1.57584749
0.7	0.5	0.1	-0.06914104	-0.06914104
0.7	0.5	0.5	0.09204405	0.09204405
0.7	0.5	1	0.27248249	0.27248249

The convergence of the method was demonstrated in Table 2.3. SPM approximate solutions of the skin friction are presented for varying magnetic parameter values at different iterations. As can be seen from the table, converging results were reached after relatively very few iterations. The results also showed that the method worked for larger magnetic parameter values and convergence was achieved at even fewer iterations.

Table 2.3: *SPM approximate solutions of* $f''(0)$ *at different orders of approximation for* $s = -0.5,\ \Omega = 0.5,\ \epsilon = 0.1$.

M	3rd order	4th order	6th order	9th order	10th order
0	-1.17935081	-1.17935081	-1.17935963	-1.17935957	-1.17935957
1	-1.44059145	-1.44062852	-1.44062948	-1.44062948	-1.44062948
5	-2.22678443	-2.22679794	-2.22679790	-2.22679790	-2.22679790
10	-2.94707748	-2.94708358	-2.94708356	-2.94708356	-2.94708356
15	-3.53171816	-3.53172178	-3.53172177	-3.53172177	-3.53172177
20	-4.03688009	-4.03688254	-4.03688254	-4.03688254	-4.03688254
25	-4.48819198	-4.48819378	-4.48819378	-4.48819378	-4.48819378
30	-4.89990358	-4.89990498	-4.89990498	-4.89990498	-4.89990498
40	-5.63719670	-5.63719763	-5.63719763	-5.63719763	-5.63719763
50	-6.29158545	-6.29158613	-6.29158613	-6.29158613	-6.29158613

Table 2.4 shows the asymptotic solutions of $f''(0)$ for large perturbation parameter. The results in

the table show that the SPM works even for large parameter values. The convergence rate was seen to improve with increase in the parameter value.

Table 2.4: *Comparison of the SPM and SQLM approximate solutions of $f''(0)$ for large M at different values of ϵ, and M for $s = \Omega = 1$.*

M	ϵ	Order	SPM	SQLM
10	0.1	11	-3.16660302	-3.16660302
25	0.1	7	-4.70893064	-4.70893064
50	0.1	6	-6.51327850	-6.51327850
100	0.1	5	-9.10616039	-9.10616039
150	0.1	5	-11.10954274	-11.10954274
10	0.5	12	-1.93017839	-1.93017839
25	0.5	8	-2.73025340	-2.73025340
50	0.5	7	-3.70083628	-3.70083628
100	0.5	5	-5.11780454	-5.11780454
150	0.5	5	-6.22016614	-6.22016614
10	0.8	14	-0.95524152	-0.95524152
25	0.8	8	-1.21528866	-1.21528866
50	0.8	7	-1.56942012	-1.56942012
100	0.8	6	-2.11085400	-2.11085400
150	0.8	5	-2.54030986	-2.54030986

Figure 2.2 shows the effect of the velocity ratio parameter ϵ, on the velocity profile. From Figure 2.2, it can be seen that the velocity decreases with increase in the values of $\epsilon < 1$. This implies that a considerable decrease was observed in the boundary layer with an increase in ϵ. Increased values of ϵ means that the free stream velocity surpasses the stretching velocity, which in turn results in increase in pressure and straining motion near the stagnation point thus reducing the boundary layer thickness. Similar observations were made in parallel studies carried out by Ishak et al. (2009) and Qi and Hong-Qing (2009).

The effect of the magnetic parameter M, on the velocity profile $f'(\eta)$, is displayed in Fig. 2.3. The velocity profile decreases with increase in the magnetic parameter. This happens for the same reason as for the decrease in the skin friction coefficient in Table 2.1. Similar results have been reported in a study carried out by Al-sudais (2012).

Figure 2.4 illustrates the effect of the permeability parameter Ω, on the velocity profile. It can be observed that as Ω increases, the velocity profile decreases. This is because the porous medium results into a drag force called the Darcy force which decelerates the fluid in the boundary layer. This behavior on permeability parameter correlate with those obtained by Al-sudais (2012) and Salem and Fathy (2012).

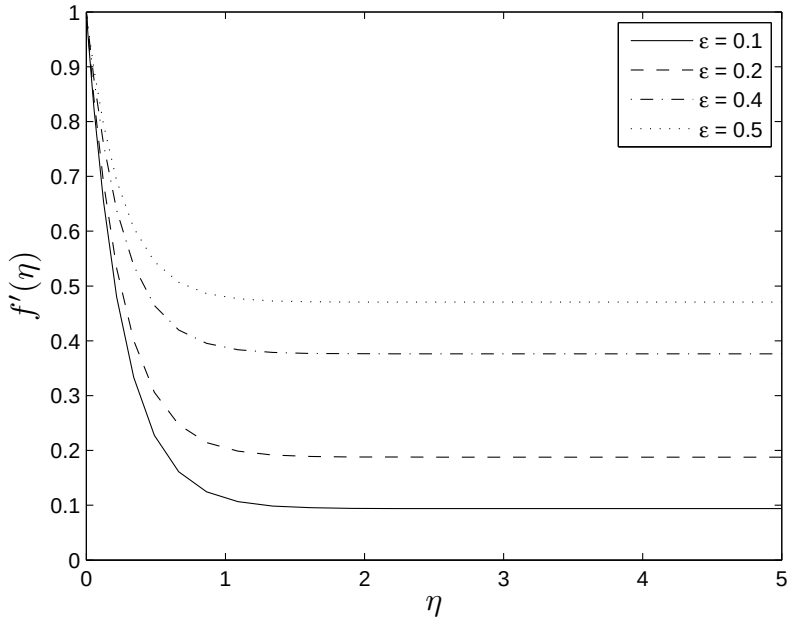

Figure 2.2: *Effect of the velocity ratio parameter on the velocity profile,* $M = 15,\ \Omega = 1,\ s = -0.5,\ N = 60,\ L = 20.$

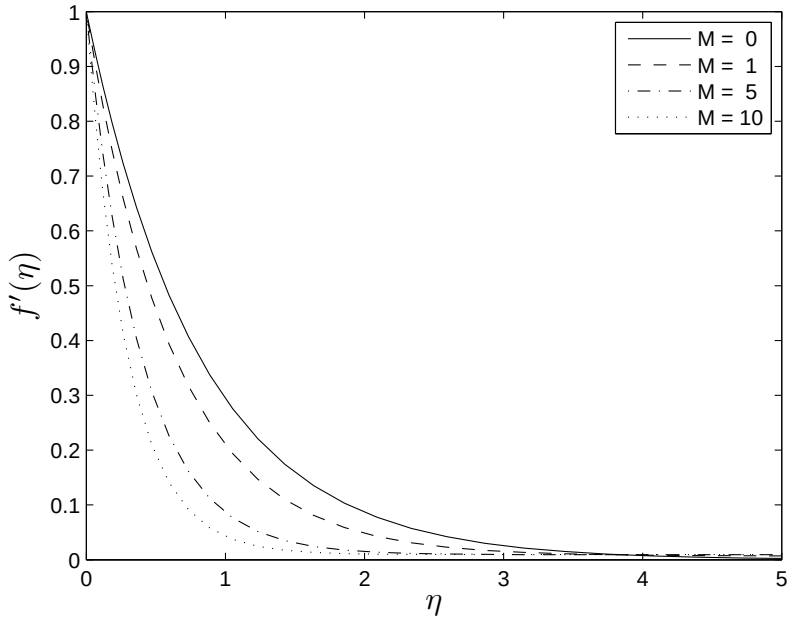

Figure 2.3: *Effect of the magnetic parameter* M *on the velocity profile,* $\Omega = 0.5,\ s = -0.5.$

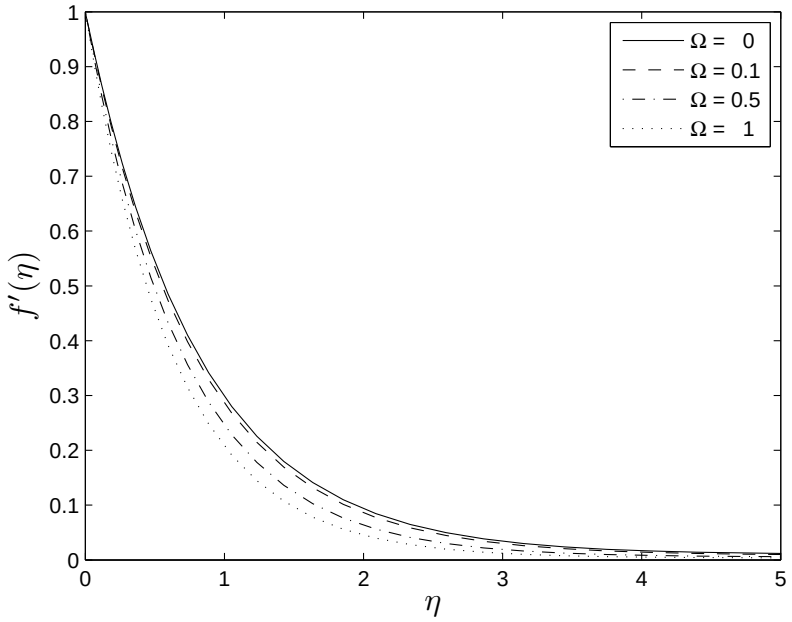

Figure 2.4: *Effect of the permeability parameter* Ω *on the velocity profile,* $M = 0.5,\ s = -0.5$.

The effect of suction and injection on the velocity profile is shown in Figures 2.5 and 2.6 respectively. From the figures, it can be seen that for both cases, the velocity decreased with an increase in suction and injection with effect being more pronounced for the suction case. For $\epsilon = 0.1$, suction implied a decrease in skin friction coefficient as seen in Table 2.1 which was caused by the increased thickness of the momentum boundary layer hence decelerating the flow near the surface of the wall.

Figure 2.7 presents the skin friction coefficient $f''(0)$ against the magnetic parameter. As seen and discussed earlier in Table 2.3, the figure concurs with the earlier results.

In Figure 2.8 the permeability parameter Ω was shown to reduce the skin friction coefficient as seen earlier in Table 2.1. A similar effect of suction and injection was observed in Figure 2.9 on the skin friction coefficient as with the velocity profiles in Figures 2.5 and 2.6. Both suction and injection were seen to decrease the skin friction with effect prominent with the suction case.

Figure 2.10 presents the effect of the Prandtl number Pr on the temperature profile. From the figure it was observed that the temperature profile is reduce with an increase in Pr. The effect was even more pronounced for small Pr because the thermal boundary layer thickness is comparatively large. Similar observations were made in a parallel study by Al-sudais (2012).

Figure 2.11 presents the effect of the temperature index constant n, on the temperature profile. The

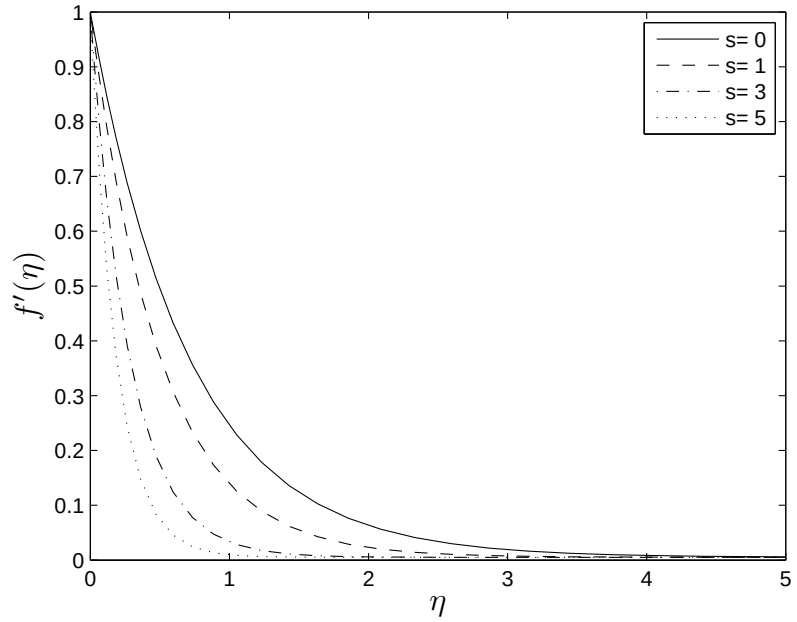

Figure 2.5: *Effect of suction,* $s > 0$ *on the velocity profile,* $\Omega = 0.5,\ M = 0.5$.

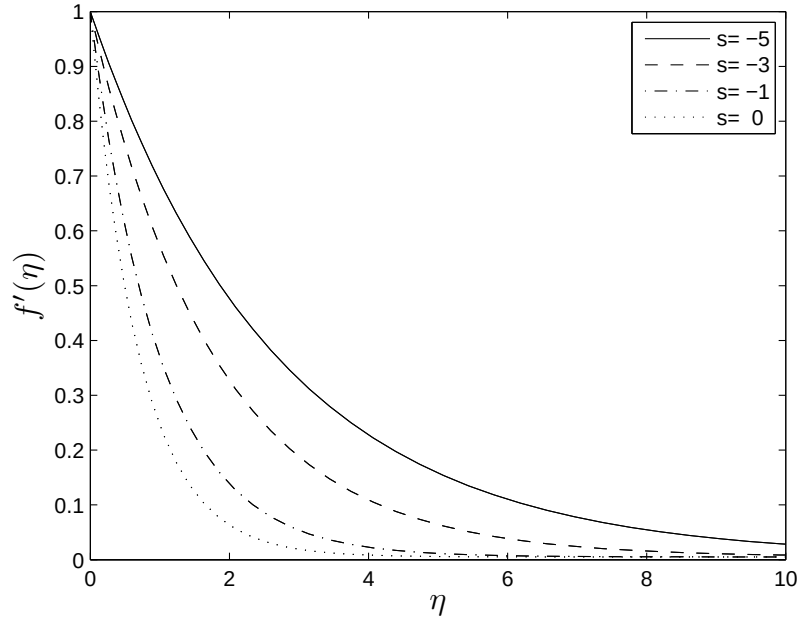

Figure 2.6: *Effect of injection,* $s < 0$ *on the velocity profile,* $\Omega = 0.5,\ M = 0.5$.

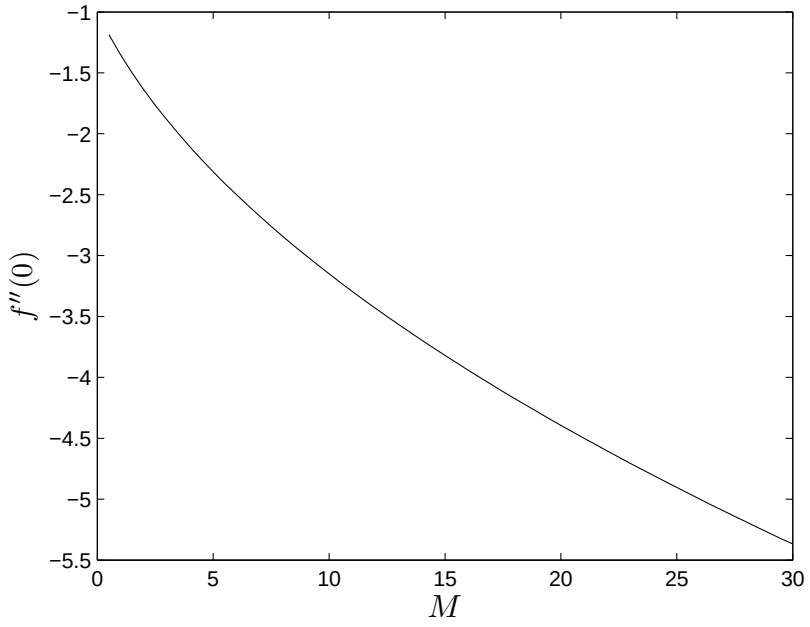

Figure 2.7: *Effect of the magnetic parameter on the skin friction coefficient,* $\Omega = 0.5,\ s = -0.5$.

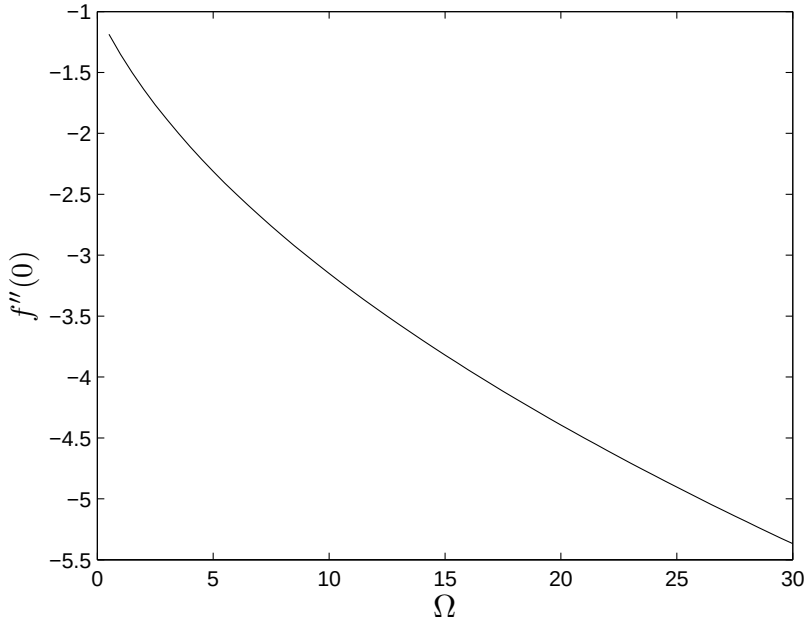

Figure 2.8: *Effect of the permeability parameter on the skin friction coefficient,* $M = 0.5,\ s = -0.5$.

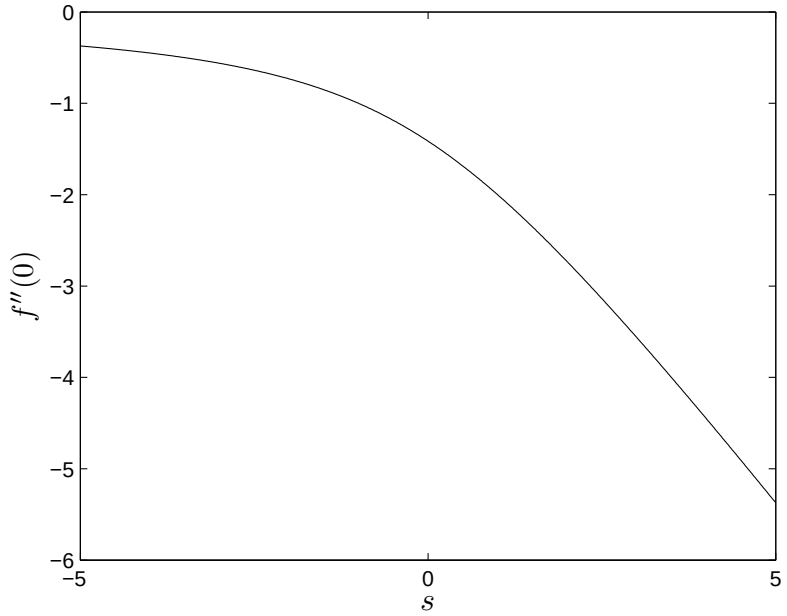

Figure 2.9: *Effect of suction/injection on the skin friction coefficient,* $M = 0.5$, $\Omega = 0.5$.

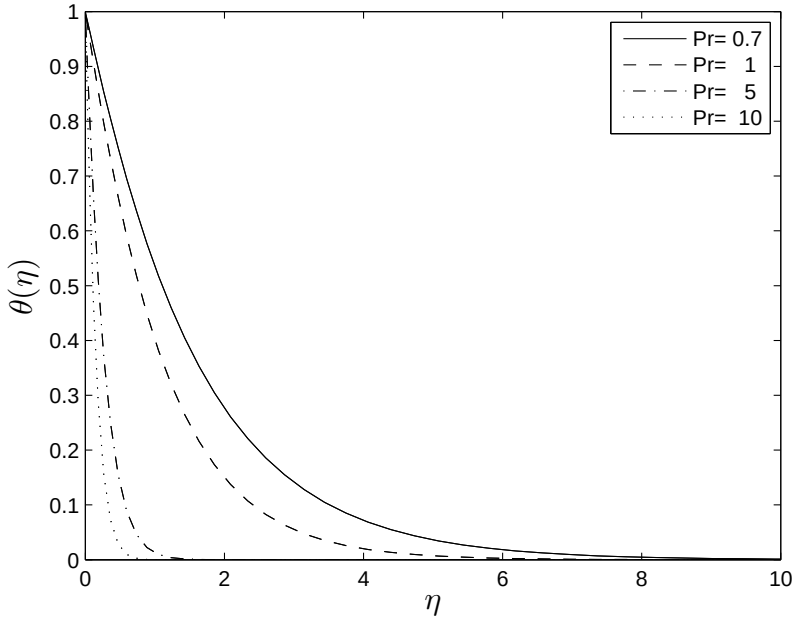

Figure 2.10: *Effect of the Prandtl number* Pr *on the temperature profile,* $n = 0.5$, $\gamma = 0.5$.

temperature decreases with an increase in n because the thermal boundary layer thickness decreases with an increase in this parameter. These results are in agreement with those of a parallel study carried out by Ishak et al. (2009).

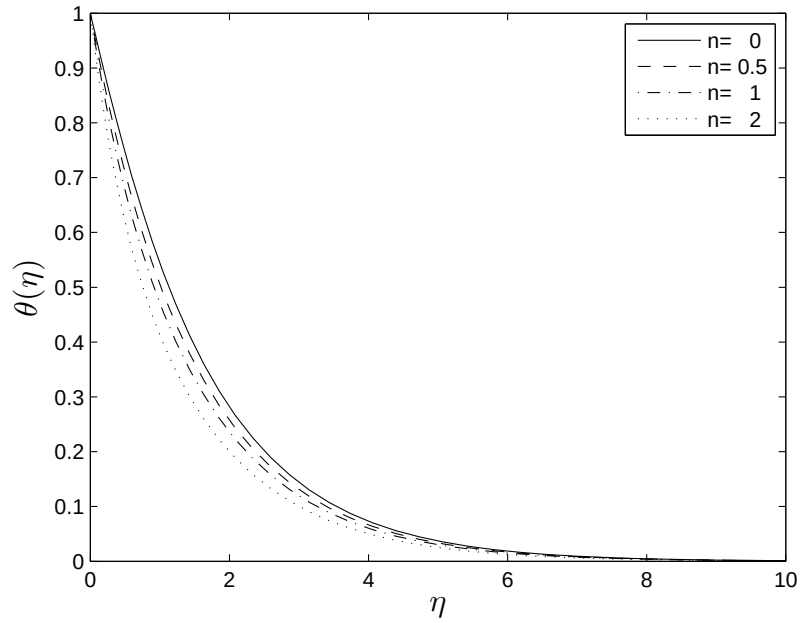

Figure 2.11: *Effect of the constant n on the temperature profile, $Pr = 0.7$, $\gamma = 0.1$.*

The effect of the heat generation parameter on the temperature profile is shown in Figure 2.12. The temperature increases with an increase in the heat generation parameter. The heat sink parameter on the other hand was observed to decrease the temperature profile in Figure 2.13. It is physically expected that the temperature increases when a heat source is introduced into the system and the opposite when volumetric heat supply is decreased. These findings are consistent with those of Sharma and Singh (2009) in a similar investigation.

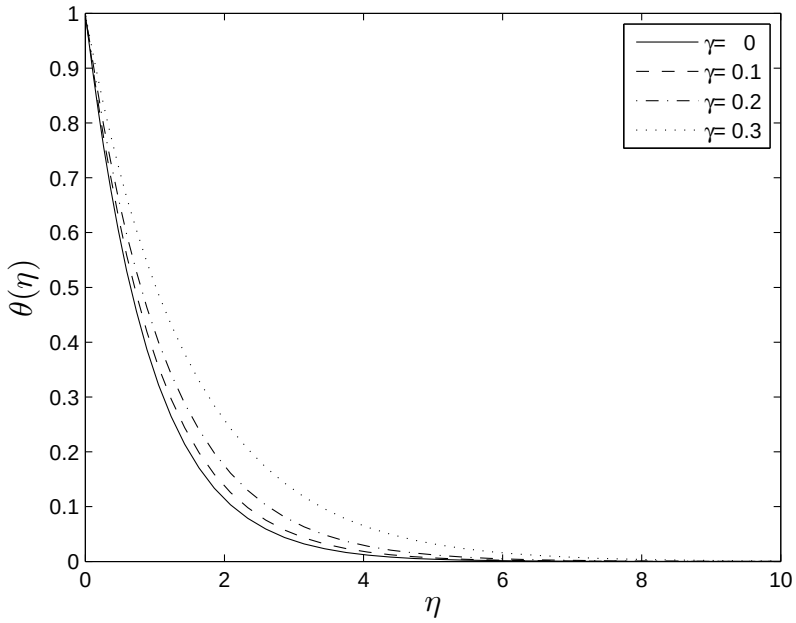

Figure 2.12: *Effect of heat source,* $\gamma > 0$ *on the temperature profile,* $n = 0.5,\ Pr = 1.$

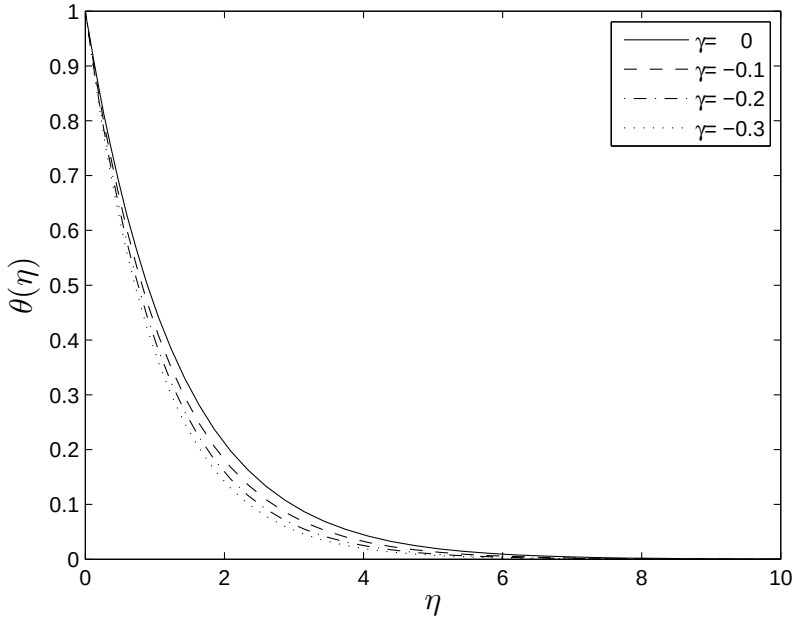

Figure 2.13: *Effect of heat sink,* $\gamma < 0$ *on the temperature profile,* $n = 0.5,\ Pr = 0.75.$

3

Unsteady Heat and Mass Transfer by MHD Mixed Convection Flow over an Impulsively Stretched Vertical Surface with Chemical Reaction Effect

3.1. Introduction

In the past few decades, the study of mixed convection flow with the heat and mass transfer under the effect of magnetic field and chemical reaction has attracted the interest of a considerable number of researchers because of its numerous applications in several branches of science and engineering and in transport processes. These applications include the industry for drying, cooling of nuclear reactors, chemical vapor deposition on surfaces and Magneto hydrodynamic (MHD) power generators (Pal and Talukdar, 2010; Dulal and Mondal, 2011). In the design of chemical process equipment, distribution of temperature and moisture over agriculture fields, combined heat and mass transfer plays an essential role (Pal and Talukdar, 2010; Dulal and Mondal, 2011). In addition, Magneto-hydrodynamic (MHD) flow plays a crucial role in the polymer, petroleum and agriculture industries (Pal and Talukdar, 2010; Dulal and Mondal, 2011).

The problem of unsteady heat and mass transfer due to MHD mixed convection flow over an impulsively stretched vertical surface with chemical reaction effect has been studied numerically in this dissertation. The problem considered extends the analysis of EL-Kabeir and Rashad (2012) by introducing chemical reaction effects. EL-Kabeir and Rashad (2012) previously used the implicit finite difference method known as the Keller - box to analyze the melting effect on unsteady heat and mass transfer mixed convection flow over an impulsively stretched vertical surface in a quiescent fluid in

the absence of a chemical reaction. Recently, researchers have shown an increased interest in the study of the combined effects of heat and mass transfer with chemical reactions due to its numerous importance to scientists and engineers. The effect of chemical reaction with heat transfer cannot be neglected because of its universal occurrence in many branches of science and engineering. Possible application of this type of flow can be found in many engineering processes such as oxidation of solid materials, production of polymers, food processing, synthesis of ceramic materials and tubular reactors (Pal and Talukdar, 2010).

The equations describing unsteady heat and mass transfer due to MHD mixed convection flow over an impulsively stretched vertical surface with chemical reaction effect are systems of nonlinear partial differential equations (PDEs) defined on a semi-infinite domain in both time and space. The unsteady PDE equations are more difficult to solve when compared to that of steady flows which are often modeled by nonlinear ordinary differential equations (ODEs). To simplify the analysis of the class of nonlinear PDEs describing the unsteady boundary layer flow, Williams and Rhyne (1980) presented a convenient transformation converting the infinite time scale $\tau = [0, \infty)$ to a finite domain $\xi = [0, 1]$ of integration. In recent times, there has been an increasing number of research that utilize the transformation of Williams and Rhyne (1980) on the solution of unsteady flows using perturbation expansions for $\xi < 1$. These investigations includes the study of Seshadri et al. (2002) who used the perturbation series approach for the solution of unsteady mixed convection flow along a heated vertical plate due to impulsive motion. The perturbation series approach was also employed by Nazar et al. (2004a,b) to obtain first-order perturbation approximation of the solution of unsteady boundary layer flow due to a stretching surface in a rotating fluid and unsteady mixed convection boundary layer flow near the stagnation point on a vertical surface in a porous medium. In addition, Roslinda et al. (2004) obtained first-order perturbation approximation of the solution of the unsteady boundary layer flow in the region of the stagnation point on a stretching sheet using the perturbation series approach.

The limitation of the perturbation series approach used by Seshadri et al. (2002); Nazar et al. (2004a,b) and Roslinda et al. (2004) is that the perturbation series differential equations, despite being linear, cannot be solved exactly beyond the first term or second term. This observation was highlighted by Liao (2006a) who noted that the difficulty in obtaining higher order solutions was due to the appearance of a combination of error function terms and exponential function term in the first solutions. In the work of Seshadri et al. (2002); Nazar et al. (2004a,b) and Roslinda et al.

(2004), only the first order solutions were presented. It was pointed out by Liao (2006a,b) that the perturbation results were only valid for a minimal frame of time.

An analytical approach was reported by Liao (2006a) as an alternative approach to overcome some of the limitations of the perturbation method. The approach is based on the homotopy analysis method (HAM) and gives results which are uniformly valid for all time. Ever since, many researchers have utilized the method in solving unsteady flow problems. These includes Liao (2006b), Xu et al. (2006, 2007), Cheng et al. (2005), Xu and Liao (2005), Ali and Mehmood (2008), Mehmood et al. (2008), Takhar et al. (2008) Sajid et al. (2008, 2009), Kumari and Nath (2009, 2010), Hayat et al. (2010), Nadeem et al. (2010). According to Liao (2006a), one major advantage of the homotopy analysis method (HAM) over the standard perturbation method for the solution of unsteady boundary layer flow problems is that the (HAM) provides flexibility in the choice of initial approximation and linear operator which can be chosen carefully so that the higher order approximation can be integrated analytically. This HAM advantage contradicts the conclusion earlier drawn by researchers about the perturbation methods that analytical solution cannot be obtained beyond first order approximation for higher order perturbation equations in unsteady flow problems. In the application of the HAM technique, the nonlinear PDEs modeling unsteady flow problems were reduced to an infinite number of linear ordinary differential equations which are governed by an auxiliary linear operator that can be used to control the convergence of the solution (Liao, 2006b).

The aim of this chapter is firstly, to introduce a new approach called the spectral perturbation method (SPM) for solving nonlinear PDEs. In this work, we apply for the first time, the spectral perturbation method (SPM) to solve nonlinear PDEs describing the unsteady heat and mass transfer by MHD mixed convection flow over an impulsively stretched vertical surface with chemical reaction effect. The SPM, combines the standard perturbation approach with the Chebyshev pseudo-spectral method to generate numerical solution of higher order perturbation equations describing the flow which are not possible to solve analytically. With the SPM, solutions to partial differential equations can be obtained by applying discretization only in the space direction. Applying discretization only in the space direction and integrating using the Chebyshev spectral collocation method makes the SPM computationally efficient. The Chebyshev pseudo-spectral method was employed because of its high level accuracy. Also, in using the spectral methods, only few grid points are required to yield accurate results. In addition, using the spectral method to integrate the perturbation equations, very accurate solutions that are valid for the entire time domain are obtained. In Chapter 2, the

SPM was used for the solution of boundary value problems (ODEs). Hence, in this chapter, the SPM will be extended to nonlinear partial differential equations. Another aim of this chapter is to extend the analysis of EL-Kabeir and Rashad (2012) by adding chemical reaction effects. Results generated using the spectral perturbation method (SPM) were compared and validated using the spectral relaxation method (SRM) and the two methods were found to be in excellent agreement. The spectral relaxation method (SRM) is an innovative iterative method that is useful for obtaining solutions to nonlinear equations. The SRM is based on simple decoupling and rearrangement of the governing nonlinear equations in a Gauss-Seidel manner. The resulting sequence of linear differential equations are then discretized and solved using the Chebyshev pseudo-spectral method. The SRM has been used successfully by considerable number of investigators for the solution of ODE and PDE problems, (see for instance, Motsa et al. (2012, 2013, 2014), Kameswaran et al. (2013, 2014), Motsa and Makukula (2013), Motsa (2014), Shateyi (2013), Shateyi and Marewo (2013) Shateyi and Makinde (2013), Shateyi and Prakash (2014), Makukula et al. (2014), Sibanda et al. (2014)). The results obtained showed that the proposed spectral perturbation method (SPM) can be used efficiently to solve partial differential equations by applying discretization only in the space direction.

3.2. Mathematical Formulation

Following Kumari and Nath (2010); EL-Kabeir and Rashad (2012); Chamkha and El-Kabeir (2013), the unsteady, laminar heat and mass transfer due to MHD mixed convection boundary layer flow of an electrically conducting fluid over a heated vertical linearly stretched sheet with a supporting external laminar flow in the presence of a chemical reaction was investigated. The geometry of the problem is shown in Figure 3.1. A uniform magnetic field was applied in the transverse direction y normal to the plate. It was assumed that the wall is impulsively stretched with a velocity u, which is proportional to the distance ax along the sheet surface. The sheet surface was maintained at a variable temperature $T = T_w = T_\infty + bx$ and a variable concentration $C = C_w = C_\infty + dx$. The stream was kept at a constant temperature T_∞ and a constant concentration C_∞ far from the sheet surface. Initially ($t < 0$), the temperature T_∞ and concentration C_∞ of the ambient fluid saturated porous medium are quiescent. At $t = 0$, the fluid is impulsively set in motion with velocity U and both the temperature and concentration of the sheet are suddenly increased from T_∞ toT_w ($T_w > T_\infty$) and C_∞ toC_w ($C_w > C_\infty$) and subsequently maintained at that temperature and concentration. The magnetic Reynolds number is assumed to be small so that the induced magnetic

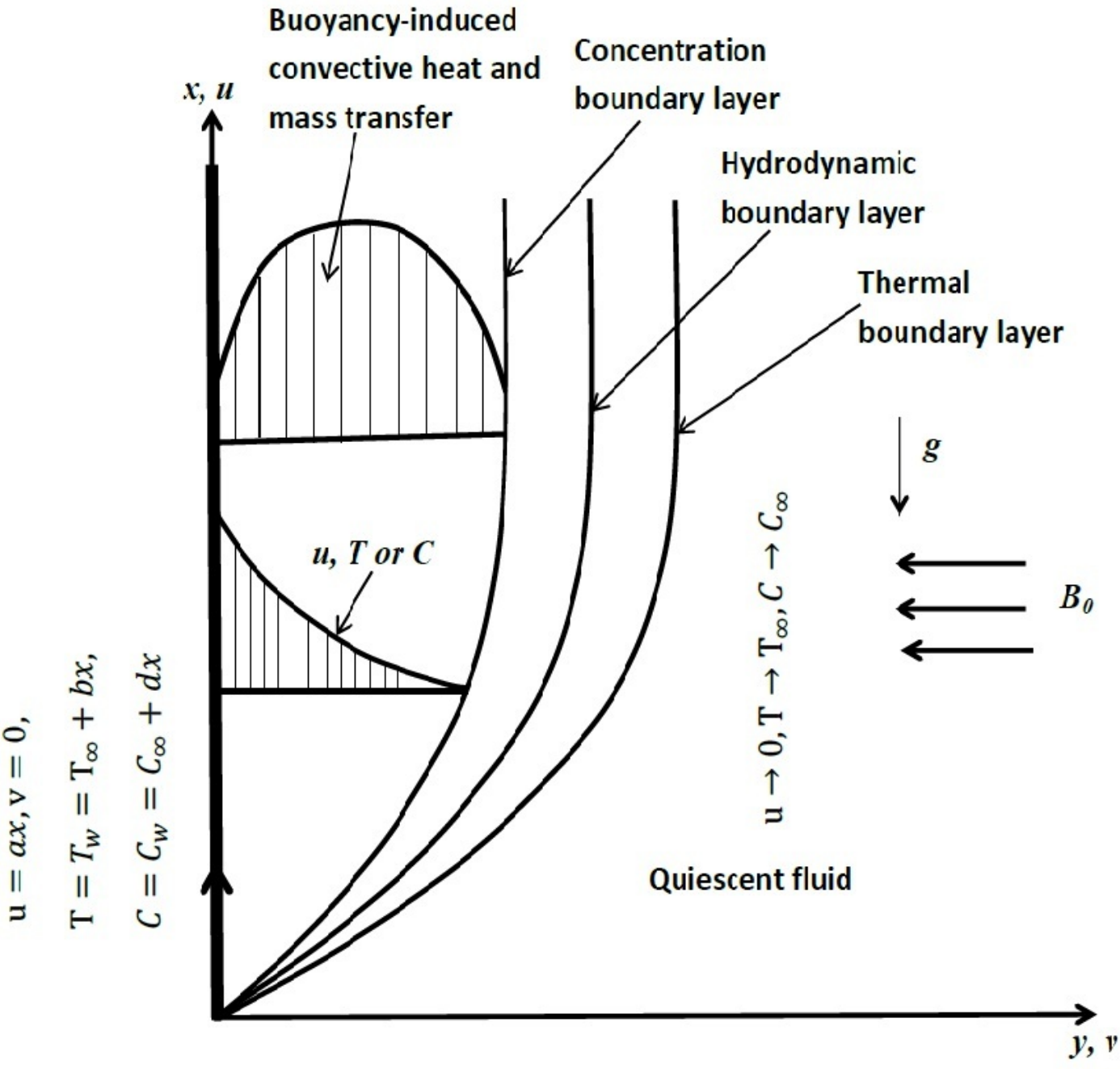

Figure 3.1: *Flow model and physical coordinate system.*

field is neglected. In addition, the hall effect and electric field are assumed to be negligible. The small magnetic Reynolds number assumption uncouples the Naiver-Stokes equation from Maxwell's equations (EL-Kabeir and Rashad, 2012; Chamkha and El-Kabeir, 2013). All physical properties are assumed constant except the density in the buoyancy force term. By invoking the boundary layer and Boussineq approximations, the simplified basic two-dimensional boundary layer equations governing the flow of an unsteady heat and mass transfer by MHD flow over an impulsively stretched vertical surface with chemical reaction effect were derived from EL-Kabeir and Rashad (2012); Chamkha and El-Kabeir (2013) and written below as follows;

$$\frac{\partial u}{\partial x} + \frac{\partial v}{\partial y} = 0, \tag{3.1}$$

$$\frac{\partial u}{\partial t} + u\frac{\partial u}{\partial x} + v\frac{\partial u}{\partial y} = \nu\frac{\partial^2 u}{\partial y^2} + g\beta_T(T - T_\infty) + g\beta_c(C - C_\infty) - \frac{\sigma B_0^2}{\rho}u, \tag{3.2}$$

$$\frac{\partial T}{\partial t} + u\frac{\partial T}{\partial x} + \nu\frac{\partial T}{\partial y} = \alpha\frac{\partial^2 T}{\partial y^2}, \tag{3.3}$$

$$\frac{\partial C}{\partial t} + u\frac{\partial C}{\partial x} + v\frac{\partial C}{\partial y} = D_m\frac{\partial^2 C}{\partial y^2} - K(C - C_\infty). \tag{3.4}$$

where t, u and v are the time, fluid tangential velocity and normal velocity components along the x and y axes respectively, T is the temperature, C is the concentration, g is the acceleration due to gravity, ρ is the fluid density, ν is the kinematic viscosity, α is the thermal diffusivity, D_m is the chemical molecular diffusivity, σ is the fluid electrical conductivity, B_0 is the magnetic induction, K is the dimensional chemical reaction parameter, β_T is the thermal expansion coefficient and β_c is the concentration coefficient.

The appropriate initial and boundary conditions for this problem were given by Hayat et al. (2010) as:

$$\begin{aligned}
&t < 0: \quad u = 0, \quad v = 0, \quad T = T_w, \quad C = C_w, \quad \forall\, x,\, y,\\
&t \geq 0 : u = ax, \quad v = 0, \quad T = T_w = T_\infty + bx, \quad C = C_w = C_\infty + dx, \quad \text{at} \quad y = 0,\\
&t \geq 0 : u \to 0, \quad T \to T_\infty, \quad C \to C_\infty \quad \text{as} \quad y \to \infty,
\end{aligned} \tag{3.5}$$

where a, b and d are constants.

The stream function ψ was introduced and defined as given by EL-Kabeir and Rashad (2012); Chamkha and El-Kabeir (2013);

$$u = \frac{\partial \psi}{\partial y}, \quad v = -\frac{\partial \psi}{\partial x}. \tag{3.6}$$

Further, it is convenient to choose the time scale ξ so that the region of the time integration is finite. Such transformations were introduced by Williams and Rhyne (1980). The transformations are expressed as:

$$\xi = 1 - \exp(-\tau), \quad \tau = at, \tag{3.7}$$

with b, a positive constant and t is the time variable. The Williams and Rhyne (1980) transformations (3.7) are used to convert from the infinite (original) time scale $0 \leq \tau < \infty$ to the finite scale $0 \leq \xi \leq 1$ so that the interval of integration is collapsed from an infinite domain to a finite domain.

The similarity variables given by Chamkha and El-Kabeir (2013) was used and written below as;

$$\begin{aligned} &\eta = \sqrt{\frac{a}{\nu \xi}} y, \quad \psi = \sqrt{a \nu \xi}\, x f(\xi, \eta), \\ &\theta(\xi, \eta) = \frac{T - T_\infty}{T_w - T_\infty}, \quad \phi(\xi, \eta) = \frac{C - C_\infty}{C_w - C_\infty}. \end{aligned} \tag{3.8}$$

Equation (3.1) is identically satisfied and the governing equations (3.2) - (3.4) along with the boundary conditions (3.5) can be presented in the form

$$f''' + \frac{\eta}{2}(1-\xi) f'' + \xi \left[f f'' - (f')^2 - Ha f' + \lambda(\theta + N\phi) \right] = \xi(1-\xi) \frac{\partial f'}{\partial \xi}, \tag{3.9}$$

$$\frac{1}{Pr} \theta'' + \frac{1}{2} \eta (1-\xi) \theta' + \xi \left[f\theta' - f'\theta \right] = \xi(1-\xi) \frac{\partial \theta}{\partial \xi}, \tag{3.10}$$

$$\frac{1}{Sc} \phi'' + \frac{1}{2} \eta (1-\xi) \phi' + \xi \left[f\phi' - f'\phi - \gamma\phi \right] = \xi(1-\xi) \frac{\partial \phi}{\partial \xi}, \tag{3.11}$$

subject to the boundary conditions;

$$f(\xi, 0) = 0, \quad f'(\xi, 0) = 1, \quad f'(\xi, \infty) = 0, \tag{3.12}$$

$$\theta(\xi, 0) = 1, \quad \theta(\xi, \infty) = 0, \tag{3.13}$$

$$\phi(\xi, 0) = 1, \quad \phi(\xi, \infty) = 0. \tag{3.14}$$

In the above equations, the prime denotes the derivative with respect to η and the parameters are

defined as;

$$Ha = \frac{\sigma B_0^2}{\rho a}, \quad N = \frac{\beta_c(C_w - C_\infty)}{\beta_T(T_w - T_\infty)}, \quad \lambda = \frac{\left(g\beta(T_w - T_\infty)x/\nu^2\right)}{(U_e/\nu)^2} = \frac{Gr_x}{Re_x^2},$$
$$Pr = \frac{\nu}{\alpha}, \quad Sc = \frac{\nu}{D}, \quad \gamma = \frac{K}{a}, \tag{3.15}$$

where Ha is the magnetic number (square of Hartman number), N is concentration to the thermal buoyancy ratio, λ is mixed convection parameter, γ is dimensionless chemical reaction parameter, Pr is Prandtl number, and Sc is Schmidt number. It can be noted that $\lambda > 0$ equals to the aiding flow case and $\lambda < 0$ equals to the opposing flow case. Also, Gr_x, Re_x are the local Grashof number and the local Reynold number, respectively.

The expressions for the skin friction coefficients C_{fx}, local Nusselt number Nu_x and local Sherwood number Sh_x are given in EL-Kabeir and Rashad (2012); Chamkha and El-Kabeir (2013) as;

$$C_{fx} = \frac{-\mu(\partial u/\partial y)_{y=0}}{\rho U_e^2} = -Re_x^{-1/2}\xi^{-1/2}f''(\xi, 0), \tag{3.16}$$
$$Nu_x = \frac{-x(\partial T/\partial y)_{y=0}}{T_w - T_\infty} = -Re_x^{-1/2}\xi^{-1/2}\theta'(\xi, 0), \tag{3.17}$$
$$Sh_x = \frac{-x(\partial C/\partial y)_{y=0}}{C_w - C_\infty} = -Re_x^{-1/2}\xi^{-1/2}\phi'(\xi, 0). \tag{3.18}$$

For the initial unsteady state flow, when $\xi = 0$, corresponding to $\tau = 0$, equations (3.9 - 3.11) becomes:

$$f''' + \frac{\eta}{2}f'' = 0, \tag{3.19}$$
$$\frac{1}{Pr}\theta'' + \frac{\eta}{2}\theta' = 0, \tag{3.20}$$
$$\frac{1}{Sc}\phi'' + \frac{\eta}{2}\phi' = 0, \tag{3.21}$$

subject to the boundary conditions,

$$f(0) = 0,\ f'(0) = 1,\ f'(\infty) = 0,\ \theta(0) = 1,\ \theta(\infty) = 0,\ \phi(0) = 1,\ \phi(\infty) = 0. \tag{3.22}$$

Equations (3.19 - 3.21) alongside the boundary conditions (3.22) admit closed form analytical solu-

tions given by Hayat et al. (2010) as;

$$f(0,\eta) = \eta \operatorname{erfc}\left(\frac{\eta}{2}\right) + \frac{2}{\sqrt{\pi}}\left[1 - \exp\left(-\frac{\eta^2}{4}\right)\right], \tag{3.23}$$

$$\theta(0,\eta) = \operatorname{erfc}\left(\frac{\sqrt{Pr}\eta}{2}\right), \tag{3.24}$$

$$\phi(0,\eta) = \operatorname{erfc}\left(\frac{\sqrt{Sc}\eta}{2}\right), \tag{3.25}$$

where the complementary error function erfc, is defined as

$$\operatorname{erfc}(\eta) = \frac{2}{\sqrt{\pi}}\int_{\eta}^{\infty} \exp(-t^2)\mathrm{d}t. \tag{3.26}$$

3.3. Method of solution

In this section, the spectral perturbation method (SPM) was used to solve the partial differential equations (3.9 - 3.11) subject to the boundary conditions (3.12 - 3.14). Perturbation methods in general construct a solution for a problem by generating asymptotic expansions of the perturbation parameter (Liao, 2003a). In perturbation methods, higher order perturbation approximation are difficult to get which may result in less accurate results if only one or two series solutions are used. For instance, the perturbation approach utilized by Seshadri et al. (2002) and Nazar et al. (2004a) yields only the first order approximate solutions. Below, the spectral perturbation method is used to solve equations (3.9 - 3.11).

3.3.1 Spectral Perturbation Method (SPM)

In the spectral perturbation method (SPM), series equations are generated using the standard perturbation approach and then solve the series equations integrated in the space direction η numerically using the Chebyshev spectral collocation method. With the spectral methods, higher order perturbation equations can easily be solved. Following Seshadri et al. (2002); Nazar et al. (2004a); Liao (2006a), a series expansion was constructed to approximate $f(\xi,\eta)$, $\theta(\xi,\eta)$ and $\phi(\xi,\eta)$ solution by

regarding ξ as a small parameter and looking for a perturbation approximation in the form

$$f(\xi,\eta)=\sum_{k=0}^{+\infty}\xi^k f_k(\eta), \tag{3.27}$$

$$\theta(\xi,\eta)=\sum_{k=0}^{+\infty}\xi^k \theta_k(\eta), \tag{3.28}$$

$$\phi(\xi,\eta)=\sum_{k=0}^{+\infty}\xi^k \phi_k(\eta). \tag{3.29}$$

Substituting (3.27 - 3.29) in equations (3.9 - 3.11)and boundary conditions (3.12 - 3.14) and balancing terms of equal power of ξ, we obtained,

$$f_0'''+\frac{\eta}{2}f_0''=0,\quad f_0(0)=0,\quad f_0'(0)=1,\quad f_0'(\infty)=0, \tag{3.30}$$

$$\theta_0''+Pr\frac{\eta}{2}\theta_0'=0,\quad \theta_0(0)=1,\quad \theta_0(\infty)=0, \tag{3.31}$$

$$\phi_0''+Sc\frac{\eta}{2}\phi_0'=0,\quad \phi_0(0)=1,\quad \phi_0(\infty)=0 \tag{3.32}$$

$$f_k'''+\frac{\eta}{2}f_k''-kf_k'=\frac{\eta}{2}f_{k-1}''-(k-1)f_{k-1}'+Haf_{k-1}'-\lambda\theta_{k-1}-\lambda N\phi_{k-1}$$
$$+\sum_{i=0}^{k-1}\left[f_{k-1-i}'f_i'-f_{k-1-i}f_i''\right] \tag{3.33}$$

$$f_k(0)=0,\quad f_k'(0)=0,\quad f_k'(\infty)=0,\quad k\geq 1. \tag{3.34}$$

$$\theta_k''+\frac{\eta}{2}Pr\theta_k'-Prk\theta_k=\frac{\eta}{2}Pr\theta_{k-1}'-Pr(k-1)\theta_{k-1}$$
$$-\sum_{i=0}^{k-1}\mathrm{Pr}\left[f_{k-1-i}\theta_i'-f_{k-1-i}'\theta_i\right] \tag{3.35}$$

$$\theta_k(0)=0,\quad \theta_k(\infty)=0,\quad k\geq 1. \tag{3.36}$$

$$\phi_k''+\frac{\eta}{2}Sc\phi_k'-Sck\phi_k=\frac{\eta}{2}Sc\phi_{k-1}'-Sc(k-1)\phi_{k-1}+\gamma Sc\phi_{k-1}$$
$$-\sum_{i=0}^{k-1}Sc\left[f_{k-1-i}\phi_i'-f_{k-1-i}'\phi_i\right] \tag{3.37}$$

$$\phi_k(0)=0,\quad \phi_k(\infty)=0,\quad k\geq 1. \tag{3.38}$$

The Chebyshev spectral collocation method was used to integrate (3.33 - 3.38). The spectral method is based on the Chebyshev polynomials defined on the domain $[-1,1]$ by

$$T_l(x)=\cos\left[l\cos^{-1}(x)\right]. \tag{3.39}$$

Before the spectral method was implemented, the physical domain on which the governing equation was defined was first transformed to the region $[-1, 1]$ where the spectral method can then be applied. This can be done with the aid of the domain truncation procedure, the problem was solved in the interval $[0, L]$ in place of $[0, \infty)$, where L is the scaling parameter taken to be large. This leads to the transformation

$$x = \frac{2\eta}{L} - 1, \quad -1 \leq x \leq 1 \tag{3.40}$$

The Gauss-lobatto collocation points (Hussaini and Zang, 1987; Don and Solomonoff, 1995; Trefethen, 2000) were used to define the Chebyshev nodes $[-1, 1]$ described as

$$xj = \cos\left(\frac{\pi j}{N_x}\right), \quad -1 \leq x \leq 1, \quad j = 0, 1, 2..., N_x, \tag{3.41}$$

where $(N_x + 1)$ is the total number of collocation points.

The spectral collocation method introduces a differential matrix D. The differential matrix D is used to approximate the derivatives of the unknown variables $f_k(\eta), \theta_k(\eta), \phi_k(\eta)$ at the collocation points can be defined as;

$$\left.\frac{df_k}{d\eta}\right|_{\eta=\eta j} = \sum_{l=0}^{N_x} \mathbf{D}_{jl} f_k(x_l) = \mathbf{D}F_k, \quad j = 0, 1, ..., N_x, \tag{3.42}$$

$$\left.\frac{d\theta_k}{d\eta}\right|_{\eta=\eta j} = \sum_{l=0}^{N_x} \mathbf{D}_{jl} \theta_k(x_l) = \mathbf{D}\Theta_k, \quad j = 0, 1, ..., N_x, \tag{3.43}$$

$$\left.\frac{d\phi_k}{d\eta}\right|_{\eta=\eta j} = \sum_{l=0}^{N_x} \mathbf{D}_{jl} \phi_k(x_l) = \mathbf{D}\Phi_k, \quad j = 0, 1, ..., N_x, \tag{3.44}$$

where $(N_x + 1)$ is the number of collocation points, $\mathbf{D} = 2D/L$, and

$$\mathbf{F}_k = [f_k(x_0), f_k(x_1), ..., f_k(x_{N_x})]^T, \tag{3.45}$$

$$\mathbf{\Theta}_k = [\theta_k(x_0), \theta_k(x_1), ..., \theta_k(x_{N_x})]^T, \tag{3.46}$$

$$\mathbf{\Phi}_k = [\phi_k(x_0), \phi_k(x_1), ..., \phi_k(x_{N_x})]^T, \tag{3.47}$$

is the vector function at the collocation points. The higher order derivatives are obtained as powers

of $\mathbf{D}$, that is;

$$f_k^{(p)} = \mathbf{D}^p \mathbf{F}_k, \tag{3.48}$$

$$\theta_k^{(p)} = \mathbf{D}^p \mathbf{\Theta}_k, \tag{3.49}$$

$$\phi_k^{(p)} = \mathbf{D}^p \mathbf{\Phi}_k, \tag{3.50}$$

where p is the order of the derivatives. The matrix $\mathbf{D}$ is of size $(N_x + 1) \times (N_x + 1)$ and its entries have been defined earlier in Chapter 2.

Substituting (3.42 - 3.50) in (3.33 - 3.37) gives

$$\mathbf{A}_{1,k-1}\mathbf{F}_k = \mathbf{B}_{1,k-1}, \tag{3.51}$$

$$\mathbf{A}_{2,k-1}\mathbf{\Theta}_k = \mathbf{B}_{2,k-1}, \tag{3.52}$$

$$\mathbf{A}_{3,k-1}\mathbf{\Phi}_k = \mathbf{B}_{3,k-1}, \tag{3.53}$$

subject to the following boundary conditions

$$\sum_{l=0}^{N_x} \mathbf{D}_{0l} f_k(x_l) = 0, \quad \sum_{l=0}^{N_x} \mathbf{D}_{N_x l} f_k(x_l) = 0, \quad f_k(x_{N_x}) = 0, \tag{3.54}$$

$$\theta_k(x_{N_x}) = 0, \quad \theta_k(x_0) = 0, \tag{3.55}$$

$$\phi_k(x_{N_x}) = 0, \quad \phi_k(x_0) = 0, \tag{3.56}$$

where $\mathbf{A}_{1,k-1}, \mathbf{A}_{2,k-1}, \mathbf{A}_{3,k-1}, \mathbf{B}_{1,k-1}, \mathbf{B}_{2,k-1}$, and $\mathbf{B}_{3,k-1}$ are defined as;

$$\mathbf{A}_{1,k-1} = \mathbf{D}^3 + \text{diag}\left(\frac{\boldsymbol{\eta}}{\mathbf{2}}\right)\mathbf{D}^2 - k\mathbf{D}, \tag{3.57}$$

$$\mathbf{A}_{2,k-1} = \mathbf{D}^2 + \text{diag}\left(\frac{\boldsymbol{\eta}}{\mathbf{2}}Pr\right)\mathbf{D} - k\,Pr\mathbf{I}, \tag{3.58}$$

$$\mathbf{A}_{3,k-1} = \mathbf{D}^2 + \text{diag}\left(\frac{\boldsymbol{\eta}}{\mathbf{2}}Sc\right)\mathbf{D} - k\,Sc\mathbf{I}, \tag{3.59}$$

$$\mathbf{B}_{1,k-1} = \frac{\boldsymbol{\eta}}{\mathbf{2}}\left(\mathbf{D}^2\mathbf{F}_{k-1}\right) - (k-1)\,\mathbf{D}\mathbf{F}_{k-1} + Ha\,(\mathbf{D}\mathbf{F}_{k-1}) - \lambda\mathbf{\Theta}_{k-1} - \lambda N\mathbf{\Phi}_{k-1} + \text{Sum}\mathbf{F}, \tag{3.60}$$

$$\mathbf{B}_{2,k-1} = \frac{\boldsymbol{\eta}}{\mathbf{2}}Pr\,(\mathbf{D}\mathbf{\Theta}_{k-1}) - Pr\,(k-1)\,\mathbf{\Theta}_{k-1} - \text{Sum}\mathbf{\Theta}, \tag{3.61}$$

$$\mathbf{B}_{3,k-1} = \frac{\boldsymbol{\eta}}{\mathbf{2}}Sc\,(\mathbf{D}\mathbf{\Phi}_{k-1}) - Sc\,(k-1)\,\mathbf{\Phi}_{k-1} + \gamma Sc\mathbf{\Phi}_{k-1} - \text{Sum}\mathbf{\Phi}, \tag{3.62}$$

where $\boldsymbol{\eta} = [\eta_0, \eta_1, \cdots \eta_{N_x},]$,Sum$\mathbf{F}$, Sum$\boldsymbol{\Theta}$ and Sum$\boldsymbol{\Phi}$ are defined as;

$$\begin{aligned}
\text{Sum}\mathbf{F} &= \sum_{i=0}^{k-1} \left[\left(\mathbf{DF}_{k-1-i}\right) \left(\mathbf{DF}_i\right) - \mathbf{F}_{k-1-i} \left(\mathbf{D}^2\mathbf{F}_i\right) \right], \\
\text{Sum}\boldsymbol{\Theta} &= Pr \sum_{i=0}^{k-1} \left[\left(\mathbf{DF}_{k-1-i}\right) \boldsymbol{\Theta}_i - \mathbf{F}_{k-1-i} \left(\mathbf{D}\boldsymbol{\Theta}_i\right) \right], \\
\text{Sum}\boldsymbol{\Phi} &= Sc \sum_{i=0}^{k-1} \left[\left(\mathbf{DF}_{k-1-i}\right) \boldsymbol{\Phi}_i - \mathbf{F}_{k-1-i} \left(\mathbf{D}\boldsymbol{\Phi}_i\right) \right],
\end{aligned}$$

with $\mathbf{I}$ representing an $(N_x+1)\times(N_x+1)$ identity matrix and diag() is a diagonal matrix obtained from the vector $(x_0, x_1, ..., x_{N_x},)$. The boundary conditions (3.54) are imposed on the first , $N_x th$ row (second from the last row) and (N_x+1)st row (last row) rows and first and last columns of (3.51) to obtain

$$\left[\begin{array}{c|ccc|c}
\mathbf{D}_{0,0} & \mathbf{D}_{0,1} & \cdots \quad \cdots & \mathbf{D}_{0,N_x-1} & \mathbf{D}_{0,N_x} \\
\hline
 & & \mathbf{A}_{1,k-1} & & \\
\hline
\mathbf{D}_{N_x,0} & \mathbf{D}_{N_x,1} & \cdots \quad \cdots & \mathbf{D}_{N_x,N_x-1} & \mathbf{D}_{N_x,N_x} \\
\hline
0 & 0 & \cdots \quad \cdots & 0 & 1
\end{array}\right]
\left[\begin{array}{c}
f_k(x_0) \\
\hline
f_k(x_1) \\
\vdots \\
\vdots \\
f_k(x_{N_x-1}) \\
\hline
f_k(x_{N_x})
\end{array}\right]
=
\left[\begin{array}{c}
0 \\
\hline
B_{1,k-1}(x_1) \\
\vdots \\
B_{1,k-1}(x_{N_x-1}) \\
\hline
0 \\
\hline
0
\end{array}\right], \tag{3.63}$$

while the boundary conditions (3.55) and (3.56) are imposed the first and last rows and columns of equations (3.52) and (3.53) respectively to obtain

$$\left[\begin{array}{c|ccc|c}
1 & 0 & \cdots \quad \cdots & 0 & 0 \\
\hline
 & & \mathbf{A}_{2,k-1} & & \\
\hline
0 & 0 & \cdots \quad \cdots & 0 & 1
\end{array}\right]
\left[\begin{array}{c}
\theta_k(x_0) \\
\hline
\theta_k(x_1) \\
\vdots \\
\vdots \\
\hline
\theta_k(x_{N_x})
\end{array}\right]
=
\left[\begin{array}{c}
0 \\
\hline
B_{2,k-1}(x_1) \\
\vdots \\
B_{2,k-1}(x_{N_x-1}) \\
\hline
0
\end{array}\right], \tag{3.64}$$

and

$$\left[\begin{array}{c|ccc|c} 1 & 0 & \cdots & 0 & 0 \\ \hline & & & & \\ & & \mathbf{A}_{3,k-1} & & \\ & & & & \\ \hline 0 & 0 & \cdots & 0 & 1 \end{array}\right] \left[\begin{array}{c} \phi_k(x_0) \\ \hline \phi_k(x_1) \\ \vdots \\ \vdots \\ \hline \phi_k(x_{N_x}) \end{array}\right] = \left[\begin{array}{c} 0 \\ \hline B_{3,k-1}(x_1) \\ \vdots \\ B_{3,k-1}(x_{N_x-1}) \\ \hline 0 \end{array}\right]. \tag{3.65}$$

Hence, starting from a known F_0, Θ_0, Φ_0, the solutions F_k, Θ_k, Φ_k, $k \geq 1$ can be obtained from equations (3.63 - 3.65) as;

$$\mathbf{F}_k = \mathbf{A}_{1,k-1}^{-1}\mathbf{B}_{1,k-1}, \tag{3.66}$$

$$\mathbf{\Theta}_k = \mathbf{A}_{2,k-1}^{-1}\mathbf{B}_{3,k-1}, \tag{3.67}$$

$$\mathbf{\Phi}_k = \mathbf{A}_{3,k-1}^{-1}\mathbf{B}_{4,k-1}. \tag{3.68}$$

3.3.2 Spectral Relaxation Technique (SRM)

In this section the development of the spectral relaxation method (SRM) to obtain solutions of the governing partial differential equations (3.9 - 3.11) is discussed. To start the SRM algorithm, it is convenient to reduce the order of equation (3.9) from three to two. To this end, we first set $f' = u$, so that equation (3.9) becomes

$$u'' + (1-\xi)\left(\frac{\eta}{2}u' - \xi\frac{\partial u}{\partial \xi}\right) + \xi\left[fu' - u^2 - Hau + \lambda\theta + \lambda N\phi\right] = 0. \tag{3.69}$$

The spectral relaxation method (SRM) (Motsa et al., 2012, 2013, 2014; Kameswaran et al., 2013, 2014; Motsa and Makukula, 2013; Motsa, 2014; Shateyi, 2013; Shateyi and Marewo, 2013; Shateyi and Makinde, 2013; Shateyi and Prakash, 2014; Makukula et al., 2014; Sibanda et al., 2014) uses the Gauss-Seidel concept to decouple the governing nonlinear systems of equations (3.9 - 3.11). From the decoupled equations, an iteration scheme was developed by evaluating linear terms in the current iteration level denoted by $(r+1)$ and nonlinear terms in the previous iteration level denoted by (r). Implementing the SRM on the resulting system of nonlinear partial differential equations yields the

following linear partial differential equations;

$$u''_{r+1} + a_{1,r}u'_{r+1} + a_{2,r}u_{r+1} + a_{3,r} = \xi(1-\xi)\frac{\partial u_{r+1}}{\partial \xi}, \tag{3.70}$$

$$f'_{r+1} = u_{r+1}, \tag{3.71}$$

$$\theta''_{r+1} + b_{1,r}\theta'_{r+1} + b_{2,r}\theta_{r+1} = \xi(1-\xi)\frac{\partial \theta_{r+1}}{\partial \xi}, \tag{3.72}$$

$$\phi''_{r+1} + c_{1,r}\phi'_{r+1} + c_{2,r}\phi_{r+1} = \xi(1-\xi)\frac{\partial \phi_{r+1}}{\partial \xi}, \tag{3.73}$$

$$u_{r+1}(0,\xi) = \theta_{r+1}(0,\xi) = \phi_{r+1}(0,\xi) = 1,\ f_{r+1}(0,\xi) = 0,$$

$$u_{r+1}(\infty,\xi) = \theta_{r+1}(\infty,\xi) = \phi_{r+1}(\infty,\xi) = 0, \tag{3.74}$$

where the coefficient parameters $a_{1,r}, a_{2,r}, a_{3,r}, b_{1,r}, b_{2,r}, c_{1,r}$ and $c_{2,r}$ are defined as;

$$a_{1,r} = \left(\frac{1}{2}\eta(1-\xi) + \xi f_r\right), \quad a_{2,r} = -\xi Ha, \quad a_{3,r} = -\xi\left(u_r^2 + \lambda(\theta_r + N\phi_r)\right),$$
$$b_{1,r} = Pr\left(\frac{1}{2}\eta(1-\xi) + \xi f_r\right), \quad b_{2,r} = -\xi Pr(u_r)$$
$$c_{1,r} = Sc\left(\frac{1}{2}\eta(1-\xi) + \xi f_r\right), \quad c_{2,r} = -\xi Sc(u_r + \gamma).$$

The initial approximations for solving equations (3.70 - 3.74) were obtained as the solutions at $\xi = 0$. Hence, $f_0(\xi,\eta)$, $\theta_0(\xi,\eta)$, $\phi_0(\xi,\eta)$ were given in equations (3.23 - 3.25) and $u_0(\xi,\eta)$ is given as;

$$u_0(\xi,\eta) = \text{erfc}\left(\frac{\eta}{2}\right). \tag{3.75}$$

Equations (3.70 - 3.74) can be solved iteratively for the unknown functions starting from the initial approximations given in (3.22 - 3.25) and (3.75). The iteration schemes (3.70), (3.72) and (3.73) were solved iteratively for $u_{r+1}(\xi,\eta)$, $\theta_{r+1}(\xi,\eta)$ and $\phi_{r+1}(\xi,\eta)$ when $r = 0, 1, 2, \cdots$ The solution for u_{r+1} was utilized in (3.71) which was, in turn, solved for f_{r+1}. To solve equations (3.70 - 3.73), the equations are discretized using the Chebyshev spectral collocation method in the $\eta-$direction and the implicit finite difference method in the $\xi-$direction. The underlying idea behind the Chebyshev spectral collocation method has been explained above. The finite difference scheme was used with centering about a mid-point between ξ^{n+1} and ξ^n. The mid-point is defined as $\xi^{n+\frac{1}{2}} = \left(\xi^{n+1} + \xi^n\right)/2$. Thus, using the centering about $\xi^{n+\frac{1}{2}}$ to any function, say $u(\xi,\eta)$ and its associated derivative we

obtained,

$$u\left(\eta_j, \xi^{n+\frac{1}{2}}\right) = u_j^{n+\frac{1}{2}} = \frac{u_j^{n+1} + u_j^n}{2}, \quad \left(\frac{\partial u}{\partial \xi}\right)^{n+\frac{1}{2}} = \frac{u_j^{n+1} - u_j^n}{\Delta \xi}. \tag{3.76}$$

The spectral method was first applied to equations (3.70 - 3.73), before applying the finite differences to obtain

$$\left[\mathbf{D}^2 + \mathbf{a}_{1,r}\mathbf{D} + \mathbf{a}_{2,r}\right] U_{r+1} + \mathbf{a}_{3,r} = \xi\left(1-\xi\right)\frac{dU_{r+1}}{d\xi}, \tag{3.77}$$

$$u_{r+1}\left(x_0, \xi\right) = 0, \quad u_{r+1}\left(x_{N_x}, \xi\right) = 1,$$

$$\mathbf{D}F_{r+1} = U_{r+1}, \quad f_{r+1}\left(x_{N_x}, \xi\right) = 0, \tag{3.78}$$

$$\left[\mathbf{D}^2 + \mathbf{b}_{1,r}\mathbf{D} + \ \mathbf{b}_{2,r}\right] \Theta_{r+1} = \xi\left(1-\xi\right)\frac{d\Theta_{r+1}}{d\xi}, \tag{3.79}$$

$$\theta_{r+1}\left(x_0, \xi\right) = 0, \quad \theta_{r+1}\left(x_{N_x}, \xi\right) = 1$$

$$\left[\mathbf{D}^2 + \mathbf{c}_{1,r}\mathbf{D} + \mathbf{c}_{2,r}\right] \Phi_{r+1} = \xi\left(1-\xi\right)\frac{d\Phi_{r+1}}{d\xi}, \tag{3.80}$$

$$\phi_{r+1}\left(x_0, \xi\right) = 0, \quad \phi_{r+1}\left(x_{N_x}, \xi\right) = 1,$$

where

$$U_{r+1} = \begin{bmatrix} u_{r+1}(x_0,\xi) \\ u_{r+1}(x_1,\xi) \\ \vdots \\ u_{r+1}(x_{N_x-1},\xi) \\ u_{r+1}(x_{N_x},\xi) \end{bmatrix}, \; F_{r+1} = \begin{bmatrix} f_{r+1}(x_0,\xi) \\ f_{r+1}(x_1,\xi) \\ \vdots \\ f_{r+1}(x_{N_x-1},\xi) \\ f_{r+1}(x_{N_x},\xi) \end{bmatrix}, \; \mathbf{a}_{3,r} = \begin{bmatrix} a_{3,r}(x_0,\xi) \\ a_{3,r}(x_1,\xi) \\ \vdots \\ a_{3,r}(x_{N_x-1},\xi) \\ a_{3,r}(x_{N_x},\xi) \end{bmatrix}, \tag{3.81}$$

$$\mathbf{a}_{1,r} = \begin{bmatrix} a_{1,r}(x_0,\xi) & & & & \\ & a_{1,r}(x_1,\xi) & & & \\ & & \ddots & & \\ & & & \ddots & \\ & & & & a_{1,r}(x_{N_x},\xi) \end{bmatrix}, \tag{3.82}$$

$$\mathbf{a}_{2,r} = \begin{bmatrix} a_{2,r}(x_0,\xi) & & & & \\ & a_{2,r}(x_1,\xi) & & & \\ & & \ddots & & \\ & & & \ddots & \\ & & & & a_{2,r}(x_{N_x},\xi) \end{bmatrix}, \tag{3.83}$$

$$\Theta_{r+1} = \begin{bmatrix} \theta_{r+1}(x_0,\xi) \\ \theta_{r+1}(x_1,\xi) \\ \vdots \\ \theta_{r+1}(x_{N_x-1},\xi) \\ \theta_{r+1}(x_{N_x},\xi) \end{bmatrix}, \ \mathbf{b}_{1,r} = \begin{bmatrix} b_{1,r}(x_0,\xi) & & & & \\ & b_{1,r}(x_1,\xi) & & & \\ & & \ddots & & \\ & & & \ddots & \\ & & & & b_{1,r}(x_{N_x},\xi) \end{bmatrix}, \tag{3.84}$$

$$\mathbf{b}_{2,r} = \begin{bmatrix} b_{2,r}(x_0,\xi) & & & & \\ & b_{2,r}(x_1,\xi) & & & \\ & & \ddots & & \\ & & & \ddots & \\ & & & & b_{2,r}(x_{N_x},\xi) \end{bmatrix}, \tag{3.85}$$

$$\Phi_{r+1} = \begin{bmatrix} \phi_{r+1}(x_0,\xi) \\ \phi_{r+1}(x_1,\xi) \\ \vdots \\ \phi_{r+1}(x_{N_x-1},\xi) \\ \phi_{r+1}(x_{N_x},\xi) \end{bmatrix}, \ \mathbf{c}_{1,r} = \begin{bmatrix} c_{1,r}(x_0,\xi) & & & & \\ & c_{1,r}(x_1,\xi) & & & \\ & & \ddots & & \\ & & & \ddots & \\ & & & & c_{1,r}(x_{N_x},\xi) \end{bmatrix}, \tag{3.86}$$

$$\mathbf{c}_{2,r} = \begin{bmatrix} c_{2,r}(x_0,\xi) & & & & \\ & c_{2,r}(x_1,\xi) & & & \\ & & \ddots & & \\ & & & \ddots & \\ & & & & c_{2,r}(x_{N_x},\xi) \end{bmatrix}. \tag{3.87}$$

Next, the finite difference scheme was applied on (3.77 - 3.80), in the ξ-direction with centering about

the mid-point $\xi^{n+\frac{1}{2}}$ to obtain the following systems of decoupled equations

$$\mathbf{A}_1\mathbf{U}_{r+1}^{n+1} = \mathbf{B}_1\mathbf{U}_{r+1}^{n} + \mathbf{K}_1, \tag{3.88}$$

$$\mathbf{A}_2\mathbf{\Theta}_{r+1}^{n+1} = \mathbf{B}_2\mathbf{\Theta}_{r+1}^{n} + \mathbf{K}_2, \tag{3.89}$$

$$\mathbf{A}_3\mathbf{\Phi}_{r+1}^{n+1} = \mathbf{B}_3\mathbf{\Phi}_{r+1}^{n} + \mathbf{K}_3, \tag{3.90}$$

$$\mathbf{DF}_{r+1}^{n+1} = \mathbf{U}_{r+1}^{n+1}, \tag{3.91}$$

subject to the following initial and boundary conditions

$$u_{r+1}(x_{N_x}, \xi^n) = \theta_{r+1}(x_{N_x}, \xi^n) = \phi_{r+1}(x_{N_x}, \xi^n) = 1, \tag{3.92}$$

$$u_{r+1}(x_0, \xi^n) = \theta_{r+1}(x_0, \xi^n) = \phi_{r+1}(x_0, \xi^n) = 0, \tag{3.93}$$

$$f_{r+1}(x_{N_x}, \xi^n) = 0, \quad n = 0, 1, 2, ..., \tag{3.94}$$

$$f_{r+1}\left(\eta_j, 0\right) = \eta \text{erfc}\left(\frac{\eta_j}{2}\right) + \frac{2}{\sqrt{\pi}}\left[1 - \exp\left(-\frac{\eta_j^2}{4}\right)\right], \tag{3.95}$$

$$u_{r+1}\left(\eta_j, 0\right) = \text{erfc}\left(\frac{\eta_j}{2}\right), \tag{3.96}$$

$$\theta_{r+1}\left(\eta_j, 0\right) = \text{erfc}\left(\frac{\sqrt{Pr}\eta_j}{2}\right), \tag{3.97}$$

$$\phi_{r+1}\left(\eta_j, 0\right) = \text{erfc}\left(\frac{\sqrt{Sc}\eta_j}{2}\right), \quad j = 0, 1, 2, \cdots, N_x. \tag{3.98}$$

The matrices above are defined as follows;

$$\mathbf{A}_1 = \frac{1}{2}\left(\mathbf{D}^2 + \mathbf{a}_{1,r}^{n+\frac{1}{2}}\mathbf{D} + \mathbf{a}_{2,r}\right) - \frac{\xi^{n+\frac{1}{2}}\left(1-\xi^{n+\frac{1}{2}}\right)}{\Delta\xi}\mathbf{I}, \tag{3.99}$$

$$\mathbf{A}_2 = \frac{1}{2}\left(\mathbf{D}^2 + \mathbf{b}_{1,r}^{n+\frac{1}{2}}\mathbf{D} + \mathbf{b}_{2,r}\right) - \frac{Pr\xi^{n+\frac{1}{2}}\left(1-\xi^{n+\frac{1}{2}}\right)}{\Delta\xi}\mathbf{I}, \tag{3.100}$$

$$\mathbf{A}_3 = \frac{1}{2}\left(\mathbf{D}^2 + \mathbf{c}_{1,r}^{n+\frac{1}{2}}\mathbf{D} + \mathbf{c}_{2,r}\right) - \frac{Sc\xi^{n+\frac{1}{2}}\left(1-\xi^{n+\frac{1}{2}}\right)}{\Delta\xi}\mathbf{I}, \tag{3.101}$$

$$\mathbf{B}_1 = -\frac{1}{2}\left(\mathbf{D}^2 + \mathbf{a}_{1,r}^{n+\frac{1}{2}}\mathbf{D} + \mathbf{a}_{2,r}\right) - \frac{\xi^{n+\frac{1}{2}}\left(1-\xi^{n+\frac{1}{2}}\right)}{\Delta\xi}\mathbf{I}, \tag{3.102}$$

$$\mathbf{B}_2 = -\frac{1}{2}\left(\mathbf{D}^2 + \mathbf{b}_{1,r}^{n+\frac{1}{2}}\mathbf{D} + \mathbf{b}_{2,r}\right) - \frac{Pr\xi^{n+\frac{1}{2}}\left(1-\xi^{n+\frac{1}{2}}\right)}{\Delta\xi}\mathbf{I}, \tag{3.103}$$

$$\mathbf{B}_3 = -\frac{1}{2}\left(\mathbf{D}^2 + \mathbf{c}_{1,r}^{n+\frac{1}{2}}\mathbf{D} + \mathbf{c}_{2,r}\right) - \frac{Sc\xi^{n+\frac{1}{2}}\left(1-\xi^{n+\frac{1}{2}}\right)}{\Delta\xi}\mathbf{I}, \tag{3.104}$$

$$\mathbf{K}_1 = -\mathbf{a}_{3,r}^{n+\frac{1}{2}}, \tag{3.105}$$

$$\mathbf{K}_2 = \mathbf{O}, \tag{3.106}$$

$$\mathbf{K}_3 = \mathbf{O}, \tag{3.107}$$

where $\mathbf{I}$ is an $(N_x+1)\times(N_x+1)$, U, F, Θ, and Φ are the vectors of the functions u, f, θ, and ϕ when evaluated at the grid points and $\mathbf{O}$ is a vector of zeros of size $(N_x+1)\times 1$. The boundary conditions (3.92 - 3.94) were imposed on the first and last rows of (3.88 - 3.91) as follows;

$$\begin{bmatrix} 1 & 0 & \cdots & 0 & 0 \\ \hline & & & & \\ & & \mathbf{A}_{1,k-1} & & \\ & & & & \\ \hline 0 & 0 & \cdots & 0 & 1 \end{bmatrix} \begin{bmatrix} u_{r+1,0}^{n+1} \\ \hline u_{r+1,1}^{n+1} \\ \vdots \\ \vdots \\ \hline u_{r+1,N_x}^{n+1} \end{bmatrix} = \begin{bmatrix} 0 & 0 & \cdots & 0 & 0 \\ \hline & & & & \\ & & \mathbf{B}_{1,k-1} & & \\ & & & & \\ \hline 0 & 0 & \cdots & 0 & 0 \end{bmatrix} \begin{bmatrix} u_{r+1,0}^{n} \\ \hline u_{r+1,1}^{n} \\ \vdots \\ \vdots \\ \hline u_{r+1,N_x}^{n} \end{bmatrix} + \begin{bmatrix} 0 \\ \hline \\ \mathbf{K}_1 \\ \\ \hline 1 \end{bmatrix}, \tag{3.108}$$

$$\left[\begin{array}{c|c|c} 1 & 0 \quad \cdots \quad 0 & 0 \\ \hline & \mathbf{A}_{2,k-1} & \\ \hline 0 & 0 \quad \cdots \quad 0 & 1 \end{array}\right]\left[\begin{array}{c} \theta^{n+1}_{r+1,0} \\ \hline \theta^{n+1}_{r+1,1} \\ \vdots \\ \vdots \\ \hline \theta^{n+1}_{r+1,N_x} \end{array}\right] = \left[\begin{array}{c|c|c} 0 & 0 \quad \cdots \quad 0 & 0 \\ \hline & \mathbf{B}_{2,k-1} & \\ \hline 0 & 0 \quad \cdots \quad 0 & 0 \end{array}\right]\left[\begin{array}{c} \theta^{n}_{r+1,0} \\ \hline \theta^{n}_{r+1,1} \\ \vdots \\ \vdots \\ \hline \theta^{n}_{r+1,N_x} \end{array}\right] + \left[\begin{array}{c} 0 \\ \hline \\ \mathbf{K}_2 \\ \\ \hline 1 \end{array}\right], \quad (3.109)$$

$$\left[\begin{array}{c|c|c} 1 & 0 \quad \cdots \quad 0 & 0 \\ \hline & \mathbf{A}_{3,k-1} & \\ \hline 0 & 0 \quad \cdots \quad 0 & 1 \end{array}\right]\left[\begin{array}{c} \phi^{n+1}_{r+1,0} \\ \hline \phi^{n+1}_{r+1,1} \\ \vdots \\ \vdots \\ \hline \phi^{n+1}_{r+1,N_x} \end{array}\right] = \left[\begin{array}{c|c|c} 0 & 0 \quad \cdots \quad 0 & 0 \\ \hline & \mathbf{B}_{3,k-1} & \\ \hline 0 & 0 \quad \cdots \quad 0 & 0 \end{array}\right]\left[\begin{array}{c} \phi^{n}_{r+1,0} \\ \hline \phi^{n}_{r+1,1} \\ \vdots \\ \vdots \\ \hline \phi^{n}_{r+1,N_x} \end{array}\right] + \left[\begin{array}{c} 0 \\ \hline \\ \mathbf{K}_3 \\ \\ \hline 1 \end{array}\right], \quad (3.110)$$

$$\left[\begin{array}{c|c|c} & & \\ & \mathbf{D} & \\ & & \\ \hline 0 & 0 \quad \cdots \quad 0 & 1 \end{array}\right]\left[\begin{array}{c} \\ f^{n+1}_{r+1,1} \\ \vdots \\ \vdots \\ \hline f^{n+1}_{r+1,N_x} \end{array}\right] = \left[\begin{array}{c} \\ u^{n+1}_{r+1,1} \\ \vdots \\ \\ \hline u^{n}_{r+1,N_x-1} \\ \hline 0 \end{array}\right], \quad (3.111)$$

where

$$u^n_{r+1,j} = u_{r+1}\left(x_j, \xi^n\right),\ \theta^n_{r+1,j} = \theta_{r+1}\left(x_j, \xi^n\right),\ \phi^n_{r+1,j} = \phi_{r+1}\left(x_j, \xi^n\right),\ j = 0, 1, 2, 3, \cdots, N_x. \quad (3.112)$$

Hence, starting from the initial approximations $f_0(\xi, \eta)$, $u_0(\xi, \eta)$, $\theta_0(\xi, \eta)$, $\phi_0(\xi, \eta)$, given by equations (3.22 - 3.25) and (3.75), equations (3.88 - 3.91) can be solved iteratively to give approximate solutions $u_{r+1}\left(\xi, \eta\right)$, $\theta_{r+1}\left(\xi, \eta\right)$, $\phi_{r+1}\left(\xi, \eta\right)$, $r = 0, 1, 2, 3, \cdots$, until a solution that converges to within a given level of accuracy was obtained. The solution u_{r+1} was used in equation (3.78) which was, in turn, used to find f_{r+1}.

3.4. Results and discussion

In this section, the spectral perturbation method (SPM) and spectral relaxation method (SRM) results for the set of nonlinear partial differential equations (3.9 - 3.14) is presented. Numerical computation were carried out using the proposed spectral perturbation method (SPM) and spectral

relaxation method (SRM) discussed in the previous sections for the velocity, temperature and concentration profiles as well as the local skin friction, Nusselt and Sherwood number for different values of the significant physical parameters. Results are given using tabular and graphical formats. The SPM series was used to generate results from the initial analytical solution at $\xi = 0$ up to results close to the steady state values at $\xi = 1$. The accuracy of the computed SPM results was validated against numerical results obtained using the SRM. The results presented in this chapter were generated using $L = 30$, which was found to give accurate results through numerical experimentation. Increasing the value of L did not change the results to a significant extent. The number of collocation points used was $N_x = 100$ for both SPM and SRM. The values of Prandtl number Pr used in this study was chosen to be ($Pr = 0.7$) which represents the Pr for air, water($Pr = 1 - 10$). The values of Schmidt number were chosen to be Hydrogen ($Sc = 0.20$), Water ($Sc = 0.60$), Ammonia($Sc = 0.78$), Carbon dioxide ($Sc = 0.94$) and Propyl Benzene ($Sc = 2.62$). The buoyancy force parameter (ratio of the buoyancy force due to the thermal diffusion) N takes the values 0.5 or 1.0 for low concentration. All graphs and tables therefore corresponded to these values except otherwise indicated. The values of all other physical parameters governing the fluid flow were chosen based on values earlier used in literature. In order to further test the accuracy of the SPM and the SRM, a residual error analysis was conducted. The SPM residual error of the governing partial differential equations (3.9 - 3.11) was defined as;

$$Res(f) = D^3F + \frac{\eta}{2}(1-\xi)D^2F + \xi\left[(D^2F)(F) - (DF)^2 - Ha(DF) + \lambda(\Theta + N\Phi)\right] - \xi\,(1-\xi)\,\frac{\partial(DF)}{\partial\xi}, \tag{3.113}$$

$$Res(\theta) = \left(\frac{1}{Pr}\right)\left[D^2\Theta + \frac{\eta}{2}(1-\xi)D\Theta + \xi\left[(D\Theta)(F) - (DF)(\Theta)\right] - \xi\,(1-\xi)\,\frac{\partial\Theta}{\partial\xi}\right], \tag{3.114}$$

$$Res(\phi) = \left(\frac{1}{Sc}\right)\left[D^2\Phi + \frac{\eta}{2}(1-\xi)D\Phi + \xi\left[(D\Theta)(F) - (DF)(\Phi) - \gamma\Phi\right] - \xi\,(1-\xi)\,\frac{\partial\Phi}{\partial\xi}\right]. \tag{3.115}$$

While the SRM residual error of the governing partial differential equations (3.9 - 3.11) was defined as;

$$Res(f) = D^2U + \frac{\eta}{2}(1-\xi)(DU) + \xi\left[(DU)(F) - (U)^2 - HaU + \lambda(\Theta + N\Phi)\right] - \xi\,(1-\xi)\,\frac{\partial U}{\partial\xi}, \tag{3.116}$$

$$Res(\theta) = \left(\frac{1}{Pr}\right)\left[D^2\Theta + \frac{\eta}{2}(1-\xi)D\Theta + \xi\left[(D\Theta)(F) - (U)(\Theta)\right] - \xi\,(1-\xi)\,\frac{\partial\Theta}{\partial\xi}\right], \tag{3.117}$$

$$Res(\phi) = \left(\frac{1}{Sc}\right)\left[D^2\Phi + \frac{\eta}{2}(1-\xi)D\Phi + \xi\left[(D\Theta)(F) - (U)(\Phi) - \gamma\Phi\right] - \xi\left(1-\xi\right)\frac{\partial\Phi}{\partial\xi}\right]. \quad (3.118)$$

In the equations (3.116 - 3.118), $U = F'$. Also, U, F, Θ and Φ were defined as ;

$$\frac{U_{r+1}^{n+1} + U_r^{n+1}}{2}, \quad \frac{F_{r+1}^{n+1} + F_r^{n+1}}{2}, \quad \frac{\Theta_{r+1}^{n+1} + \Theta_r^{n+1}}{2}, \quad \text{and} \quad \frac{\Phi_{r+1}^{n+1} + \Phi_r^{n+1}}{2}. \quad (3.119)$$

In addition, $\frac{\partial U}{\partial \xi}$, $\frac{\partial \Theta}{\partial \xi}$, and $\frac{\partial \Phi}{\partial \xi}$ were defined as;

$$\frac{U_{r+1}^{n+1} - U_r^{n+1}}{\Delta\xi}, \quad \frac{\Theta_{r+1}^{n+1} - \Theta_r^{n+1}}{\Delta\xi}, \quad \text{and} \quad \frac{\Phi_{r+1}^{n+1} - \Phi_r^{n+1}}{\Delta\xi}. \quad (3.120)$$

Table 3.1 displays a comparison between the spectral perturbation method (SPM) and the spectral relaxation method (SRM) approximate solution of the skin friction coefficient ($f''(0,\xi)$) at various values of Hartman number Ha. It can be observed from the table that the two sets of results are in excellent agreement. Also, from the table, it was noticed that the effect of the Hartman number was to reduce the skin friction coefficient when $\xi = 0.5$. The physical reasoning behind this result, is as a consequence of the presence of transverse magnetic field on the flow. The transverse magnetic field sets in a Lorenz drag force caused by electromagnetism. This Lorenz drag force in turn produces a retarding force on the velocity field and thus, as the Hartman number increase, the retarding force also increases Hence, the boundary layer thickness decreases consequently reducing the shear stress at the sheet. It can be seen from Table 3.1 that results which are consistent with nine decimal digits were achieved with only four iteration. The number of grid points N_t used in the $\xi -$ direction is 10000 .

Table 3.1: *Comparison of the SPM and SRM approximate solutions of $f''(0,\xi)$ at different values of Ha, when $\xi = 0.5$, $\gamma = 1$, $Sc = 0.6$, $Pr = 1.5$, $\lambda = 0.5$ and $N = 1$.*

Ha	Order	SPM	It	N_t (Grid Points)	SRM	Difference (SPM - SRM)
0	21	-0.5412625054	4	10000	-0.5412625050	-0.0000000004
0.1	22	-0.5687336457	4	10000	-0.5687336453	-0.0000000004
0.3	20	-0.6223191104	4	10000	-0.6223191101	-0.0000000003
0.5	22	-0.6741858388	4	10000	-0.6741858385	-0.0000000003
0.7	18	-0.7244358040	4	10000	-0.7244358038	-0.0000000002
0.9	17	-0.7731640397	4	10000	-0.7731640396	-0.0000000002
1.0	18	-0.7969854223	4	10000	-0.7969854222	-0.0000000001
1.5	21	-0.9110740515	4	10000	-0.9110740517	0.0000000002
1.7	21	-0.9545424370	4	10000	-0.9545424373	0.0000000003
2.0	11	-1.0176356556	4	10000	-1.0176356559	0.0000000003

Table 3.2: *Comparison of the SPM and SRM approximate solutions of $\theta'(0,\xi)$ at different values of λ, and Pr, when $\xi = 0.5$, $\gamma = 1$, $Sc = 0.6$, $Ha = 1$, and $N = 1$.*

λ	Pr	Order	SPM	It	N_t(Grid Points)	SRM	Difference (SPM - SRM)
0	0.7	23	-0.6278318239	4	10000	-0.6278318241	0.0000000002
0	1.5	24	-0.9704104930	4	10000	-0.9704104933	0.0000000003
0	3	28	-1.4270081804	4	10000	-1.4270081807	0.0000000003
0	5	20	-1.8845313181	4	10000	-1.8845313184	0.0000000003
0	7	21	-2.2577308115	4	10000	-2.2577308118	0.0000000003
0	10	23	-2.7291527800	4	10000	-2.7291527804	0.0000000004
0.5	0.7	22	-0.6472110257	4	10000	-0.6472110257	0.0000000000
0.5	1.5	21	-0.9913518847	4	10000	-0.9913518848	0.0000000001
0.5	3	18	-1.4486322487	4	10000	-1.4486322488	0.0000000001
0.5	5	20	-1.9063010552	4	10000	-1.9063010554	0.0000000002
0.5	7	20	-2.2794797565	4	10000	-2.2794797567	0.0000000002
0.5	10	20	-2.7508106579	4	10000	-2.7508106582	0.0000000003
3	0.7	20	-0.7301529363	4	10000	-0.7301529361	-0.0000000002
3	1.5	19	-1.0836580237	4	10000	-1.0836580235	-0.0000000002
3	3	17	-1.5462651227	4	10000	-1.5462651224	-0.0000000003
3	5	17	-2.0061038392	4	10000	-2.0061038389	-0.0000000003
3	7	17	-2.3800671239	4	10000	-2.3800671235	-0.0000000004
3	10	16	-2.8518007075	4	10000	-2.8518007072	-0.0000000003

Table 3.2 gives a comparison of the spectral perturbation method (SPM) and the spectral relaxation method (SRM) solutions of the local Nusselt number for varying Prandtl number Pr and mixed convection parameter λ. A comparison of the two result indicates that the SPM results are in good agreement with the SRM results for nine to ten decimal places. It can be observed from the table that the heat transfer rate reduces with an increase in Pr. The heat transfer rate is decreased by increase in Pr due to the reducing manner of the thermal boundary layer thickness with increment in Pr. We remark that the number of iterations needed to give the SRM solutions in Table 3.2 is four. The number of grid points N_t used in generating the results in Table 3.2 is 10000.

A comparison of the spectral perturbation method (SPM) and the spectral relaxation method (SRM) approximate solution for the mass transfer coefficient for different values of the concentration to thermal buoyancy ratio N, mixed convection parameter λ, chemical reaction parameter γ and Schmidt number Sc is shown in Table 3.3. The mass transfer coefficient decreased with an increase in N, λ, γ and Sc. The mass transfer rate is reduce by an increase in N, λ, γ and Sc due to the reducing manner of the solutal boundary layer thickness with increment in these parameters. Table 3.3 shows that the SPM results are in good agreement with the (SRM) solutions. This shows that the SPM is a

Table 3.3: *Comparison of the SPM and SRM approximate solutions of $\phi'(0,\xi)$at different values of λ, N, γ, and Sc, when $Ha = 1$, $\xi = 0.5$, and $Pr = 1.5$.*

N	λ	γ	Sc	Order	SPM	It	N_t	SRM	Difference (SPM - SRM)
0.1	0	0	0.2	24	-0.3010787178	3	10000	-0.3010787179	0.0000000001
0.1	0	0	0.6	24	-0.5741354094	3	10000	-0.5741354096	0.0000000002
0.1	0	0	0.78	24	-0.6683346542	3	10000	-0.6683346544	0.0000000002
0.1	0	0	0.94	25	-0.7440222118	3	10000	-0.7440222120	0.0000000002
0.1	0	0	2.62	21	-1.3244650947	3	10000	-1.3244650949	0.0000000002
0.5	0.5	0.5	0.2	21	-0.3742245763	3	10000	-0.3742245763	0.0000000000
0.5	0.5	0.5	0.6	19	-0.6919154177	3	10000	-0.6919154178	0.0000000001
0.5	0.5	0.5	0.78	21	-0.8000959702	3	10000	-0.8000959703	0.0000000001
0.5	0.5	0.5	0.94	19	-0.8867166724	3	10000	-0.8867166726	0.0000000002
0.5	0.5	1	0.2	21	-1.5463570186	3	10000	-1.5463570189	0.0000000003
1	3	1	0.2	23	-0.4803470113	4	10000	-0.4803470114	0.0000000001
1	3	1	0.6	19	-0.8467369401	4	10000	-0.8467369404	0.0000000003
1	3	1	0.78	19	-0.9691750885	4	10000	-0.9691750888	0.0000000003
1	3	1	0.94	19	-1.0667279295	4	10000	-1.0667279299	0.0000000004
1	3	1	2.62	16	-1.8022963261	4	10000	-1.8022963268	0.0000000007

viable method for solving the model equations. In the SRM results in Table 3.3, a uniform grid with $N_t = 10000$ was used in the $\xi -$ direction to generate the results that are consistent to at least nine decimal places. It can be observed from the table that only four iterations was required to obtain the SRM solution. This is so because for larger number of grid points N_t, only few iterations are required to give converged results.

Table 3.4: *Approximate numerical values of the skin friction $f''(0,\xi)$ for various ξ and N_t (Grid Points) computed using the SRM, when $\lambda = 0.5$, $N = 1$ and $Ha = 1$.*

ξ	N_t (Grid Points)				
	500	1000	2000	5000	10000
0.1	-0.61019890	-0.61019891	-0.61019891	-0.61019891	-0.61019891
0.3	-0.70310508	-0.70310509	-0.70310509	-0.70310509	-0.70310509
0.5	-0.79698541	-0.79698542	-0.79698542	-0.79698542	-0.79698542
0.6	-0.84421553	-0.84421554	-0.84421554	-0.84421554	-0.84421554
0.7	-0.89160155	-0.89160156	-0.89160156	-0.89160156	-0.89160156
0.8	-0.93911733	-0.93911734	-0.93911734	-0.93911734	-0.93911734
0.9	-0.98672992	-0.98672993	-0.98672993	-0.98672993	-0.98672993
0.95	-1.01053770	-1.01053772	-1.01053773	-1.01053773	-1.01053773
0.98	-1.02476406	-1.02476403	-1.02476406	-1.02476407	-1.02476407

Tables 3.4 - 3.6 give the approximate numerical values of the skin friction $f''(0,\xi)$, the heat transfer rate $\theta'(0,\xi)$, and the mass transfer rate $\phi'(0,\xi)$ respectively for various values of ξ and grid points (N_t) computed using the SRM. The results presented in these tables were computed using the same

Table 3.5: *Approximate numerical values of the heat transfer rate $\theta'(0,\xi)$ for various ξ and grid points N_t computed using the SRM, when $Pr = 1.5$, $\lambda = 0.5$, $N = 1$ and $Ha = 1$.*

ξ	N_t (Grid Points)				
	500	1000	2000	5000	10000
0.1	-0.75235582	-0.75235580	-0.75235579	-0.75235579	-0.75235579
0.3	-0.87320803	-0.87320801	-0.87320800	-0.87320800	-0.87320800
0.5	-0.99135192	-0.99135189	-0.99135188	-0.99135188	-0.99135188
0.6	-1.04931600	-1.04931598	-1.04931597	-1.04931597	-1.04931597
0.7	-1.10646916	-1.10646913	-1.10646912	-1.10646912	-1.10646912
0.8	-1.16271393	-1.16271390	-1.16271389	-1.16271389	-1.16271389
0.9	-1.21781799	-1.21781794	-1.21781792	-1.21781792	-1.21781792
0.95	-1.24469323	-1.24469313	-1.24469310	-1.24469310	-1.24469310
0.98	-1.26030666	-1.26030636	-1.26030628	-1.26030626	-1.26030625

Table 3.6: *Approximate numerical values of the mass transfer rate $\phi'(0,\xi)$ for various ξ and grid points N_t computed using the SRM, when $Sc = 0.6$,$\gamma = 1$,$\lambda = 0.5$, $N = 1$ and $Ha = 1$.*

ξ	N_t (Grid Points)				
	500	1000	2000	5000	10000
0.1	-0.51175555	-0.51175548	-0.51175546	-0.51175546	-0.51175546
0.3	-0.65570423	-0.65570416	-0.65570413	-0.65570413	-0.65570413
0.5	-0.79217956	-0.79217949	-0.79217947	-0.79217947	-0.79217947
0.6	-0.85756619	-0.85756612	-0.85756610	-0.85756610	-0.85756610
0.7	-0.92101828	-0.92101820	-0.92101818	-0.92101818	-0.92101818
0.8	-0.98250113	-0.98250106	-0.98250103	-0.98250103	-0.98250103
0.9	-1.04196826	-1.04196818	-1.04196816	-1.04196816	-1.04196816
0.95	-1.07093123	-1.07093115	-1.07093113	-1.07093113	-1.07093113
0.98	-1.08807104	-1.08807097	-1.08807095	-1.08807095	-1.08807095

Table 3.7: *Comparison of the SPM and SRM numerical values of the skin friction $f''(0,\xi)$ at different values of ξ when $\lambda = 0.5$, $N = 1$ and $Ha = 1$.*

ξ	Order	SPM	SPM Time(sec)	SRM	N_t (Grid Points)	It	SRM Time(sec)
0.1	5	-0.61019891	0.008	-0.61019891	1000	3	7.800
0.3	8	-0.70310509	0.019	-0.70310509	1000	3	7.904
0.5	12	-0.79698542	0.037	-0.79698542	1000	3	8.322
0.6	18	-0.84421554	0.042	-0.84421554	1000	3	8.340
0.7	24	-0.89160156	0.068	-0.89160156	1000	4	10.847
0.8	36	-0.93911734	0.107	-0.93911734	1000	4	10.888
0.9	80	-0.98672993	0.330	-0.98672993	1000	4	10.923
0.95	147	-1.01053773	1.103	-1.01053773	2000	4	21.072
0.98	403	-1.02476407	5.076	-1.02476407	5000	4	49.585

Table 3.8: *Comparison of the SPM and SRM numerical values of the heat transfer rate* $\theta'(0,\xi)$ *at different values of* ξ *when* $Pr = 1.5$, $Sc = 0.6$, $\gamma = 1$, $\lambda = 0.5$, $N = 1$ *and* $Ha = 1$.

ξ	Order	SPM	SPM Time(sec)	SRM	N_t (Grid Points)	It	SRM Time(sec)
0.1	5	-0.75235579	0.008	-0.75235579	2000	2	10.910
0.3	9	-0.87320800	0.019	-0.87320800	2000	3	15.024
0.5	19	-0.99135188	0.037	-0.99135188	2000	3	15.433
0.6	19	-1.04931597	0.042	-1.04931597	2000	3	15.834
0.7	27	-1.10646912	0.068	-1.10646912	2000	3	16.064
0.8	43	-1.16271389	0.107	-1.16271389	2000	3	16.091
0.9	89	-1.21781792	0.330	-1.21781792	2000	3	16.252
0.95	180	-1.24469310	1.103	-1.24469310	2000	3	16.392
0.98	429	-1.26030625	5.076	-1.26030625	10000	3	81.792

Table 3.9: *Comparison of the SPM and SRM numerical values of the mass transfer rate* $\phi'(0,\xi)$ *at different values of* ξ *when* $Sc = 0.6$,$\gamma = 1$,$\lambda = 0.5$, $N = 1$ *and* $Ha = 1$.

ξ	Order	SPM	SPM Time(sec)	SRM	N_t (Grid Points)	It	SRM Time(sec)
0.1	5	-0.51175546	0.008	-0.51175546	2000	2	10.811
0.3	10	-0.65570413	0.019	-0.65570413	2000	2	10.824
0.5	11	-0.79217947	0.037	-0.79217947	2000	3	15.435
0.6	13	-0.85756610	0.042	-0.85756610	2000	3	15.886
0.7	21	-0.92101818	0.068	-0.92101818	2000	3	15.941
0.8	32	-0.98250103	0.107	-0.98250103	2000	3	16.046
0.9	78	-1.04196816	0.330	-1.04196816	2000	3	16.289
0.95	152	-1.07093113	1.103	-1.07093113	2000	3	16.295
0.98	333	-1.08807095	5.076	-1.08807095	2000	4	21.619

number of collocation points N_x and L. Increasing the grid points improves the accuracy of the results until the results match exactly to within eight decimal places. As observed from Table 3.4, for small value of ξ, full convergence to at least eight decimal digits was reached with grid points $N_t = 1000$. As ξ approaches 1, more grid points N_t are required to give the converged results presented in Table 3.4. In Table 3.5, when ξ is small, the number of grid points N_t required to give converged results that are consistent to at least eight decimal digits was 2000. The number of grid points N_t was progressively increased as ξ tends closer to 1. Similarly, in Table 3.6, convergence to within eight decimal places was reached when the N_t was at least 2000. We remark that for all the values of grid points N_t used in Tables 3.4 - 3.6, only four iterations were used to obtain the results.

Results given in Tables 3.7 - 3.9 give further validation of the accuracy of the SPM. The tables present a comparison of the SPM and the SRM approximate solutions for the skin friction ($f''(0,\xi)$), heat transfer rate ($\theta'(0,\xi)$), and mass transfer rate ($\phi'(0,\xi)$) at different values of the dimensionless time ξ and at different order of approximation. The solutions were obtained for $Pr = 1.5$, $Sc = 0.6$, $\gamma = 1$, $\lambda = 0.5$, $N = 1$ and $Ha = 1$. It can be observed from the tables that as the dimensionless time ξ increases, the order of the SPM approximation required to give converged results increases. This shows that when ξ is very small, only few terms of the SPM approximation are needed to give converged results and higher order of approximation are required when ξ is closer to 1. Furthermore, the column on the run time in (sec) for both SPM and SRM is displayed in Tables 3.7 - 3.9. It can be seen from the table that the desired solution for the SPM was obtained after only a few seconds. This shows the efficiency of the proposed SPM in terms of the amount of time it takes to give desired results. Comparing the SPM and the SRM computational times clearly shows that the SPM is faster than the SRM in the computation of the solution for the governing equation. This computation speed of the SPM may be explained by the fact that discretization was done only in $\eta-$ direction unlike the SRM, where discretization was done both in $\eta-$ and ξ directions. Hence, the numerical results presented in the tables, show that the two methods were in good agreement on comparison. In addition, the table further gives the number of grid points N_t and iterations (It) required to give converged SRM results that match with the SPM results to within eight decimal places. It can be observed from the Tables that for the time ξ closer to 1, both the values of grid points N_t and iterations required to obtain the results presented in Tables 3.7 - 3.9 increase.

The velocity profile $f'(\xi,\eta)$ for different values of ξ is shown in Fig. 3.2. It can be seen that increasing the values of ξ tends to reduce the velocity distribution in the boundary layer. The influence of ξ

on the temperature profile $\theta(\xi, \eta)$ is displayed in Figure 3.3. The influence of ξ is to reduce the temperature distribution. It can be observed from Figure 3.4 that the effect of increasing ξ on the concentration distribution $\phi(\xi, \eta)$ in the solutal boundary is to reduce the solutal boundary layer. Similar observations in Figure 3.2 were made in earlier studies by Aurangzaib et al. (2013), while related effect in Figure 3.3 were observed in similar studies by Ishak et al. (2006) and in Figure 3.4 by Dulal and Mondal (2011) and Aurangzaib et al. (2013).

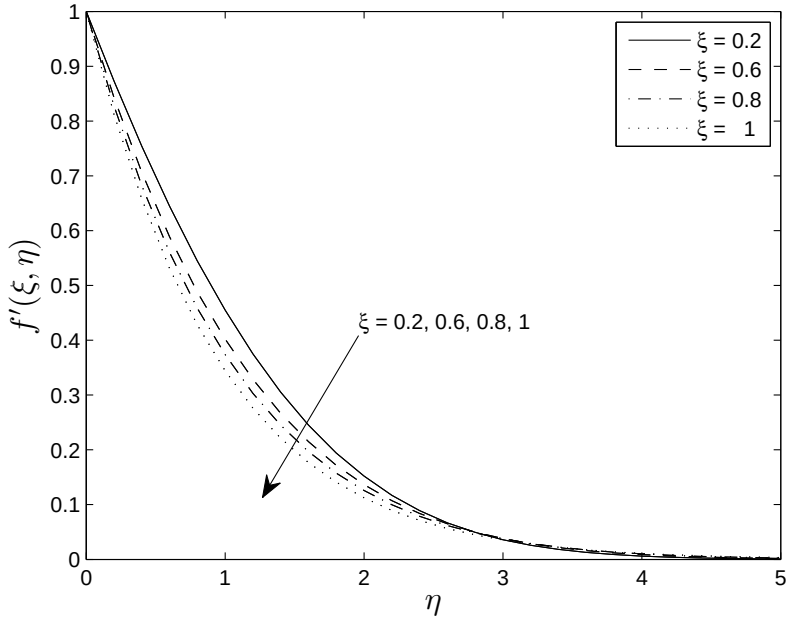

Figure 3.2: *Effects of ξ on velocity distribution $f'(\eta)$, when $Ha = 1,\ Sc = 0.6,\ \gamma = 1,\ Pr = 1.5,\ N = 1,\ \lambda = 0.5,\ L = 30,\ N_x = 100$.*

Figures 3.5 - 3.7 illustrates the effect of the Hartman number (Ha) on the fluid velocity $f'(\xi, \eta)$, temperature $\theta(\xi, \eta)$, and concentration $\phi(\xi, \eta)$, respectively. It was observed from Figure 3.5 that as Ha increases, there is a reduction in the fluid velocity. This is due to an increase in the strength of the magnetic field normal to the flow direction in an electrically conducting fluid which result in a drag Lorenz force acting in the opposite direction to that of the flow. Hence, applying moderate magnetic field stabilizes the flow. Figure 3.6 shows the influence of Ha on the temperature distribution. It is clear that the thermal boundary layer increases with an increase in Ha. Therefore, an increase in the values of Ha, causes an increase in temperature. Figure 3.7 presents the effect of Ha on the concentration distribution. An increase in Ha leads to an increase in the concentration profiles. This is because application of magnetic field heats up the fluid and thereby decreasing the heat and

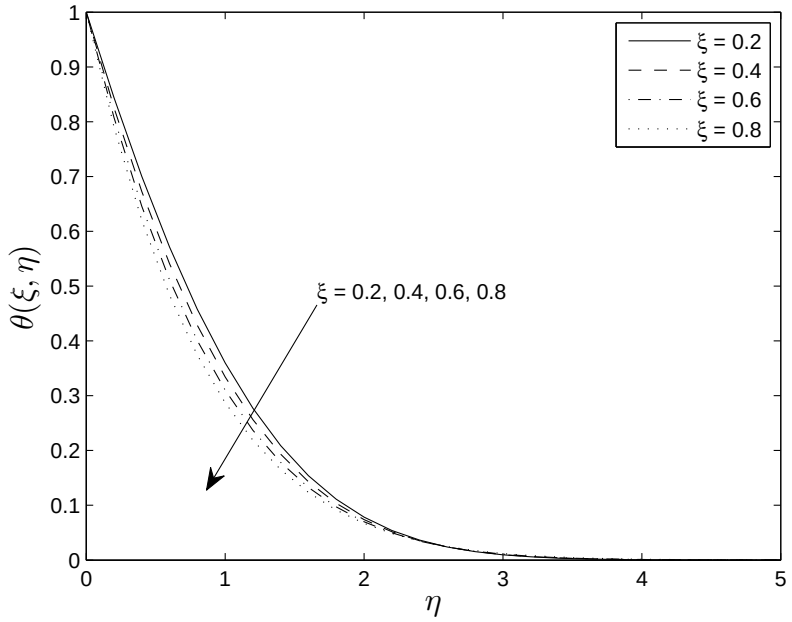

Figure 3.3: *Effect of* ξ *on temperature distribution* $\theta(\eta)$, *when* $N = 1,\ Sc = 0.6,\ Ha = 1,\ Pr = 1.5,\ \lambda = 0.5,\ \gamma = 1,\ L = 30,\ N_x = 100.$

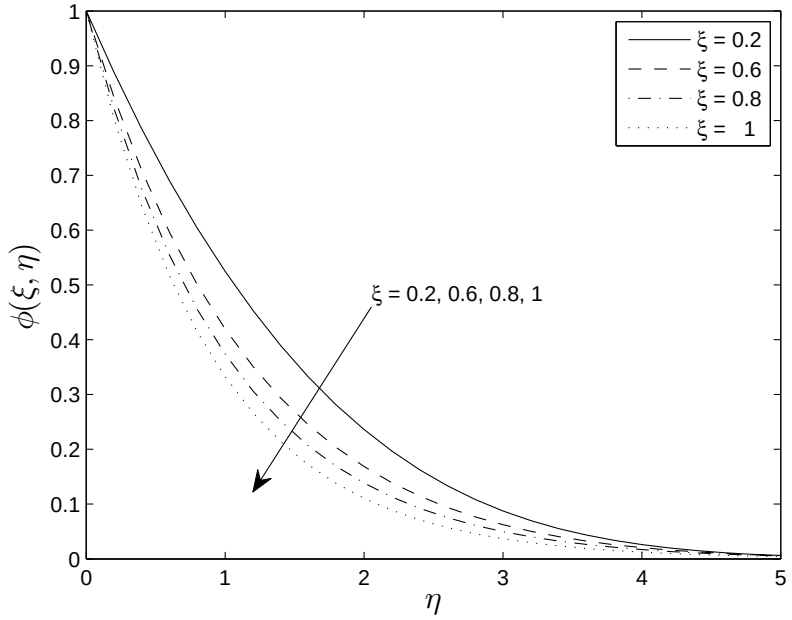

Figure 3.4: *Effect of* ξ *on concentration distribution* $\phi(\xi, \eta)$ *when* $\lambda = 0.5,\ Pr = 1.5,\ Sc = 0.6,\ \gamma = 1,\ Ha = 1,\ N = 1,\ L = 30,\ N_x = 100.$

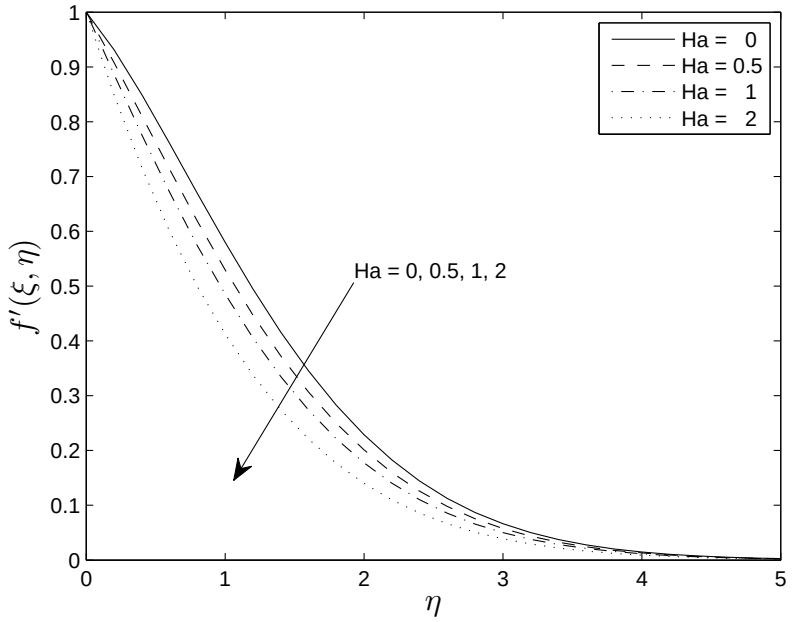

Figure 3.5: *Effect of Hartmann number Ha on velocity distribution* $f'(\eta)$, *when* $\xi = 0.5,\ Sc = 0.6,\ \gamma = 1,\ Pr = 1.5,\ N = 1,\ \lambda = 1,\ L = 30,\ N_x = 100.$

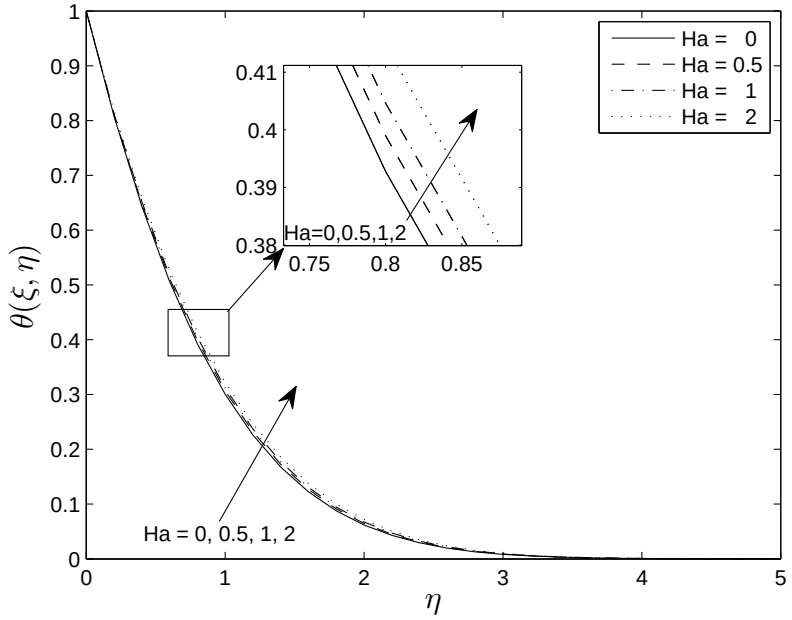

Figure 3.6: *Effect of Hartman number Ha on temperature profile* $\theta(\xi,\eta)$ *when* $\xi = 0.5,\ \lambda = 1,\ Sc = 0.6,\ \gamma = 1,\ Pr = 1.5,\ N = 1,\ L = 30,\ N_x = 100.$

mass transfers from the wall. This causes an increase in the fluid temperature and concentration profiles. The effect of the Hartman number on the fluid velocity $f'(\xi,\eta)$, temperature $\theta(\xi,\eta)$, and concentration $\phi(\xi,\eta)$ profiles respectively correlate with result obtained by EL-Kabeir and Rashad (2012) and Chamkha and El-Kabeir (2013).

Figures 3.8 - 3.10 shows the effect of the chemical reaction parameter γ on the velocity $f'(\xi,\eta)$, temperature $\theta(\xi,\eta)$ and the solute concentration $\phi(\xi,\eta)$ profiles. We note that both the fluid velocity and concentration distributions are reduced with increasing values of γ (which represents severe destructive reactant). A reverse effect was observed for the temperature distribution which in this case increases with an increment in γ. This result, however, implies that the increase in γ makes the concentration of the diffusing species to decrease. The reduction in the concentration of the diffusing species reduces mass diffusion, consequently showing down the fluid motion and increasing the fluid temperature. These findings are consistent with those of Chamkha and El-Kabeir (2013) in a similar investigation.

The influence of mixed convection parameter λ on the velocity $f'(\xi,\eta)$, temperature $\theta(\xi,\eta)$ and concentration $\phi(\xi,\eta)$ profiles are given in Figures 3.11 - 3.13 respectively. When the mixed convection parameter value was increased, there was an increase in the boundary layer of the velocity profile while the temperature and concentration profiles decreases. The faster moving fluid removes the heat and species, thereby causing stabilization and reduction in the growth of the thermal and diffusion boundary layers along the vertical walls. This behavior can be clearly seen in Figures 3.11 - 3.13. These observations are consistent with those of Chamkha and El-Kabeir (2013).

Figures 3.14 - 3.16 depicts the impact of the concentration to thermal buoyancy ratio N on the velocity $f'(\xi,\eta)$, temperature $\theta(\xi,\eta)$ and concentration $\phi(\xi,\eta)$ distributions respectively. It was observed that the boundary layer thickness increases with increasing values of N on the velocity distribution while there was a reduction in the temperature and solute concentration distributions.

Figure 3.17 illustrate the influence of the Prandtl number Pr on the temperature $\theta(\xi,\eta)$ distribution. We note that an increase in Pr leads to a decrease in the temperature distribution which in turn yields a reduction in the thermal boundary layer thickness. These results are in agreement with studies by Dulal and Mondal (2011), and Hayat et al. (2010).

The impact of Schmidt number Sc on the concentration profile $\phi(\xi,\eta)$ is shown in Figure 3.18. We note that the concentration profile $\phi(\xi,\eta)$ reduces with an increase in Sc. These findings are

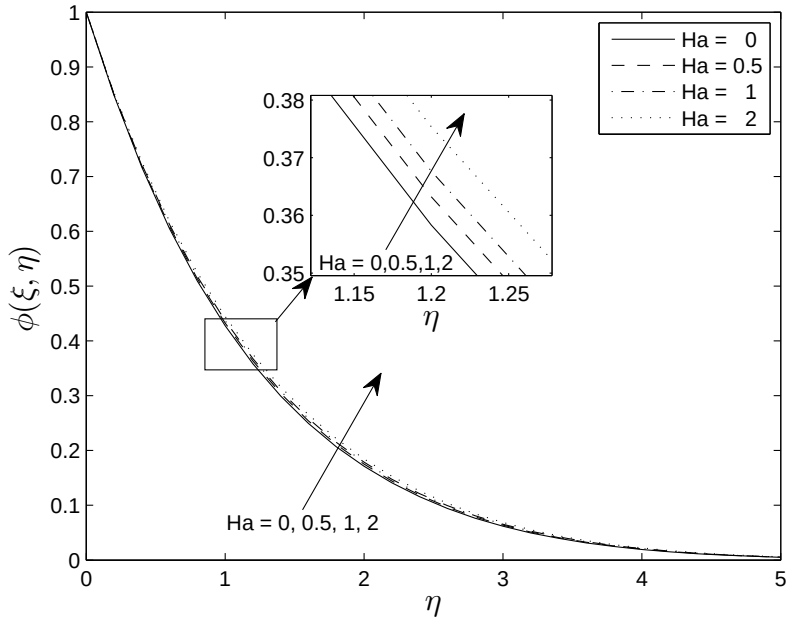

Figure 3.7: *Effect of Hartman number* Ha *on concentration distribution* $\phi(\xi,\eta)$ *when* $\xi = 0.5,\ \lambda = 1,\ Pr = 1.5,\ Sc = 0.6,\ \gamma = 1,\ N = 1,\ L = 30,\ N_x = 100.$

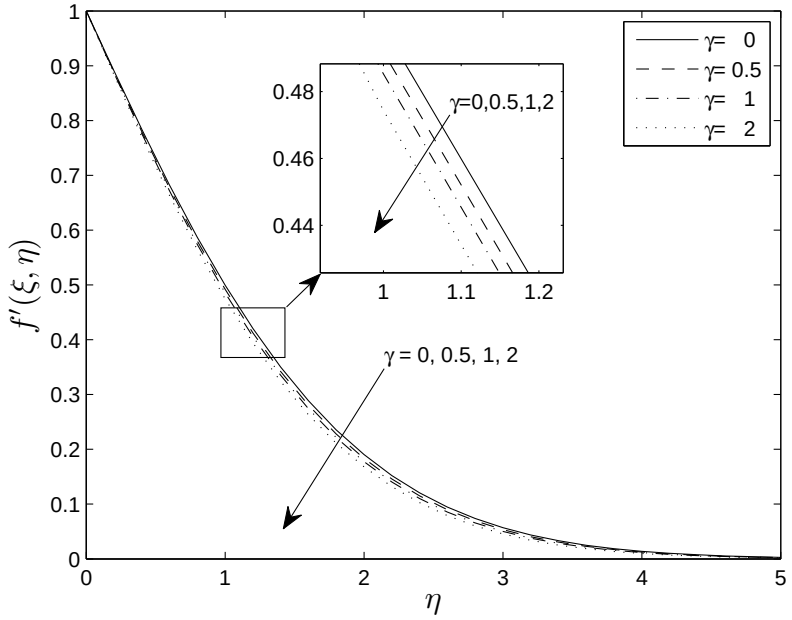

Figure 3.8: *Effect of Chemical reaction parameter* γ *on velocity distribution* $f'(\xi,\eta)$, *when* $\xi = 0.5,\ Sc = 0.6,\ Ha = 1,\ Pr = 1.5,\ N = 1,\ \lambda = 1,\ L = 30,\ N_x = 100.$

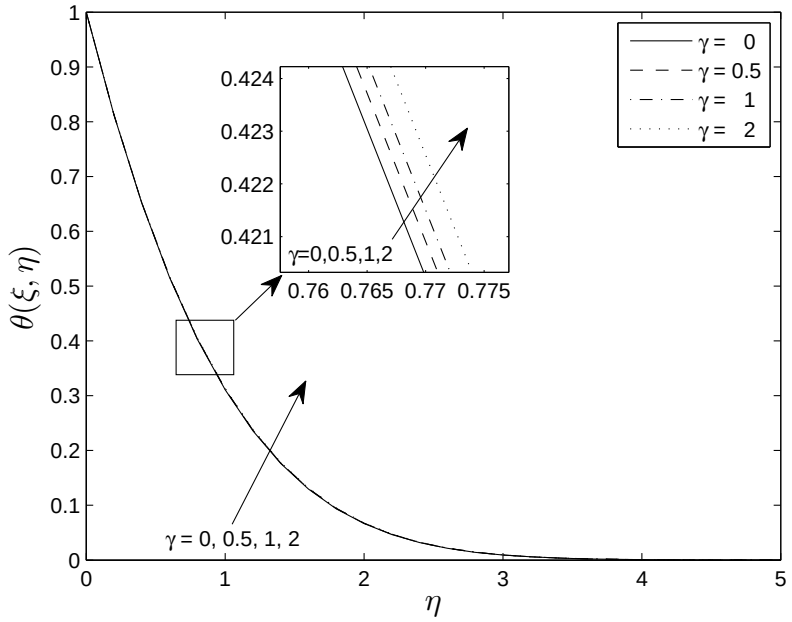

Figure 3.9: *Effect of chemical reaction parameter* γ *on temperature profile* $\theta(\xi,\eta)$*, when* $\xi = 0.5,\ Ha = 1,\ Sc = 0.6,\ N = 1,\ \lambda = 1,\ Pr = 1.5,\ L = 30,\ N_x = 100.$

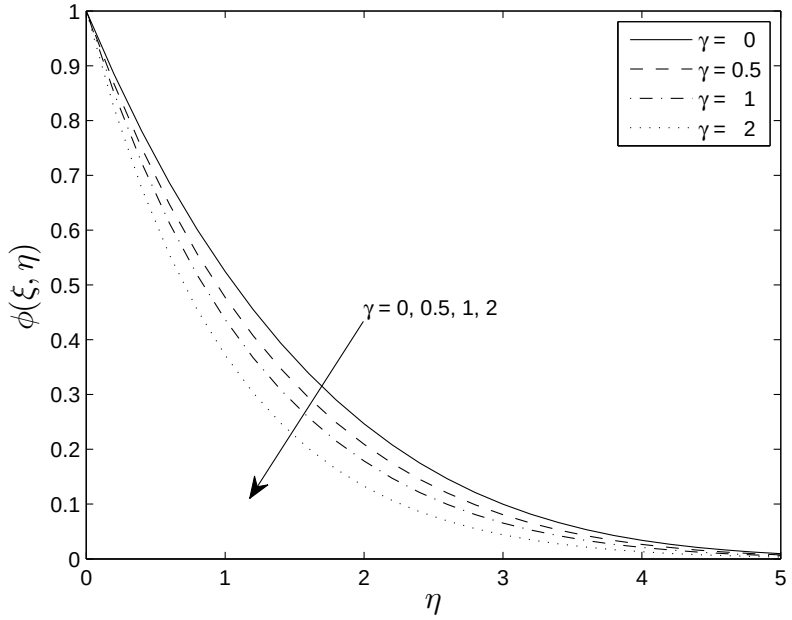

Figure 3.10: *Effect of Chemical reaction parameter* γ *on concentration distribution* $\phi(\xi,\eta)$ *when* $\xi = 0.5,\ \lambda = 1,\ Pr = 1.5,\ Sc = 0.6,\ Ha = 1,\ N = 1,\ L = 30,\ N_x = 100.$

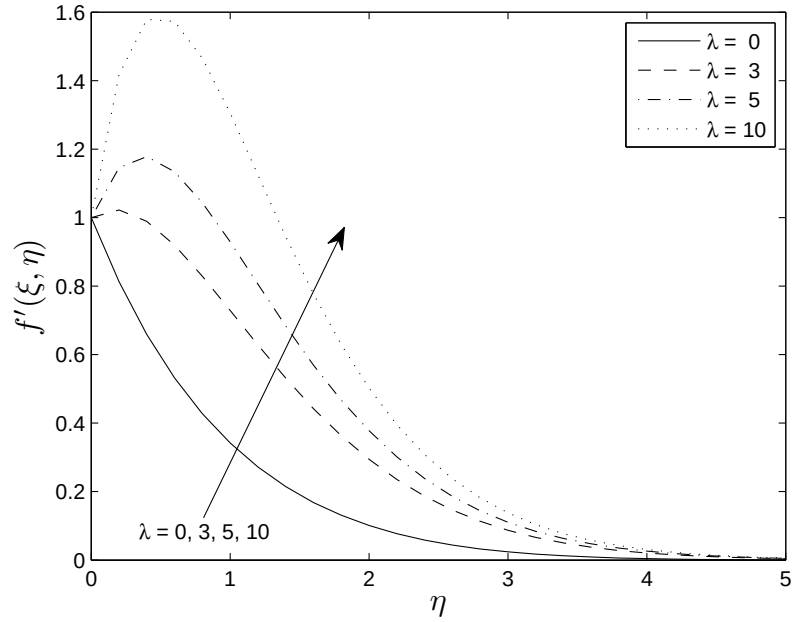

Figure 3.11: *Effect of Mixed convection parameter* λ *on velocity distribution* $f'(\xi,\eta)$, *when* $\xi = 0.5,\ Sc = 0.6,\ Ha = 1,\ Pr = 0.7,\ N = 1,\ \gamma = 1,\ L = 30,\ N_x = 100.$

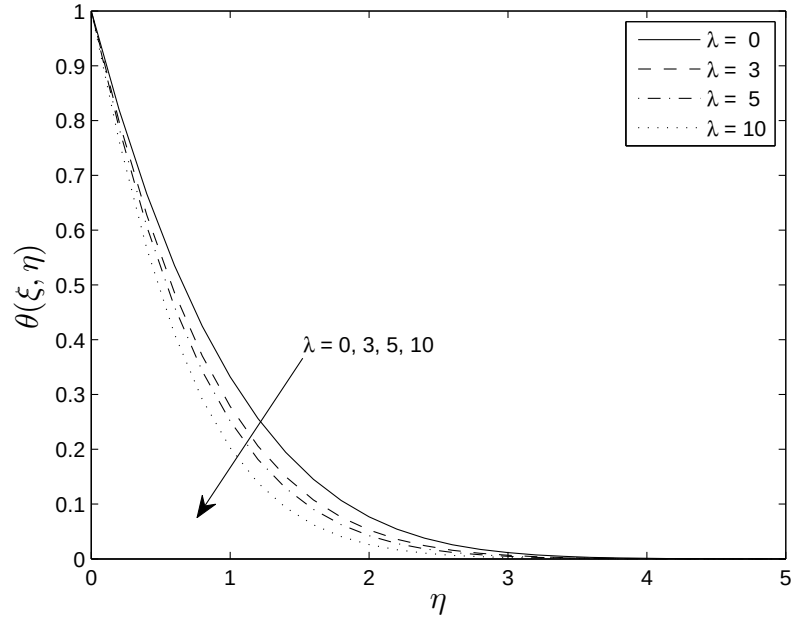

Figure 3.12: *Effect of Mixed convection parameter* λ *on temperature distribution* $\theta(\xi,\eta)$, *when* $\xi = 0.5,\ Sc = 0.6,\ Ha = 1,\ Pr = 0.7,\ N = 1,\ \gamma = 1,\ L = 30,\ N_x = 100.$

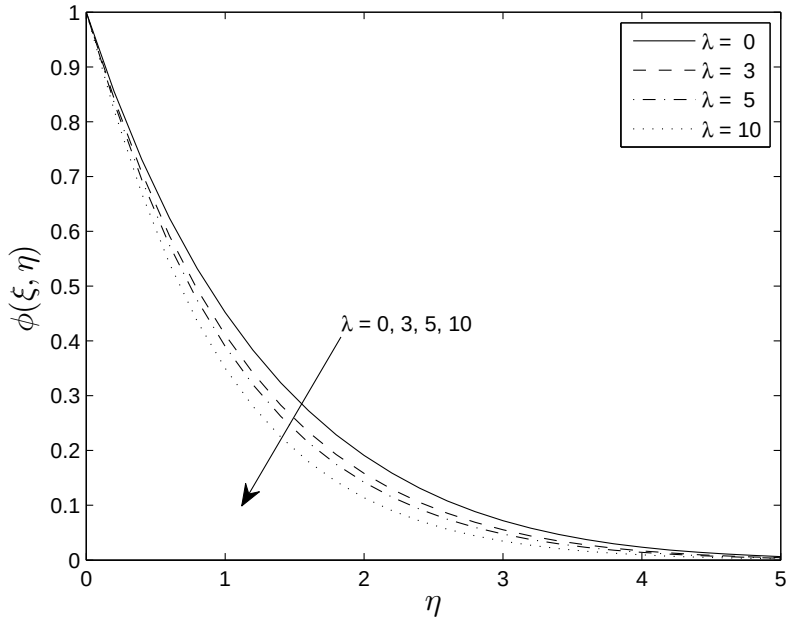

Figure 3.13: *Effect of Mixed convection parameter* λ *on concentration distribution* $\phi(\xi,\eta)$ *when* $\xi = 0.5,\ Pr = 1.5,\ Sc = 0.6,\ \gamma = 1,\ Ha = 1,\ N = 1,\ L = 30,\ N_x = 100.$

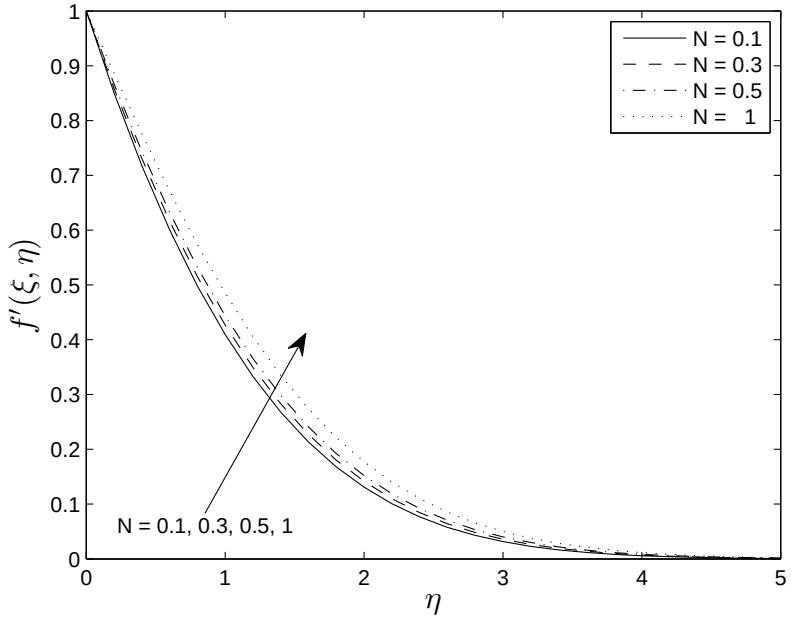

Figure 3.14: *Effect of concentration to thermal buoyancy ratio parameter* N *on velocity distribution* $f'(\xi,\eta)$, *when* $\xi = 0.5,\ Sc = 0.6,\ Ha = 1,\ Pr = 0.7,\ \lambda = 1,\ \gamma = 1,\ L = 30,\ N_x = 100.$

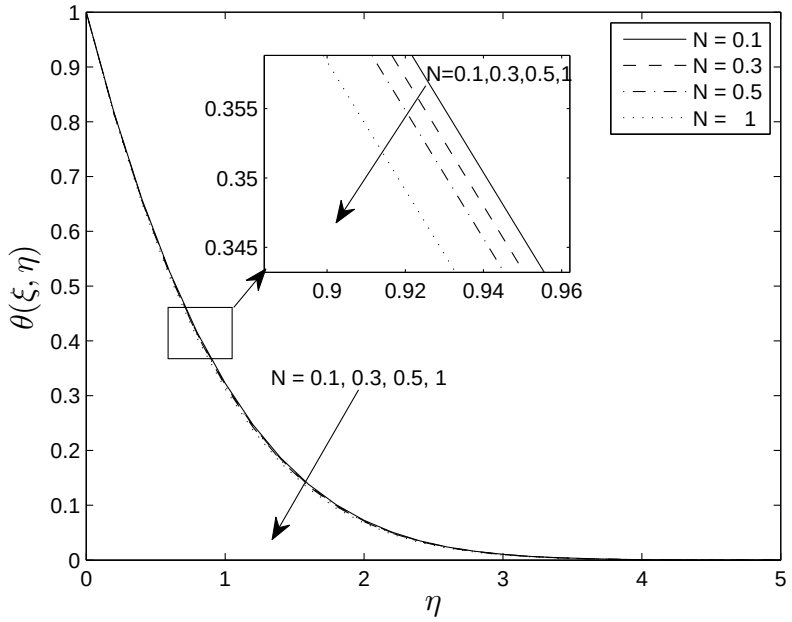

Figure 3.15: *Effect of concentration to thermal buoyancy ratio N on temperature distribution $\theta(\xi,\eta)$, when $\xi = 0.5,\ Ha = 1,\ Sc = 0.6,\ \gamma = 1,\ \lambda = 1,\ Pr = 1.5,\ L = 30,\ N_x = 100$.*

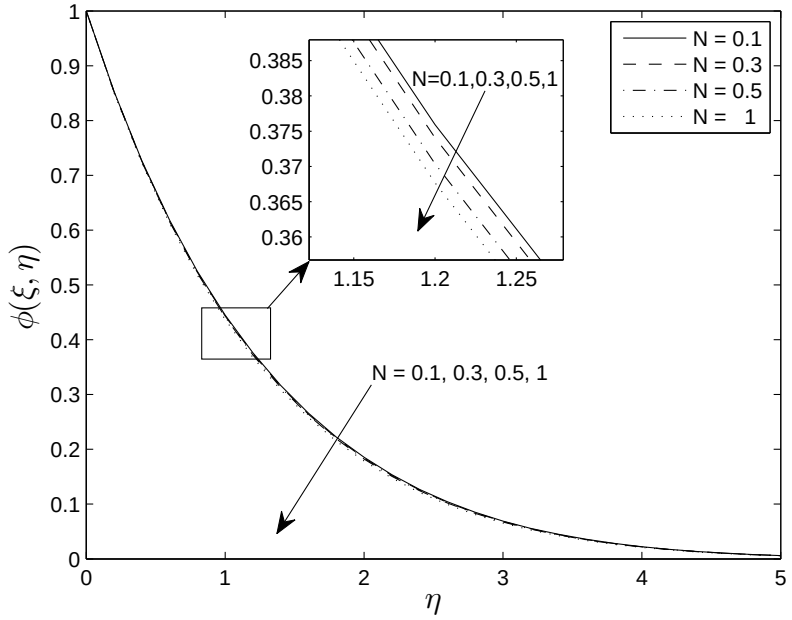

Figure 3.16: *Effect of concentration to thermal buoyancy parameter N on concentration distribution $\phi(\xi,\eta)$ when $\xi = 0.5,\ \lambda = 1,\ Pr = 1.5,\ Sc = 0.6,\ \gamma = 1,\ Ha = 1,\ L = 30,\ N_x = 100$.*

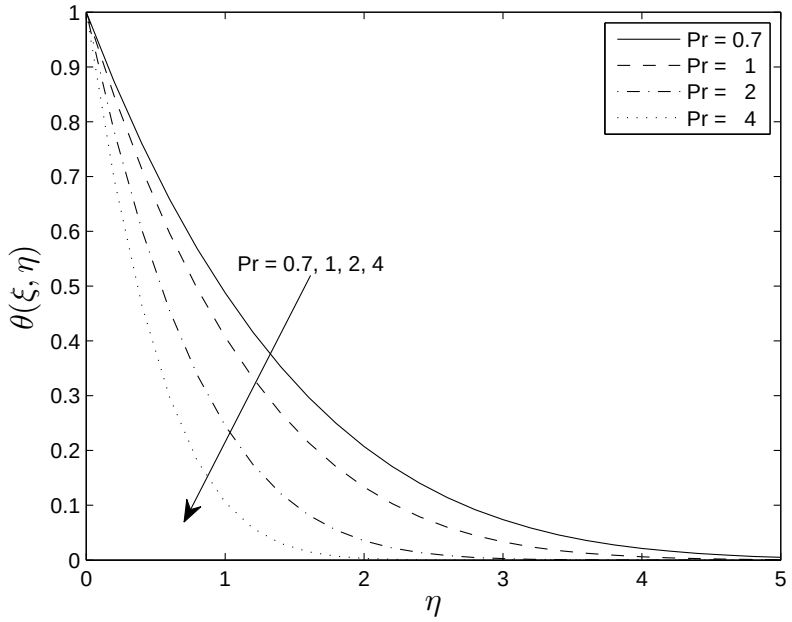

Figure 3.17: *Variation of temperature* $\theta(\xi,\eta)$ *for different values of Prandtl number* Pr*, when* $\xi = 0.5,\ Ha = 1,\ Sc = 0.6,\ \gamma = 1,\ \lambda = 1,\ N = 1,\ L = 30,\ N_x = 100.$

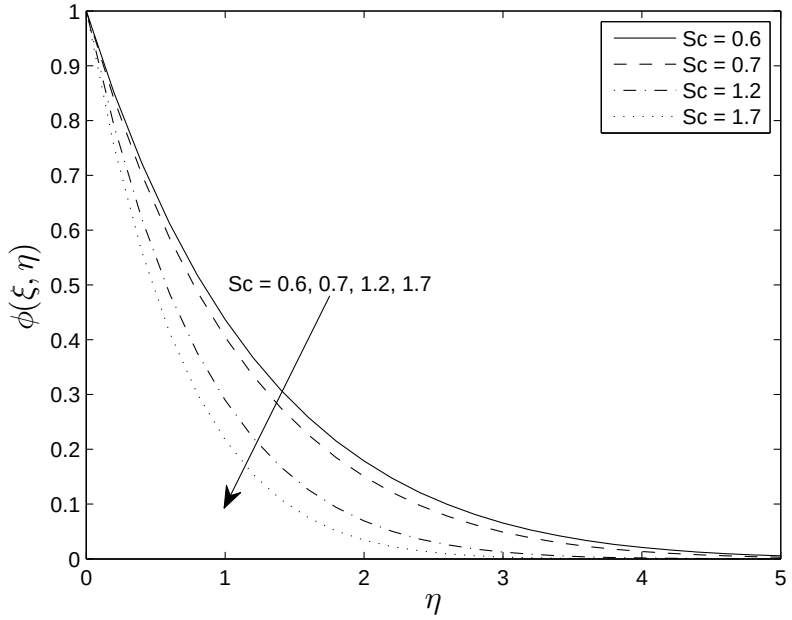

Figure 3.18: *Effect of Schmidt number* Sc *on concentration distribution* $\phi(\xi,\eta)$ *when* $\xi = 0.5,\ \lambda = 1,\ Pr = 1.5,\ N = 1,\ \gamma = 1,\ Ha = 1,\ L = 30,\ N_x = 100.$

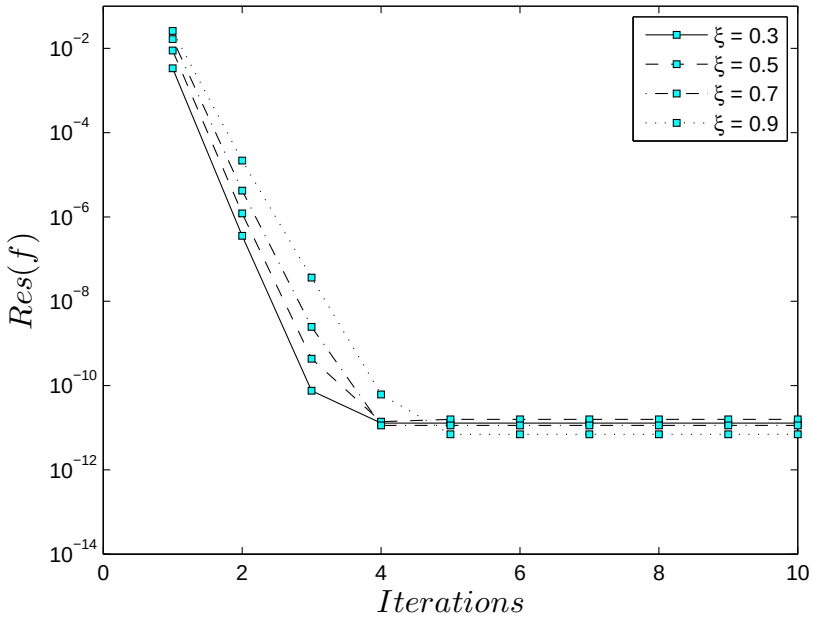

Figure 3.19: *Residual error curve* $Res(f)$ *against SRM iterations when* $\xi = 0.3, 0.5, 0.7, 0.9,\ Ha = 1,\ Sc = 0.6,\ \gamma = 1,\ \lambda = 1,\ N = 1,$ *grid ponts* $N_t = 5000,\ L = 30,\ N_x = 100.$

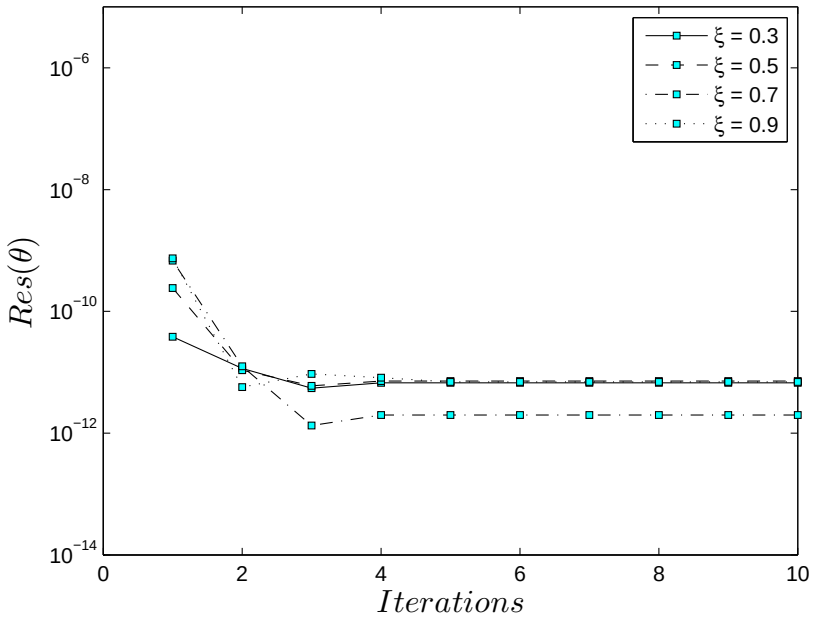

Figure 3.20: *Residual error curve* $Res(\theta)$ *against SRM iterations when* $\xi = 0.3, 0.5, 0.7, 0.9,\ Ha = 1,\ Sc = 0.6,\ \gamma = 1,\ \lambda = 1,\ N = 1,$ *grid ponts* $N_t = 5000,\ L = 30,\ N_x = 100.$

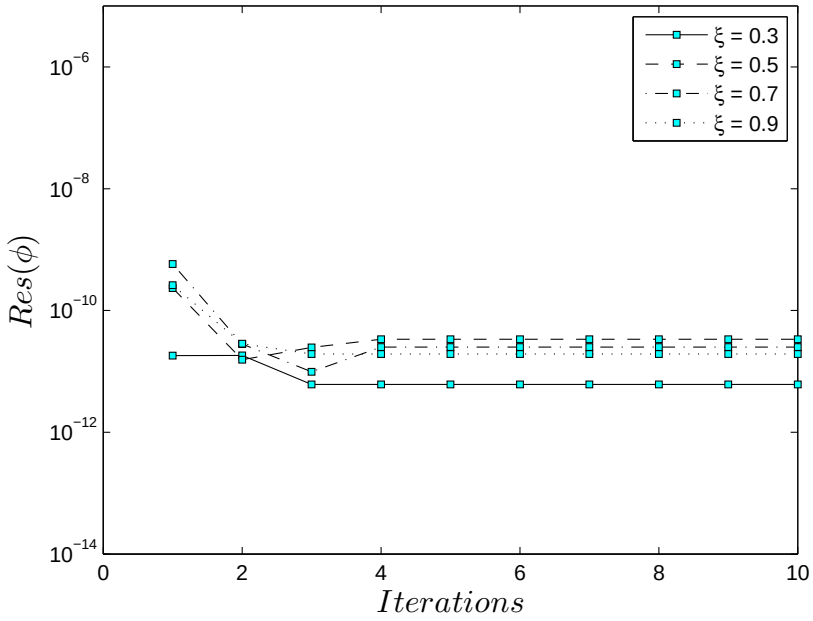

Figure 3.21: *Residual error curve* $Res(\phi)$ *against SRM iterations when* $\xi = 0.3, 0.5, 0.7, 0.9,\ Ha = 1,\ Sc = 0.6,\ \gamma = 1,\ \lambda = 1,\ N = 1,$ *grid ponts* $N_t = 5000,\ L = 30,$ *and* $N_x = 100.$

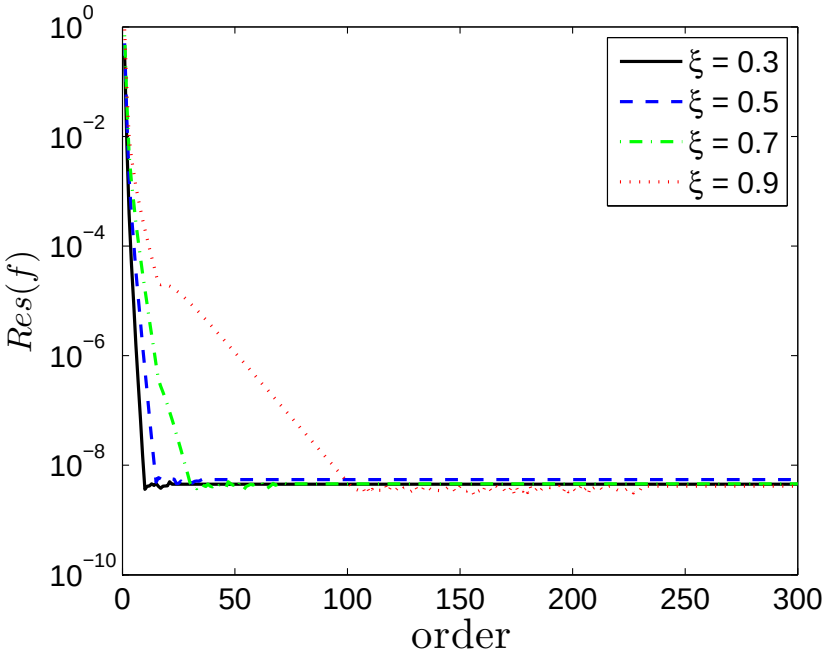

Figure 3.22: *Residual error curve* $Res(f)$ *against increasing SPM approximation order when* $\xi = 0.3, 0.5, 0.7, 0.9,\ Ha = 1,\ Sc = 0.6,\ \gamma = 1,\ \lambda = 1,\ N = 1,$ *grid pontsN*$_t = 5000,\ L = 30,$ *and* $N_x = 100.$

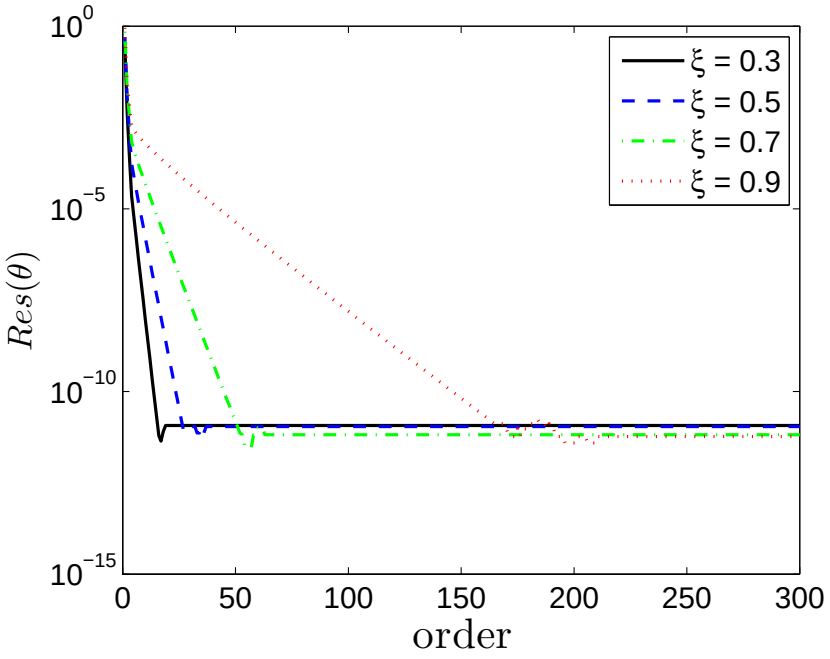

Figure 3.23: *Residual error curve* $Res(\theta)$ *against increasing SPM approximation order when* $\xi = 0.3, 0.5, 0.7, 0.9,\ Ha = 1,\ Sc = 0.6,\ \gamma = 1,\ \lambda = 1,\ N = 1,\ L = 30,$ *and* $N_x = 100$.

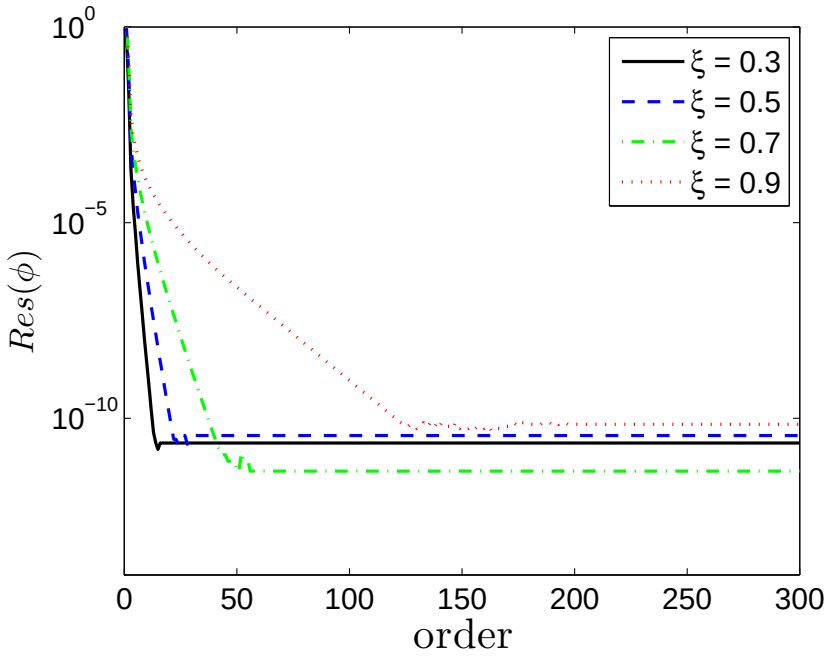

Figure 3.24: *Residual error curve* $Res(\phi)$ *against increasing SPM approximation order when* $\xi = 0.3, 0.5, 0.7, 0.9,\ Ha = 1,\ Sc = 0.6,\ \gamma = 1,\ \lambda = 1,\ N = 1,\ L = 30,$ *and* $N_x = 100$.

consistent with those of Hayat et al. (2010).

Figures 3.19 - 3.21 displays the variation of the SRM residual errors in f, θ and ϕ respectively against the number of iterations. The results are given for different values of the time ξ. From the graphs, it can be seen that for small value of time ξ, convergence to accurate result to within a specific level below 10^{-10} can be achieved with few iterations of the SRM. In addition, it can be observed from the Figures that the residual error curves for $f(\xi, \eta)$, $\theta(\xi, \eta)$, $\phi(\xi, \eta)$ level at a certain level below 10^{-10} for all values of ξ considered.

Figures 3.22 - 3.24 shows the residual error in f, θ and ϕ respectively, against increasing orders of the SPM approximation at different values of time ξ. It can be observed that the residual errors decrease sharply with an increase in the order of approximation. Also, it can be seen that the residual error curves tend to plateau at more or less a fixed level for the different values of time ξ considered. The interpretation of these results is that the SPM will converge up to a specific saturation level which corresponds to the level at which the curves levels off. In the equation for $f(\xi, \eta)$, the residual error curve levels off at a fixed level below 10^{-8} for all values of ξ. In the equation for $\theta(\xi, \eta)$, it can be seen that the residual error curve levels off at a certain level below 10^{-10} and below 10^{-10} in the equation for $\phi(\xi, \eta)$. Furthermore, we note that as ξ approaches 1, the plateau is reached at higher orders of the SPM approximation. This observation is in line with the results presented in Tables 3.7 - 3.9 where it was noted that when ξ is small, only few terms of the SPM approximation are required to obtain converged results that are accurate up to eight decimal digits and more terms are required as ξ tends closer to 1. In addition, this observation can be linked with the well known fact that the standard perturbation based methods give accurate results when the series expansion is with respect to a small parameter. It is interesting to note that with the SPM, accurate results can be obtained even when ξ approaches 1, albeit with a higher orders of the SPM approximation.

4

Unsteady Three Dimensional MHD Flow and Mass Transfer in a Porous Space

4.1. Introduction

The investigations of boundary layer flow and heat transfer problems due to a stretching sheet have attracted much attention from researchers due to its applications in various engineering and manufacturing processes (Takhar et al., 2001; Kumari and Nath, 2009; Hayat et al., 2010). Such engineering applications include cooling of metallic sheets and aerodynamic extrusion of plastic sheets (Hayat et al., 2010). In addition, applications in manufacturing processes occur in glass blowing, metal extrusion, spinning of metal, fiber spinning, continuous casting and continuous stretching of plastic films (Kumari and Nath, 2009; Hayat et al., 2010). Magneto-hydrodynamic (MHD) flow also plays a crucial role in the metallurgical process such as annealing, drawing and copper wire thinning (Kumari and Nath, 2009).

In recent years, literature surveys established that many researchers have diverted their attention towards unsteady flows. In this chapter, the unsteady three dimensional MHD flow and mass transfer in a porous space described by systems of partial differential equations PDEs was investigated. Many researchers have utilized the Williams and Rhyne (1980) transformation to find solutions of different aspect of the unsteady three dimensional boundary layer flow problems using various analytical and numerical methods. These includes Takhar et al. (2001) who numerically solved the equations for unsteady three-dimensional MHD boundary layer flow due to the impulsive motion of a stretching surface using the implicit finite difference method. The homotopy analysis was used by Kumari and Nath (2009) to generate analytical solution of unsteady three-dimensional MHD boundary layer flow

and heat transfer due to an impulsively stretched plane surface. Mehmood et al. (2008) presented an analytic solution obtained by homotopy analysis for unsteady three dimensional MHD boundary-layer flow due to the impulsive motion of a stretching surface. Hayat et al. (2010) employed the homotopy analysis method to unsteady three dimensional MHD flow and mass transfer in a porous space. Series solutions of unsteady three-dimensional MHD flow and heat transfer in the boundary layer over an impulsively stretching plate were presented by Xu et al. (2007). Numerical investigation of unsteady three-dimensional MHD flow and mass transfer in a porous space in the presence of thermal radiation was carried out Olanrewaju et al. (2012) using the sixth-order Runge-Kutta Fehlberg method with shooting technique.

In this chapter, we aimed at extending the use of the spectral perturbation method (SPM) to a four systems of equations. The equation modeling an unsteady three dimensional MHD flow and mass transfer in a porous space previously studied by Hayat et al. (2010) was considered in this chapter. The use and accuracy of the SPM has been demonstrated in Chapters 2 and 3. We showed that the SPM can be used as an alternative numerical approach for solving both nonlinear ODEs and PDEs. In the research by Hayat et al. (2010), an analytic approach was used for the solution of this same problem and only graphical results were reported. Numerical simulations of the equations using the spectral perturbation method (SPM) and the spectral relaxation method (SRM) is conducted. Results generated using the spectral perturbation method (SPM) are compared and validated using the spectral relaxation method (SRM) and the two methods show good agreement.

4.2. Mathematical Formulation

Following Takhar et al. (2001) and Hayat et al. (2010), an unsteady three dimensional flow of a viscous fluid over a stretching surface is examined. The fluid is an electrically conducting fluid in the presence of a fixed applied magnetic field B_0. The magnetic field B_0 is applied in the $z-$direction. It is assumed that the magnetic Reynolds number is small, i.e $Rm = \mu_0\, \sigma V L \ll 1$, where μ_0 is the magnetic permeability, σ is the electrical conductivity and V, L are the characteristic velocity and length respectively. The induced magnetic field is neglected under the assumption of small magnetic Reynolds number. Initially (for $t = 0$), both the fluid and the plate are stationary and have constant temperature T_∞ and concentration C_∞. At $t = 0$, the velocity components $u = ax$, $v = by$ (where u and v are the velocity in the x and y direction respectively). The surface temperature

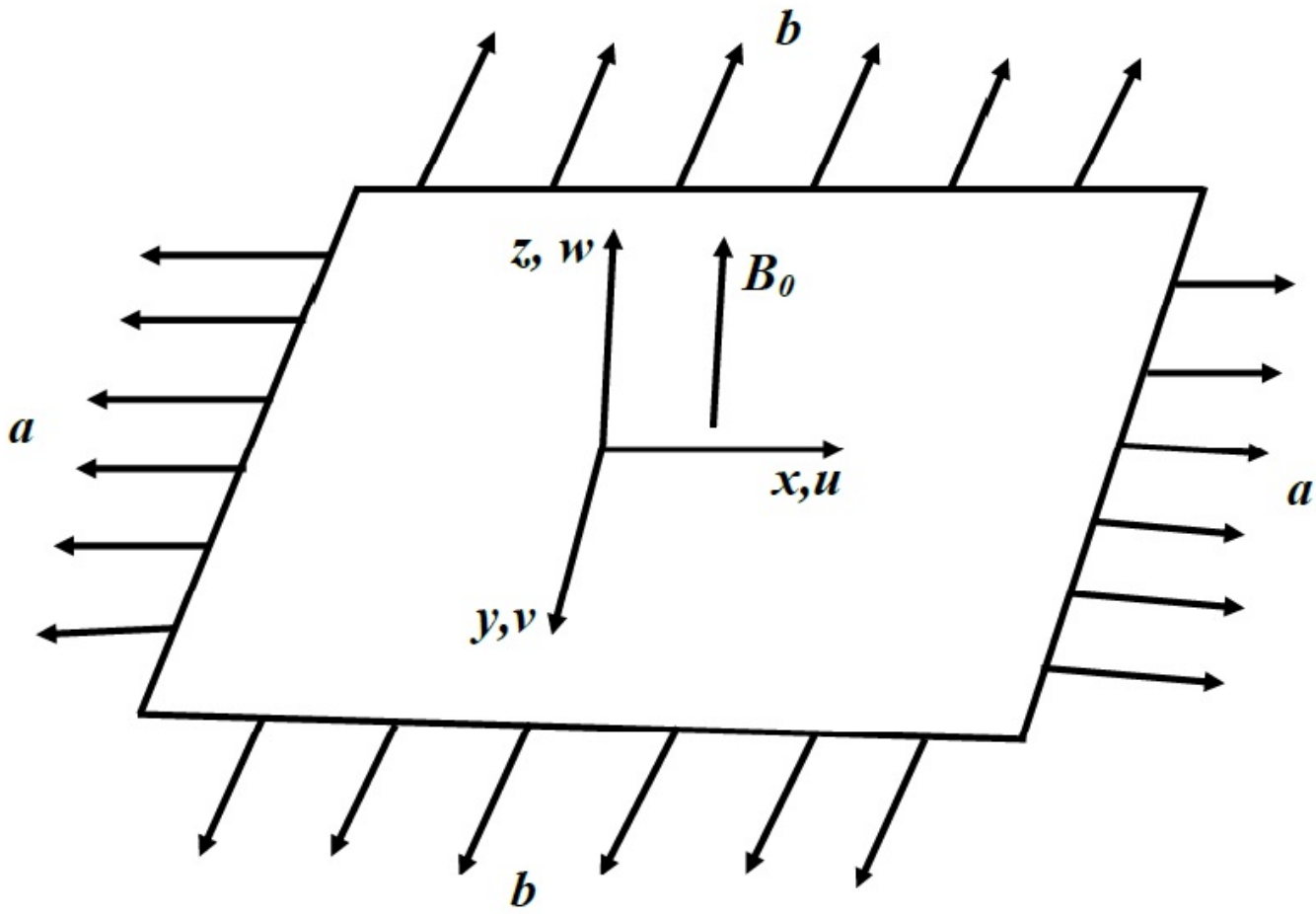

Figure 4.1: *Flow model and physical coordinate system.*

and concentration vary from T_∞ to $T_w\,(T_w > T_\infty)$ and C_∞ to $C_w\,(C_w > C_\infty)$. The physical model and coordinate system are depicted in Figure 4.1. With these assumptions, the simplified basic mathematical expression for the boundary layer equations governing the unsteady three dimensional magnetohydrodynamics (MHD) flow and mass transfer in a porous space were given by Hayat et al. (2010) as;

$$\frac{\partial u}{\partial x} + \frac{\partial v}{\partial y} + \frac{\partial w}{\partial z} = 0, \tag{4.1}$$

$$\frac{\partial u}{\partial t} + u\frac{\partial u}{\partial x} + v\frac{\partial u}{\partial y} + w\frac{\partial u}{\partial z} = \nu\frac{\partial^2 u}{\partial z^2} - \frac{\sigma B_0^2}{\rho}u - \frac{\nu\varphi}{k}u, \tag{4.2}$$

$$\frac{\partial v}{\partial t} + u\frac{\partial v}{\partial x} + v\frac{\partial v}{\partial y} + w\frac{\partial v}{\partial z} = \nu\frac{\partial^2 \nu}{\partial z^2} - \frac{\sigma B_0^2}{\rho}\nu - \frac{\nu\varphi}{k}\nu, \tag{4.3}$$

$$\frac{\partial T}{\partial t} + u\frac{\partial T}{\partial x} + \nu\frac{\partial T}{\partial y} + w\frac{\partial T}{\partial z} = \alpha\frac{\partial^2 T}{\partial z^2}, \tag{4.4}$$

$$\frac{\partial C}{\partial t} + u\frac{\partial C}{\partial x} + v\frac{\partial C}{\partial y} + w\frac{\partial C}{\partial z} = D\frac{\partial^2 C}{\partial z^2} - k_1 C. \tag{4.5}$$

Here $x, y,$ and z are the longitudinal, the transverse and the normal directions respectively. $u, v,$ and$w$ are the velocity components in the $x-y-$ and z-directions respectively, B_0 is the magnetic field applied in the $z-$ direction, ρ is the fluid density, ν is the kinematic viscosity, σ is the electrical conductivity, φ is the porosity, k is the permeability of the porous medium, C is the concentration species of the fluid, D is the diffusion coefficient of the diffusion species in the fluid and k_1 connotes the first-order homogeneous constant reaction rate.

The corresponding boundary conditions are given by Hayat et al. (2010) which are in the format

$$\begin{aligned}
&u = v = w, \quad T = T_\infty, \quad C = C_\infty, \quad t < 0,\\
&u = u_w = ax, \quad v = v_w = by, \quad w = 0, \quad T = T_w, \quad C = C_w, \quad z = 0; t \geq 0,\\
&u \to 0, \quad v \to 0, \quad T \to 0, \quad C \to 0, \quad asz \to \infty; \quad t \geq 0,
\end{aligned} \tag{4.6}$$

where the constants a and b are positive.

Further, it is convenient to choose time scale ξ so that the region of the time integration can be finite. Such transformations were introduced by Williams and Rhyne (1980). The transformations are expressed as;

$$\xi = 1 - \exp(-\tau), \quad \tau = at, \tag{4.7}$$

with b being a positive constant and t is the time variable. The Williams and Rhyne (1980) transformation (4.7) were used to convert from the infinite (original) time scale $0 \leq \tau < \infty$ to the finite scale $0 \leq \xi \leq 1$ so that the interval of integration is collapsed from an infinite domain to a finite domain.

The similarity variables given by Hayat et al. (2010) were utilized and are defined as;

$$\eta = \sqrt{\frac{a}{v\xi}}z, \quad u = ax\frac{\partial f}{\partial \eta}, \quad v = ay\frac{\partial g}{\partial \eta}, \quad w = -\sqrt{av\xi}(f+g),$$
$$\theta = \frac{T - T_\infty}{T_w - T_\infty}, \quad \phi = \frac{C - C_\infty}{C_w - C_\infty}. \tag{4.8}$$

Equation (4.1) is satisfied identically and equations (4.2) - (4.5) become :

$$f''' + (1-\xi)\left(\frac{\eta}{2}f'' - \xi\frac{\partial f'}{\partial \xi}\right) + \xi\left[(f+g)f'' - (f')^2 - M^2 f' - \lambda f'\right] = 0, \tag{4.9}$$

$$g''' + (1-\xi)\left(\frac{\eta}{2}g'' - \xi\frac{\partial g'}{\partial \xi}\right) + \xi\left[(f+g)g'' - (g')^2 - M^2 g' - \lambda g'\right] = 0, \tag{4.10}$$

$$\theta'' + Pr(1-\xi)\left(\frac{\eta}{2}\theta' - \xi\frac{\partial \theta}{\partial \xi}\right) + Pr\xi(f+g)\theta' = 0, \tag{4.11}$$

$$\phi'' + Sc(1-\xi)\left(\frac{\eta}{2}\phi' - \xi\frac{\partial \phi}{\partial \xi}\right) + Sc\xi\ (f+g)\phi' - \gamma Sc\xi\phi = 0, \tag{4.12}$$

subject to the boundary conditions

$$f(\xi,0) = 0, \quad f'(\xi,0) = 1, \quad f'(\xi,\infty) = 0, \tag{4.13}$$

$$g(\xi,0) = c, \quad g'(\xi,0) = 1, \quad g'(\xi,\infty) = 0, \tag{4.14}$$

$$\theta(\xi,0) = 1, \quad \theta(\xi,\infty) = 0, \tag{4.15}$$

$$\phi(\xi,0) = 1, \quad \phi(\xi,\infty) = 0. \tag{4.16}$$

In the above equations, the prime denotes the derivative with respect to η, ($c = b/a$ which indicate that the stretching sheet parameter is a positive constant. The problem reduces to two-dimensional case when $c = 0$. The local Hartman number M, the local porosity parameter λ, the Schmidt number Sc and the chemical reaction parameter γ are defined as;

$$M^2 = \frac{\sigma B_0^2}{\rho a}, \quad \lambda = \frac{\nu\varphi}{ak}, \quad Pr = \frac{\nu}{a}, \quad Sc = \frac{\nu}{D}, \quad \gamma = \frac{k_1}{a}. \tag{4.17}$$

The expressions of the skin friction coefficients $C_{f(x)}$ and $C_{f(y)}$ in $x-$ and $y-$ directions, local Nusselt number Nu and local Sherwood number Sh are given by Hayat et al. (2010) as;

$$C_{fx} = -\mu(\partial u/\partial z)_{z=0}/\rho(ax)^2, \quad C_{fy} = -\mu(\partial v/\partial z)_{z=0}/\rho(ay)^2,$$
$$Nu = \frac{-x(\partial T/\partial z)_{z=0}}{(T_w - T_\infty)}, \quad Sh = \frac{-x(\partial C/\partial z)_{z=0}}{(C_w - C_\infty)}. \tag{4.18}$$

Using similarity variables (4.8), we obtained;

$$Re_x^{1/2}\xi^{1/2}C_{fx} = -f_{\eta\eta}(\xi,0), \quad Re_y^{1/2}\xi^{1/2}C_{fy} = -g_{\eta\eta}(\xi,0),$$
$$NuRe_x^{1/2}\xi^{1/2} = -\theta_\eta(\xi,0), \quad ShRe_x^{1/2}\xi^{1/2} = -\phi_\eta(\xi,0), \tag{4.19}$$

where $Re_x = ax^2/v$ and $Re_y = ay^2/v$ are the local Reynolds number, $f_{\eta\eta}(\xi,0)$ and $g_{\eta\eta}(\xi,0)$ are the surface shear stresses in x and y directions, $\theta_\eta(\xi,0)$ is the surface heat transfer parameter and $\phi_\eta(\xi,0)$ is the surface mass transfer parameter.

For the initial unsteady state flow, when $\xi = 0$, corresponding to $\tau = 0$, equations (4.9 - 4.12) can be written as;

$$f''' + \frac{\eta}{2}f'' = 0, \tag{4.20}$$
$$g''' + \frac{\eta}{2}g'' = 0, \tag{4.21}$$
$$\frac{1}{Pr}\theta'' + \frac{\eta}{2}\theta' = 0, \tag{4.22}$$
$$\frac{1}{Sc}\phi'' + \frac{\eta}{2}\phi' = 0, \tag{4.23}$$

subject to the boundary conditions,

$$f(0) = 0,\ f'(0) = 1,\ f'(\infty) = 0,$$
$$g(0) = 0,\ g'(0) = c,\ g'(\infty) = 0,$$
$$\theta(0) = 1,\ \theta(\infty) = 0,$$
$$\phi(0) = 1,\ \phi(\infty) = 0. \tag{4.24}$$

Equations (4.9 - 4.12) together with the boundary conditions (4.13 - 4.16) admit the closed form analytical solution for the initial unsteady state when $\xi = 0$ which are regarded as the solution of

the equations. They are given by Hayat et al. (2010) as;

$$f(0,\eta) = \eta \operatorname{erfc}\left(\frac{\eta}{2}\right) + \frac{2}{\sqrt{\pi}}\left[1 - \exp\left(-\frac{\eta^2}{4}\right)\right], \tag{4.25}$$

$$g(0,\eta) = c\left(\eta \operatorname{erfc}\left(\frac{\eta}{2}\right) + \frac{2}{\sqrt{\pi}}\left[1 - \exp\left(-\frac{\eta^2}{4}\right)\right]\right), \tag{4.26}$$

$$\theta(0,\eta) = \operatorname{erfc}\left(\frac{\sqrt{Pr}\eta}{2}\right), \tag{4.27}$$

$$\phi(0,\eta) = \operatorname{erfc}\left(\frac{\sqrt{Sc}\eta}{2}\right), \tag{4.28}$$

where

$$\operatorname{erfc}(\eta) = 1 - \frac{2}{\sqrt{\pi}}\int_0^{\eta} \exp(-s^2)\mathrm{d}s. \tag{4.29}$$

4.3. Method of solution

In this section, the spectral perturbation method (SPM) was used to solve the partial differential equations (4.9-4.12) subject to the boundary conditions (4.13 - 4.16). Below, the use of the spectral perturbation method on the unsteady three dimensional MHD flow and mass transfer equations is demonstrated.

4.3.1 Spectral Perturbation Method (SPM)

In the spectral perturbation method (SPM), series solutions were generated using the usual perturbation approach and then integration was done numerically in the space direction η using the Chebyshev spectral collocation method. Following Seshadri et al. (2002); Nazar et al. (2004a); Liao (2006b), a series expansion was constructed to approximate $f(\xi,\eta)$, $g(\xi,\eta)$, $\theta(\xi,\eta)$, and $\phi(\xi,\eta)$ solution by regarding ξ as a small parameter and looking for a perturbation approximation in the

form

$$f(\xi,\eta)=\sum_{k=0}^{+\infty}\xi^k f_k(\eta) \tag{4.30}$$

$$g(\xi,\eta)=\sum_{k=0}^{+\infty}\xi^k g_k(\eta) \tag{4.31}$$

$$\theta(\xi,\eta)=\sum_{k=0}^{+\infty}\xi^k \theta_k(\eta), \tag{4.32}$$

$$\phi(\xi,\eta)=\sum_{k=0}^{+\infty}\xi^k \phi_k(\eta). \tag{4.33}$$

Substituting (4.30 - 4.33) in equations (4.9 - 4.13) and balancing terms of equal power of ξ, we obtain

$$f_0'''+\frac{\eta}{2}f_0''=0,\quad f_0(0)=0,\quad f_0'(0)=1,\quad f_0'(\infty)=0, \tag{4.34}$$

$$g_0'''+\frac{\eta}{2}g_0''=0,\quad g_0(0)=0,\quad g_0'(0)=c,\quad g_0'(\infty)=0, \tag{4.35}$$

$$\theta_0''+Pr\frac{\eta}{2}\theta_0'=0,\quad \theta_0(0)=1,\quad \theta_0(\infty)=0, \tag{4.36}$$

$$\phi_0''+Sc\frac{\eta}{2}\phi_0'=0,\quad \phi_0(0)=1,\quad \phi_0(\infty)=0 \tag{4.37}$$

$$f_k'''+\frac{\eta}{2}f_k''-kf_k'=\frac{\eta}{2}f_{k-1}''-(k-1)f_{k-1}'+M^2f_{k-1}'+\lambda f_{k-1}'$$
$$+\sum_{n=0}^{k-1}\left[f_{k-1-n}'f_n'-f_{k-1-n}f_n''-g_{k-1-n}f_n''\right] \tag{4.38}$$

$$f_k(0)=0,\quad f_k'(0)=1,\quad f_k'(\infty)=0,\quad k\geq 1. \tag{4.39}$$

$$g_k'''+\frac{\eta}{2}g_k''-kg_k'=\frac{\eta}{2}g_{k-1}''-(k-1)g_{k-1}'+M^2g_{k-1}'+\lambda g_{k-1}'$$
$$+\sum_{n=0}^{k-1}\left[g_{k-1-n}'g_n'-f_{k-1-n}g_n''-g_{k-1-n}g_n''\right] \tag{4.40}$$

$$g_k(0)=0,\quad g_k'(0)=1,\quad g_k'(\infty)=0,\quad k\geq 1. \tag{4.41}$$

$$\theta_k''+\frac{\eta}{2}Pr\theta_k'-Prk\theta_k=\frac{\eta}{2}Pr\theta_{k-1}'-(k-1)\theta_{k-1}$$
$$-\sum_{n=0}^{k-1}\Pr\left[f_{k-1-n}\theta_n'+g_{k-1-n}\theta_n'\right] \tag{4.42}$$

$$\theta_k(0)=0,\quad \theta_k(\infty)=0,\quad k\geq 1. \tag{4.43}$$

$$\phi_k''+\frac{\eta}{2}Sc\phi_k'-Sck\phi_k=\frac{\eta}{2}Sc\phi_{k-1}'-(k-1)\phi_{k-1}+\gamma Sc\phi_{k-1}$$
$$-\sum_{n=0}^{k-1}Sc\left[f_{k-1-n}\phi_n'+g_{k-1-n}\phi_n'\right] \tag{4.44}$$

$$\phi_k(0)=0,\quad \phi_k(\infty)=0,\quad k\geq 1. \tag{4.45}$$

The Chebyshev spectral collocation method was used to integrate equations (4.38 - 4.45). The differential matrix D was used to approximate the derivatives of the unknown variables $f_k(\xi,\eta), g_k(\xi,\eta), \theta_k(\xi,\eta), \phi_k(\xi,$ at the collocation points and can be defined as;

$$\left.\frac{df_k}{d\eta}\right|_{\eta=\eta j} = \sum_{l=0}^{N_x} \mathbf{D}_{jl} f_k(x_l) = \mathbf{D}F_k, \quad j = 0, 1, ..., N_x, \tag{4.46}$$

$$\left.\frac{dg_k}{d\eta}\right|_{\eta=\eta j} = \sum_{l=0}^{N_x} \mathbf{D}_{jl} g_k(x_l) = \mathbf{D}G_k, \quad j = 0, 1, ..., N_x, \tag{4.47}$$

$$\left.\frac{d\theta_k}{d\eta}\right|_{\eta=\eta j} = \sum_{l=0}^{N_x} \mathbf{D}_{jl} \theta_k(x_l) = \mathbf{D}\Theta_k, \quad j = 0, 1, ..., N_x, \tag{4.48}$$

$$\left.\frac{d\phi_k}{d\eta}\right|_{\eta=\eta j} = \sum_{l=0}^{N_x} \mathbf{D}_{jl} \phi_x(x_l) = \mathbf{D}\Phi_k, \quad j = 0, 1, ..., N_x, \tag{4.49}$$

where $N_x + 1$ is the number of collocation points, $\mathbf{D} = 2D/L$, and

$$\mathbf{F}_k = [f_k(x_0), f_k(x_1), ..., f_k(x_{N_x})]^T, \tag{4.50}$$

$$\mathbf{G}_k = [g_k(x_0), f_k(x_1), ..., f_k(x_{N_x})]^T, \tag{4.51}$$

$$\mathbf{\Theta}_k = [\theta_k(x_0), \theta_k(x_1), \cdots, \theta_k(x_{N_x})]^T, \tag{4.52}$$

$$\mathbf{\Phi}_k = [\phi_k(x_0), \phi_k(x_1), \cdot, \phi_k(x_{N_x})]^T, \tag{4.53}$$

is the vector function at the collocation points. The higher order derivatives was obtained as power of $\mathbf{D}$, that is

$$F_k^{(p)} = \mathbf{D}^p F_k, \tag{4.54}$$

$$G_k^{(p)} = \mathbf{D}^p G_k, \tag{4.55}$$

$$\Theta_k^{(p)} = \mathbf{D}^p \Theta_k, \tag{4.56}$$

$$\Phi_k^{(p)} = \mathbf{D}^p \Phi_k, \tag{4.57}$$

where p is the order of the derivatives. The matrix D is of size $(N_x + 1) \times (N_x + 1)$ and its entries are defined in the previous chapters.

Substituting (4.46 - 4.57) in (4.38 - 4.45) gives

$$\mathbf{A}_{1,k-1}\mathbf{F}_k = \mathbf{B}_{1,k-1}, \tag{4.58}$$

$$\mathbf{A}_{2,k-1}\mathbf{G}_k = \mathbf{B}_{2,k-1}, \tag{4.59}$$

$$\mathbf{A}_{3,k-1}\mathbf{\Theta}_k = \mathbf{B}_{3,k-1}, \tag{4.60}$$

$$\mathbf{A}_{4,k-1}\mathbf{\Phi}_k = \mathbf{B}_{4,k-1}, \tag{4.61}$$

subject to the boundary conditions

$$\sum_{l=0}^{N_x}\mathbf{D}_{0k}f_k(\eta_k) = 0, \quad \sum_{l=0}^{N_x}\mathbf{D}_{N_xk}f_k(\eta_k) = 0, \quad f_k(\eta_{N_x}) = 0, \tag{4.62}$$

$$\sum_{k=0}^{N_x}\mathbf{D}_{0k}g_k(\eta_k) = 0, \quad \sum_{k=0}^{N_x}\mathbf{D}_{N_xk}g_k(\eta_k) = 0, \quad g_k(\eta_{N_x}) = 0, \tag{4.63}$$

$$\theta_k(\eta_{N_x}) = 0, \quad \theta_k(\eta_0) = 0, \tag{4.64}$$

$$\phi_k(\eta_{N_x}) = 0, \quad \phi_k(\eta_0) = 0. \tag{4.65}$$

The coefficients $\mathbf{A}_{1,k-1}, \mathbf{A}_{2,k-1}, \mathbf{A}_{3,k-1}, \mathbf{A}_{4,k-1}, \mathbf{B}_{1,k-1}, \mathbf{B}_{2,k-1}, \mathbf{B}_{3,k-1}$ and $\mathbf{B}_{4,k-1}$ are defined as;

$$\mathbf{A}_{1,k-1} = \mathbf{D}^3 + \mathrm{diag}\left(\frac{\boldsymbol{\eta}}{\mathbf{2}}\right)\mathbf{D}^2 - k\mathbf{D} \tag{4.66}$$

$$\mathbf{A}_{2,k-1} = \mathbf{D}^3 + \mathrm{diag}\left(\frac{\boldsymbol{\eta}}{\mathbf{2}}\right)\mathbf{D}^2 - k\mathbf{D}, \tag{4.67}$$

$$\mathbf{A}_{3,k-1} = \mathbf{D}^2 + \mathrm{diag}\left(\frac{\boldsymbol{\eta}}{\mathbf{2}}Pr\right)\mathbf{D} - k\,Pr\mathbf{I}, \tag{4.68}$$

$$\mathbf{A}_{4,k-1} = \mathbf{D}^2 + \mathrm{diag}\left(\frac{\boldsymbol{\eta}}{\mathbf{2}}Sc\right)\mathbf{D} - k\,Sc\mathbf{I}, \tag{4.69}$$

$$\mathbf{B}_{1,k-1} = \frac{\eta}{2}\left(\mathbf{D}^2\mathbf{F}_{k-1}\right) - (k-1)\,\mathbf{D}\mathbf{F}_{k-1} + M^2\left(\mathbf{D}\mathbf{F}_{k-1}\right) + \lambda\left(\mathbf{D}\mathbf{F}_{k-1}\right) + \mathrm{Sum}\mathbf{F}, \tag{4.70}$$

$$\mathbf{B}_{2,k-1} = \frac{\eta}{2}\left(\mathbf{D}^2\mathbf{G}_{k-1}\right) - (k-1)\,\mathbf{D}\mathbf{G}_{k-1} + M^2\left(\mathbf{D}\mathbf{G}_{k-1}\right) + \lambda\left(\mathbf{D}\mathbf{G}_{k-1}\right) + \mathrm{Sum}\mathbf{G}, \tag{4.71}$$

$$\mathbf{B}_{3,k-1} = \frac{\eta}{2}Pr\left(\mathbf{D}\mathbf{\Theta}_{k-1}\right) - Pr\,(k-1)\,\mathbf{\Theta}_{k-1} - \mathrm{Sum}\mathbf{\Theta}, \tag{4.72}$$

$$\mathbf{B}_{4,k-1} = \frac{\eta}{2}Sc\left(\mathbf{D}\mathbf{\Phi}_{k-1}\right) - Sc\,(k-1)\,\mathbf{\Phi}_{k-1} + \gamma Sc\mathbf{\Phi}_{k-1} - \mathrm{Sum}\mathbf{\Phi}, \tag{4.73}$$

where $\boldsymbol{\eta} = [\eta_0, \eta_1, \cdots \eta_{N_x},]$, and Sum$\mathbf{F}$, Sum$\mathbf{G}$, Sum$\boldsymbol{\Theta}$, and Sum$\boldsymbol{\Phi}$, are defined as

$$\begin{aligned}
\text{Sum}\mathbf{F} &= \sum_{i=0}^{k-1} \left[(\mathbf{DF}_{k-1-i})(\mathbf{DF}_i) - \mathbf{F}_{k-1-i}\left(\mathbf{D}^2\mathbf{F}_i\right) - \mathbf{G}_{k-1-i}\left(\mathbf{D}^2\mathbf{F}_i\right) \right], \\
\text{Sum}\mathbf{G} &= \sum_{i=0}^{k-1} \left[(\mathbf{DF}_{k-1-i})(\mathbf{DF}_i) - \mathbf{F}_{k-1-i}\left(\mathbf{D}^2\mathbf{F}_i\right) - \mathbf{G}_{k-1-i}\left(\mathbf{D}^2\mathbf{G}_i\right) \right], \\
\text{Sum}\boldsymbol{\Theta} &= Pr \sum_{i=0}^{k-1} \left[\mathbf{F}_{k-1-i}(\mathbf{D}\boldsymbol{\Theta}_i) + \mathbf{G}_{k-1-i}(\mathbf{D}\boldsymbol{\Theta}_i) \right], \\
\text{Sum}\boldsymbol{\Phi} &= Sc \sum_{i=0}^{k-1} \left[\mathbf{F}_{k-1-i}(\mathbf{D}\boldsymbol{\Theta}_i) + \mathbf{G}_{k-1-i}(\mathbf{D}\boldsymbol{\Phi}_i) \right],
\end{aligned}$$

with $\mathbf{I}$ representing an $(N_x+1)\times(N_x+1)$ identity matrix and diag() is a diagonal matrix obtained from the vector $(x_0, x_1, ..., x_{N_x},)$. The boundary conditions (4.62) and (4.63) were imposed on the first , $N_x th$ row (second from the last row) and (N_x+1)st row (last row) rows and first and last columns of (4.58) and (4.59) to obtain

$$\left[\begin{array}{c|ccc|c}
\mathbf{D}_{0,0} & \mathbf{D}_{0,1} & \cdots & \mathbf{D}_{0,N_x-1} & \mathbf{D}_{0,N_x} \\ \hline
 & & \mathbf{A}_{1,k-1} & & \\ \hline
\mathbf{D}_{N_x,0} & \mathbf{D}_{N_x,1} & \cdots & \mathbf{D}_{N_x,N_x-1} & \mathbf{D}_{N_x,N_x} \\ \hline
0 & 0 & \cdots & 0 & 1
\end{array}\right]
\left[\begin{array}{c} f_k(x_0) \\ \hline f_k(x_1) \\ \vdots \\ \vdots \\ \hline f_k(x_{N_x-1}) \\ \hline f_k(x_{N_x}) \end{array}\right]
=
\left[\begin{array}{c} 0 \\ \hline B_{1,k-1}(x_1) \\ \vdots \\ B_{1,k-1}(x_{N_x-1}) \\ \hline 0 \\ \hline 0 \end{array}\right], \tag{4.74}$$

$$\left[\begin{array}{c|ccc|c}
\mathbf{D}_{0,0} & \mathbf{D}_{0,1} & \cdots & \mathbf{D}_{0,N_x-1} & \mathbf{D}_{0,N_x} \\ \hline
 & & \mathbf{A}_{2,k-1} & & \\ \hline
\mathbf{D}_{N_x,0} & \mathbf{D}_{N_x,1} & \cdots & \mathbf{D}_{N_x,N_x-1} & \mathbf{D}_{N_x,N_x} \\ \hline
0 & 0 & \cdots & 0 & 1
\end{array}\right]
\left[\begin{array}{c} g_k(x_0) \\ \hline g_k(x_1) \\ \vdots \\ \vdots \\ \hline g_k(x_{N_x-1}) \\ \hline g_k(x_{N_x}) \end{array}\right]
=
\left[\begin{array}{c} 0 \\ \hline B_{2,k-1}(x_1) \\ \vdots \\ B_{2,k-1}(x_{N_x-1}) \\ \hline 0 \\ \hline 0 \end{array}\right], \tag{4.75}$$

while the boundary conditions (4.64) and (4.65) were imposed on the first and last rows and columns

of equations (4.60) and (4.61) respectively to obtain

$$\left[\begin{array}{c|ccc|c} 1 & 0 & \cdots & 0 & 0 \\ \hline & & & & \\ & & \mathbf{A}_{3,k-1} & & \\ & & & & \\ \hline 0 & 0 & \cdots & 0 & 1 \end{array}\right] \left[\begin{array}{c} \theta_k(x_0) \\ \hline \theta_k(x_1) \\ \vdots \\ \vdots \\ \hline \theta_k(x_{N_x}) \end{array}\right] = \left[\begin{array}{c} 0 \\ \hline B_{3,k-1}(x_1) \\ \vdots \\ B_{3,k-1}(x_{N_x-1}) \\ \hline 0 \end{array}\right], \tag{4.76}$$

and

$$\left[\begin{array}{c|ccc|c} 1 & 0 & \cdots & 0 & 0 \\ \hline & & & & \\ & & \mathbf{A}_{4,k-1} & & \\ & & & & \\ \hline 0 & 0 & \cdots & 0 & 1 \end{array}\right] \left[\begin{array}{c} \phi_k(x_0) \\ \hline \phi_k(x_1) \\ \vdots \\ \vdots \\ \hline \phi_k(x_{N_x}) \end{array}\right] = \left[\begin{array}{c} 0 \\ \hline B_{4,k-1}(x_1) \\ \vdots \\ B_{4,k-1}(x_{N_x-1}) \\ \hline 0 \end{array}\right]. \tag{4.77}$$

Hence, starting from a known $F_0, G_0, \Theta_0, \Phi_0$, the solutions $F_k, G_k, \Theta_k, \Phi_k$, $k \geq 1$ can be obtained as;

$$F_k = \mathbf{A}_{1,k-1}^{-1}\mathbf{B}_{1,k-1}, \tag{4.78}$$

$$G_k = \mathbf{A}_{2,k-1}^{-1}\mathbf{B}_{2,k-1}, \tag{4.79}$$

$$\Theta_k = \mathbf{A}_{3,k-1}^{-1}\mathbf{B}_{3,k-1}, \tag{4.80}$$

$$\Phi_k = \mathbf{A}_{4,k-1}^{-1}\mathbf{B}_{4,k-1}. \tag{4.81}$$

4.3.2 Spectral Relaxation Method (SRM)

In this section, the development of the spectral relaxation method (SRM) to obtain solution of the partial differential equations (4.9 - 4.12) is discussed. To start the SRM algorithm, we first set $f' = u$ and $g' = v$, so that equations (4.9) and (4.10) becomes

$$u'' + (1-\xi)\left(\frac{\eta}{2}u' - \xi\frac{\partial u}{\partial \xi}\right) + \xi\left[(f+g)u' - u^2 - M^2u - \lambda u\right] = 0, \tag{4.82}$$

$$v'' + (1-\xi)\left(\frac{\eta}{2}v' - \xi\frac{\partial v}{\partial \xi}\right) + \xi\left[(f+g)v' - v^2 - M^2v - \lambda v\right] = 0. \tag{4.83}$$

The spectral relaxation method (SRM) (Motsa et al., 2012, 2013, 2014; Kameswaran et al., 2013,

2014; Motsa and Makukula, 2013; Motsa, 2014; Shateyi, 2013; Shateyi and Marewo, 2013; Shateyi and Makinde, 2013; Shateyi and Prakash, 2014; Makukula et al., 2014; Sibanda et al., 2014) utilizes the Gauss-Seidel idea to decouple nonlinear systems of equations (4.9) - (4.12). From the decoupled equations, an iteration scheme was developed by evaluating linear terms in the current iteration level denoted by $(r+1)$, and nonlinear terms in the previous iteration level denoted by (r). Implementing the SRM on the resulting systems of nonlinear partial differential equations yields the following linear partial differential equations;

$$u''_{r+1} + a_{1,r}u'_{r+1} + a_{2,r}u_{r+1} + a_{3,r} = \xi\left(1-\xi\right)\frac{\partial u_{r+1}}{\partial \xi}, \tag{4.84}$$

$$f'_{r+1} = u_{r+1}, \tag{4.85}$$

$$v''_{r+1} + b_{1,r}v'_{r+1} + b_{2,r}v_{r+1} + b_{3,r} = \xi\left(1-\xi\right)\frac{\partial v_{r+1}}{\partial \xi}, \tag{4.86}$$

$$g'_{r+1} = v_{r+1}, \tag{4.87}$$

$$\theta''_{r+1} + c_{1,r}\theta'_{r+1} = \xi\left(1-\xi\right)\frac{\partial \theta_{r+1}}{\partial \xi}, \tag{4.88}$$

$$\phi''_{r+1} + d_{1,r}\phi'_{r+1} + d_{2,r}\phi_{r+1} = \xi\left(1-\xi\right)\frac{\partial \phi_{r+1}}{\partial \xi}, \tag{4.89}$$

$$u_{r+1}(0,\xi) = \theta_{r+1}(0,\xi) = \phi_{r+1}(0,\xi) = 1,\ f_{r+1}(0,\xi) = g_{r+1}(0,\xi) = 0,$$

$$u_{r+1}(\infty,\xi) = v_{r+1}(\infty,\xi) = \theta_{r+1}(\infty,\xi) = \phi_{r+1}(\infty,\xi) = 0,$$

$$v_{r+1}(0,\xi) = c, \tag{4.90}$$

where the coefficient parameters $a_{1,r}, a_{2,r}, a_{3,r}, b_{1,r}, b_{2,r}, b_{3,r}, c_{1,r}, d_{1,r}$ and $d_{2,r}$ are defined as;

$$\begin{aligned}
a_{1,r} &= \frac{1}{2}\eta\left(1-\xi\right) + \xi\left(f_r + g_r\right), \quad a_{2,r} = -\xi\left(M^2+\lambda\right), \quad a_{3,r} = -\xi u_r^2,\\
b_{1,r} &= \frac{1}{2}\eta\left(1-\xi\right) + \xi\left(f_r + g_r\right), \quad b_{2,r} = -\xi\left(M^2+\lambda\right), \quad b_{3,r} = -\xi v_r^2,\\
c_{1,r} &= Pr\left(\frac{1}{2}\eta\left(1-\xi\right) + \xi\left(f_r + g_r\right)\right),\\
d_{1,r} &= Sc\left(\frac{1}{2}\eta\left(1-\xi\right) + \xi\left(f_r + g_r\right)\right), \quad d_{2,r} = -\gamma Sc\xi.
\end{aligned}$$

The initial approximation for solving equations (4.84 - 4.90) were obtained at $\xi = 0$. Hence, $f_0(\xi,\eta)$

, $g_0(\xi,\eta)$, $\theta_0(\xi,\eta)$, $\phi_0(\xi,\eta)$ were given in equations (4.25 - 4.28) and $u_0(\xi,\eta)$, $v_0(\xi,\eta)$ were given as;

$$u_0(\xi,\eta) = \operatorname{erfc}\left(\frac{\eta}{2}\right), \tag{4.91}$$

$$v_0(\xi,\eta) = c\left[\operatorname{erfc}\left(\frac{\eta}{2}\right)\right]. \tag{4.92}$$

Equations (4.84 - 4.90) can be solved iteratively for the unknown functions starting from the initial approximations given in (4.25- 4.28) and (4.91 - 4.92). The iteration schemes (4.84), (4.86), (4.88) and (4.89) were solved iteratively for $u_{r+1}(\xi,\eta)$, $v_{r+1}(\xi,\eta)$, $\theta_{r+1}(\xi,\eta)$ and $\phi_{r+1}(\xi,\eta)$ when $r = 0, 1, 2, \cdots$ The solutions for u_{r+1} and v_{r+1} were used in (4.85) and (4.87) which were, in turn, solved for f_{r+1} and g_{r+1}. To solve equations (4.84 - 4.89), the equations were discretized using the Chebyshev spectral collocation method in the $\eta-$direction and the implicit finite difference method in the $\xi-$direction. We note that equations (4.84 - 4.89) can be discretized in both directions using the Chebyshev spectral collocation method but the implicit finite difference method was used in the $\xi-$direction because the SRM being used in this study uses finite difference method in this $\xi-$direction. The finite difference scheme was used with centering about a mid-point between ξ^{n+1} and ξ^n. The mid-point is defined as $\xi^{n+\frac{1}{2}} = \left(\xi^{n+1} + \xi^n\right)/2$. Thus, using the centering about $\xi^{n+\frac{1}{2}}$ to any function, say $u(\eta,\xi)$ and its associated derivative we obtain,

$$u\left(\eta_j, \xi^{n+\frac{1}{2}}\right) = u_j^{n+\frac{1}{2}} = \frac{u_j^{n+1} + u_j^n}{2}, \quad \left(\frac{\partial u}{\partial \xi}\right)^{n+\frac{1}{2}} = \frac{u_j^{n+1} - u_j^n}{\Delta\xi}. \tag{4.93}$$

The spectral method was first applied on (4.84 - 4.89), before applying the finite differences to obtain

$$\left[\mathbf{D}^2 + \mathbf{a}_{1,r}\mathbf{D} + \mathbf{a}_{2,r}\right] U_{r+1} + \mathbf{a}_{3,r} = \xi\,(1-\xi)\,\frac{dU_{r+1}}{d\xi}, \tag{4.94}$$

$$u_{r+1}\,(x_0,\xi) = 0, \quad u_{r+1}\,(x_{N_x},\xi) = 1,$$

$$\mathbf{D}F_{r+1} = U_{r+1}, \quad f_{r+1}\,(x_{N_x},\xi) = 0, \tag{4.95}$$

$$\left[\mathbf{D}^2 + \mathbf{b}_{1,r}\mathbf{D} + \mathbf{b}_{2,r}\right] V_{r+1} + \mathbf{b}_{3,r} = \xi\,(1-\xi)\,\frac{dU_{r+1}}{d\xi}, \tag{4.96}$$

$$v_{r+1}\,(x_0,\xi) = 0, \quad v_{r+1}\,(x_{N_x},\xi) = c,$$

$$\mathbf{D}G_{r+1} = V_{r+1}, \quad g_{r+1}\,(x_{N_x},\xi) = 0, \tag{4.97}$$

$$\left[\mathbf{D}^2 + \mathbf{c}_{1,r}\mathbf{D}\right] \Theta_{r+1} = \xi\,(1-\xi)\,\frac{d\Theta_{r+1}}{d\xi}, \tag{4.98}$$

$$\theta_{r+1}\,(x_0,\xi) = 0, \quad \theta_{r+1}\,(x_{N_x},\xi) = 1$$

$$\left[\mathbf{D}^2 + \mathbf{d}_{1,r}\mathbf{D} + \mathbf{d}_{2,r}\right] \Phi_{r+1} = \xi\,(1-\xi)\,\frac{d\Phi_{r+1}}{d\xi}, \tag{4.99}$$

$$\phi_{r+1}\,(x_0,\xi) = 0, \quad \phi_{r+1}\,(x_{N_x},\xi) = 1,$$

where

$$U_{r+1} = \begin{bmatrix} u_{r+1}(x_0,\xi) \\ u_{r+1}(x_1,\xi) \\ \vdots \\ u_{r+1}(x_{N_x-1},\xi) \\ u_{r+1}(x_{N_x},\xi) \end{bmatrix},\ F_{r+1} = \begin{bmatrix} f_{r+1}(x_0,\xi) \\ f_{r+1}(x_1,\xi) \\ \vdots \\ f_{r+1}(x_{N_x-1},\xi) \\ f_{r+1}(x_{N_x},\xi) \end{bmatrix},\ \mathbf{a}_{3,r} = \begin{bmatrix} a_{3,r}(x_0,\xi) \\ a_{3,r}(x_1,\xi) \\ \vdots \\ a_{3,r}(x_{N_x-1},\xi) \\ a_{3,r}(x_{N_x},\xi) \end{bmatrix}, \tag{4.100}$$

$$\mathbf{a}_{1,r} = \begin{bmatrix} a_{1,r}(x_0,\xi) & & & & \\ & a_{1,r}(x_1,\xi) & & & \\ & & \ddots & & \\ & & & \ddots & \\ & & & & a_{1,r}(x_{N_x},\xi) \end{bmatrix}, \tag{4.101}$$

$$\mathbf{a}_{2,r} = \begin{bmatrix} a_{2,r}(x_0,\xi) & & & & \\ & a_{2,r}(x_1,\xi) & & & \\ & & \ddots & & \\ & & & \ddots & \\ & & & & a_{2,r}(x_{N_x},\xi) \end{bmatrix}, \tag{4.102}$$

$$V_{r+1} = \begin{bmatrix} v_{r+1}(x_0,\xi) \\ v_{r+1}(x_1,\xi) \\ \vdots \\ v_{r+1}(x_{N_x-1},\xi) \\ v_{r+1}(x_{N_x},\xi) \end{bmatrix}, \; G_{r+1} = \begin{bmatrix} g_{r+1}(x_0,\xi) \\ g_{r+1}(x_1,\xi) \\ \vdots \\ g_{r+1}(x_{N_x-1},\xi) \\ g_{r+1}(x_{N_x},\xi) \end{bmatrix}, \; \mathbf{b}_{3,r} = \begin{bmatrix} b_{3,r}(x_0,\xi) \\ b_{3,r}(x_1,\xi) \\ \vdots \\ b_{3,r}(x_{N_x-1},\xi) \\ b_{3,r}(x_{N_x},\xi) \end{bmatrix}, \tag{4.103}$$

$$\mathbf{b}_{1,r} = \begin{bmatrix} b_{1,r}(x_0,\xi) & & & & \\ & b_{1,r}(x_1,\xi) & & & \\ & & \ddots & & \\ & & & \ddots & \\ & & & & b_{1,r}(x_{N_x},\xi) \end{bmatrix}, \tag{4.104}$$

$$\mathbf{b}_{2,r} = \begin{bmatrix} b_{2,r}(x_0,\xi) & & & & \\ & b_{2,r}(x_1,\xi) & & & \\ & & \ddots & & \\ & & & \ddots & \\ & & & & b_{2,r}(x_{N_x},\xi) \end{bmatrix}, \tag{4.105}$$

$$\Theta_{r+1} = \begin{bmatrix} \theta_{r+1}(x_0,\xi) \\ \theta_{r+1}(x_1,\xi) \\ \vdots \\ \theta_{r+1}(x_{N_x-1},\xi) \\ \theta_{r+1}(x_{N_x},\xi) \end{bmatrix}, \; \mathbf{c}_{1,r} = \begin{bmatrix} c_{1,r}(x_0,\xi) & & & & \\ & c_{1,r}(x_1,\xi) & & & \\ & & \ddots & & \\ & & & \ddots & \\ & & & & c_{1,r}(x_{N_x},\xi) \end{bmatrix}, \tag{4.106}$$

$$\Phi_{r+1} = \begin{bmatrix} \phi_{r+1}(x_0,\xi) \\ \phi_{r+1}(x_1,\xi) \\ \vdots \\ \phi_{r+1}(x_{N_x-1},\xi) \\ \phi_{r+1}(x_{N_x},\xi) \end{bmatrix}, \ \mathbf{d}_{1,r} = \begin{bmatrix} d_{1,r}(x_0,\xi) & & & & \\ & d_{1,r}(x_1,\xi) & & & \\ & & \ddots & & \\ & & & \ddots & \\ & & & & d_{1,r}(x_{N_x},\xi) \end{bmatrix}, \quad (4.107)$$

$$\mathbf{d}_{2,r} = \begin{bmatrix} d_{2,r}(x_0,\xi) & & & & \\ & d_{2,r}(x_1,\xi) & & & \\ & & \ddots & & \\ & & & \ddots & \\ & & & & d_{2,r}(x_{N_x},\xi) \end{bmatrix}. \quad (4.108)$$

Next, the finite difference scheme was applied to equations (4.94 - 4.99), in the $\xi-$direction with centering about the mid-point $\xi^{n+\frac{1}{2}}$ to obtain the following systems of decoupled equations

$$\mathbf{A}_1 U_{r+1}^{n+1} = \mathbf{B}_1 U_{r+1}^{n} + \mathbf{K}_1, \quad (4.109)$$

$$\mathbf{D} F_{r+1}^{n+1} = U_{r+1}^{n+1}, \quad (4.110)$$

$$\mathbf{A}_2 V_{r+1}^{n+1} = \mathbf{B}_2 V_{r+1}^{n} + \mathbf{K}_2, \quad (4.111)$$

$$\mathbf{D} G_{r+1}^{n+1} = V_{r+1}^{n+1}, \quad (4.112)$$

$$\mathbf{A}_3 \Theta_{r+1}^{n+1} = \mathbf{B}_3 \Theta_{r+1}^{n} + \mathbf{K}_3, \quad (4.113)$$

$$\mathbf{A}_4 \Phi_{r+1}^{n+1} = \mathbf{B}_4 \Phi_{r+1}^{n} + \mathbf{K}_4, \quad (4.114)$$

subject to the following initial and boundary conditions

$$u_{r+1}(x_{N_x},\xi^n)=\theta_{r+1}(x_{N_x},\xi^n)=\phi_{r+1}(x_{N_x},\xi^n)=1,\quad v_{r+1}(x_{N_x},\xi^n)=c, \tag{4.115}$$

$$u_{r+1}(x_0,\xi^n)=\theta_{r+1}(x_0,\xi^n)=\phi_{r+1}(x_0,\xi^n)=1,\quad v_{r+1}(x_0,\xi^n)=0, \tag{4.116}$$

$$f_{r+1}(x_{N_x},\xi^n)=g_{r+1}(x_{N_x},\xi^n)=0, \tag{4.117}$$

$$f_{r+1}\left(\eta_j,0\right)=\eta\text{erfc}\left(\frac{\eta_j}{2}\right)+\frac{2}{\sqrt{\pi}}\left[1-\exp\left(-\frac{\eta_j^2}{4}\right)\right], \tag{4.118}$$

$$u_{r+1}\left(\eta_j,0\right)=\text{erfc}\left(\frac{\eta_j}{2}\right), \tag{4.119}$$

$$g_{r+1}\left(\eta_j,0\right)=c\left(\eta\text{erfc}\left(\frac{\eta_j}{2}\right)+\frac{2}{\sqrt{\pi}}\left[1-\exp\left(-\frac{\eta_j^2}{4}\right)\right]\right), \tag{4.120}$$

$$v_{r+1}\left(\eta_j,0\right)=c\left[\text{erfc}\left(\frac{\eta_j}{2}\right)\right], \tag{4.121}$$

$$\theta_{r+1}\left(\eta_j,0\right)=\text{erfc}\left(\frac{\sqrt{Pr}\eta_j}{2}\right), \tag{4.122}$$

$$\phi_{r+1}\left(\eta_j,0\right)=\text{erfc}\left(\frac{\sqrt{Sc}\eta_j}{2}\right),\quad j=0,1,2,\cdots,N_x. \tag{4.123}$$

The matrices above are defined as follows;

$$\mathbf{A}_1 = \frac{1}{2}\left(\mathbf{D}^2 + \mathbf{a}_{1,r}^{n+\frac{1}{2}}\mathbf{D} + \mathbf{a}_{2,r}\right) - \frac{\xi^{n+\frac{1}{2}}\left(1-\xi^{n+\frac{1}{2}}\right)}{\Delta\xi}\mathbf{I}, \tag{4.124}$$

$$\mathbf{A}_2 = \frac{1}{2}\left(\mathbf{D}^2 + \mathbf{b}_{1,r}^{n+\frac{1}{2}}\mathbf{D} + \mathbf{b}_{2,r}\right) - \frac{\xi^{n+\frac{1}{2}}\left(1-\xi^{n+\frac{1}{2}}\right)}{\Delta\xi}\mathbf{I}, \tag{4.125}$$

$$\mathbf{A}_3 = \frac{1}{2}\left(\mathbf{D}^2 + \mathbf{c}_{1,r}^{n+\frac{1}{2}}\mathbf{D}\right) - \frac{Pr\xi^{n+\frac{1}{2}}\left(1-\xi^{n+\frac{1}{2}}\right)}{\Delta\xi}\mathbf{I}, \tag{4.126}$$

$$\mathbf{A}_4 = \frac{1}{2}\left(\mathbf{D}^2 + \mathbf{d}_{1,r}^{n+\frac{1}{2}}\mathbf{D} + \mathbf{d}_{2,r}\right) - \frac{Sc\xi^{n+\frac{1}{2}}\left(1-\xi^{n+\frac{1}{2}}\right)}{\Delta\xi}\mathbf{I}, \tag{4.127}$$

$$\mathbf{B}_1 = -\frac{1}{2}\left(\mathbf{D}^2 + \mathbf{a}_{1,r}^{n+\frac{1}{2}}\mathbf{D} + \mathbf{a}_{2,r}\right) - \frac{\xi^{n+\frac{1}{2}}\left(1-\xi^{n+\frac{1}{2}}\right)}{\Delta\xi}\mathbf{I}, \tag{4.128}$$

$$\mathbf{B}_2 = -\frac{1}{2}\left(\mathbf{D}^2 + \mathbf{b}_{1,r}^{n+\frac{1}{2}}\mathbf{D} + \mathbf{b}_{2,r}\right) - \frac{\xi^{n+\frac{1}{2}}\left(1-\xi^{n+\frac{1}{2}}\right)}{\Delta\xi}\mathbf{I}, \tag{4.129}$$

$$\mathbf{B}_3 = -\frac{1}{2}\left(\mathbf{D}^2 + \mathbf{c}_{1,r}^{n+\frac{1}{2}}\mathbf{D}\right) - \frac{Pr\xi^{n+\frac{1}{2}}\left(1-\xi^{n+\frac{1}{2}}\right)}{\Delta\xi}\mathbf{I}, \tag{4.130}$$

$$\mathbf{B}_4 = -\frac{1}{2}\left(\mathbf{D}^2 + \mathbf{d}_{1,r}^{n+\frac{1}{2}}\mathbf{D} + \mathbf{d}_{2,r}\right) - \frac{Sc\xi^{n+\frac{1}{2}}\left(1-\xi^{n+\frac{1}{2}}\right)}{\Delta\xi}\mathbf{I}, \tag{4.131}$$

$$\mathbf{K}_1 = -\mathbf{a}_{3,r}^{n+\frac{1}{2}}, \tag{4.132}$$

$$\mathbf{K}_2 = -\mathbf{b}_{3,r}^{n+\frac{1}{2}}, \tag{4.133}$$

$$\mathbf{K}_3 = \mathbf{O}, \tag{4.134}$$

$$\mathbf{K}_4 = \mathbf{O}, \tag{4.135}$$

where $\mathbf{I}$ is an $(N_x+1)\times(N_x+1)$, $U, F, V, G, \Theta,$ and Φ are the vectors of the functions $u, f, v, g, \theta,$ and ϕ when evaluated at the grid points and $\mathbf{O}$ is a vector of zeros of size $(N_x+1)\times 1$. The boundary conditions (4.115 - 4.117) were imposed on the first and last rows of (4.109 - 4.114) as follows;

$$\begin{bmatrix} 1 & 0 & \cdots & 0 & 0 \\ \hline & & & & \\ & \mathbf{A}_{1,k-1} & & & \\ & & & & \\ \hline 0 & 0 & \cdots & 0 & 1 \end{bmatrix} \begin{bmatrix} u_{r+1,0}^{n+1} \\ \hline u_{r+1,1}^{n+1} \\ \vdots \\ \vdots \\ \hline u_{r+1,N_x}^{n+1} \end{bmatrix} = \begin{bmatrix} 0 & 0 & \cdots & 0 & 0 \\ \hline & & & & \\ & \mathbf{B}_{1,k-1} & & & \\ & & & & \\ \hline 0 & 0 & \cdots & 0 & 0 \end{bmatrix} \begin{bmatrix} u_{r+1,0}^{n} \\ \hline u_{r+1,1}^{n} \\ \vdots \\ \vdots \\ \hline u_{r+1,N_x}^{n} \end{bmatrix} + \begin{bmatrix} 0 \\ \hline \\ \mathbf{K}_1 \\ \\ \hline 1 \end{bmatrix}, \tag{4.136}$$

$$\left[\begin{array}{c|c|c} 1 \quad 0 \quad \cdots \quad 0 \quad 0 & & \\ \hline & \mathbf{A}_{2,k-1} & \\ \hline 0 \quad 0 \quad \cdots \quad 0 \quad 1 & & \end{array}\right]\left[\begin{array}{c} v^{n+1}_{r+1,0} \\ \hline v^{n+1}_{r+1,1} \\ \vdots \\ \vdots \\ \hline v^{n+1}_{r+1,N_x} \end{array}\right] = \left[\begin{array}{c|c|c} 0 \quad 0 \quad \cdots \quad 0 \quad 0 & & \\ \hline & \mathbf{B}_{2,k-1} & \\ \hline 0 \quad 0 \quad \cdots \quad 0 \quad 0 & & \end{array}\right]\left[\begin{array}{c} v^{n}_{r+1,0} \\ \hline v^{n}_{r+1,1} \\ \vdots \\ \vdots \\ \hline v^{n}_{r+1,N_x} \end{array}\right] + \left[\begin{array}{c} 0 \\ \hline \\ \mathbf{K}_2 \\ \\ \hline c \end{array}\right], \quad (4.137)$$

$$\left[\begin{array}{c|c|c} 1 \quad 0 \quad \cdots \quad 0 \quad 0 & & \\ \hline & \mathbf{A}_{3,k-1} & \\ \hline 0 \quad 0 \quad \cdots \quad 0 \quad 1 & & \end{array}\right]\left[\begin{array}{c} \theta^{n+1}_{r+1,0} \\ \hline \theta^{n+1}_{r+1,1} \\ \vdots \\ \vdots \\ \hline \theta^{n+1}_{r+1,N_x} \end{array}\right] = \left[\begin{array}{c|c|c} 0 \quad 0 \quad \cdots \quad 0 \quad 0 & & \\ \hline & \mathbf{B}_{3,k-1} & \\ \hline 0 \quad 0 \quad \cdots \quad 0 \quad 0 & & \end{array}\right]\left[\begin{array}{c} \theta^{n}_{r+1,0} \\ \hline \theta^{n}_{r+1,1} \\ \vdots \\ \vdots \\ \hline \theta^{n}_{r+1,N_x} \end{array}\right] + \left[\begin{array}{c} 0 \\ \hline \\ \mathbf{K}_3 \\ \\ \hline 1 \end{array}\right], \quad (4.138)$$

$$\left[\begin{array}{c|c|c} 1 \quad 0 \quad \cdots \quad 0 \quad 0 & & \\ \hline & \mathbf{A}_{4,k-1} & \\ \hline 0 \quad 0 \quad \cdots \quad 0 \quad 1 & & \end{array}\right]\left[\begin{array}{c} \phi^{n+1}_{r+1,0} \\ \hline \phi^{n+1}_{r+1,1} \\ \vdots \\ \vdots \\ \hline \phi^{n+1}_{r+1,N_x} \end{array}\right] = \left[\begin{array}{c|c|c} 0 \quad 0 \quad \cdots \quad 0 \quad 0 & & \\ \hline & \mathbf{B}_{4,k-1} & \\ \hline 0 \quad 0 \quad \cdots \quad 0 \quad 0 & & \end{array}\right]\left[\begin{array}{c} \phi^{n}_{r+1,0} \\ \hline \phi^{n}_{r+1,1} \\ \vdots \\ \vdots \\ \hline \phi^{n}_{r+1,N_x} \end{array}\right] + \left[\begin{array}{c} 0 \\ \hline \\ \mathbf{K}_4 \\ \\ \hline 1 \end{array}\right], \quad (4.139)$$

$$\left[\begin{array}{c|c|c} & & \\ & \mathbf{D} & \\ & & \\ \hline 0 \quad 0 \quad \cdots \quad 0 \quad 1 & & \end{array}\right]\left[\begin{array}{c} \\ f^{n+1}_{r+1,1} \\ \vdots \\ \vdots \\ \hline f^{n+1}_{r+1,N_x} \end{array}\right] = \left[\begin{array}{c} \\ u^{n}_{r+1,1} \\ \vdots \\ \hline u^{n}_{r+1,N_x-1} \\ 0 \end{array}\right], \quad (4.140)$$

$$\left[\begin{array}{c|c|c} & & \\ & \mathbf{D} & \\ & & \\ \hline 0 \quad 0 \quad \cdots \quad 0 \quad 1 & & \end{array}\right]\left[\begin{array}{c} \\ g^{n+1}_{r+1,1} \\ \vdots \\ \vdots \\ \hline g^{n+1}_{r+1,N_x} \end{array}\right] = \left[\begin{array}{c} \\ v^{n}_{r+1,1} \\ \vdots \\ \hline v^{n}_{r+1,N_x-1} \\ 0 \end{array}\right], \quad (4.141)$$

where

$$u^n_{r+1,j} = u_{r+1}\left(x_j, \xi^n\right),\ v^n_{r+1,j} = v_{r+1}\left(x_j, \xi^n\right),$$
$$\theta^n_{r+1,j} = \theta_{r+1}\left(x_j, \xi^n\right),\ \phi^n_{r+1,j} = \phi_{r+1}\left(x_j, \xi^n\right),\ j = 0, 1, 2, 3, \cdots, N_x. \tag{4.142}$$

Hence, starting from the initial approximations $f_0(\xi,\eta)$, $u_0(\xi,\eta)$, $g_0(\xi,\eta)$, $v_0(\xi,\eta)$, $\theta_0(\xi,\eta)$, $\phi_0(\xi,\eta)$, given by equations (4.25 - 4.28) and (4.91 - 4.92), equations (4.109 - 4.114) can be solved iteratively to give approximate solutions for $u_{r+1}\left(\xi,\eta\right)$, $v_{r+1}\left(\xi,\eta\right)$, $\theta_{r+1}\left(\xi,\eta\right)$, $\phi_{r+1}\left(\xi,\eta\right)$, $r = 0, 1, 2, 3, \cdots$, until a solution that converges to within a given level of accuracy was obtained. The solution u_{r+1} and v_{r+1} were used in equation (4.95) and (4.97) respectively to find f_{r+1} and g_{r+1}.

4.4. Results and discussion

In this section, the nonlinear partial differential Equations (4.9 - 4.12) together with the boundary conditions (4.13 - 4.16) were solved using the spectral perturbation method (SPM). The approximate numerical solutions of the skin friction coefficients $(f''(0,\xi), g''(0,\xi))$, surface heat transfer $(\theta'(0,\xi))$ and the surface mass transfer rate $(\phi'(0,\xi))$ at different values of the flow parameters were presented. Graphical results for velocity $f'(\xi,\eta)$, $g'(\xi,\eta)$, temperature $\theta(\xi,\eta)$ and concentration $\phi(\xi,\eta)$ profiles for different values of the physical parameter significant to the flow were also presented. The SPM series was utilized to generate results from the initial analytical solution at $\xi = 0$ up to results close to the steady state values at $\xi = 1$. In order to ascertain the accuracy of the SPM, comparison was made with approximate numerical solutions obtained using the spectral relaxation method (SRM) and good agreement was attained. The results presented in this chapter were generated using $L = 30$, which was found to give accurate results through numerical experimentation. Increasing the value of L did not change the results to a significant extent. The number of collocation points used in the spectral method discretization was $N_x = 100$, for both methods. The values of Prandtl number Pr used in this study was chosen to be $(Pr = 0.7)$ which represents the Pr for air, water$(Pr = 1 - 10)$. The values of Schmidt number were chosen to be $(Sc = 0.20)$ Hydrogen, $(Sc = 0.60)$ water vapor, $(Sc = 0.78)$ Ammonia, and $(Sc = 2.62)$ Propyl Benzene. All graphs and tables therefore correspond to these values except otherwise indicated. We note that the values of all physical parameters used in this study were chosen based on the values used in the literature related to this work. In addition, in order to further test the accuracy of the SPM and the SRM, a residual error analysis was conducted.

The SPM residual error of the governing partial differential equations (4.9 - 4.12) is defined as;

$$Res(f) = D^3F + (1-\xi)\left(\frac{\eta}{2}(D^2F) - \xi\frac{\partial(DF)}{\partial\xi}\right) + \xi\left[(F+G)(D^2F) - (DF)^2 - M^2(DF) - \lambda(DF)\right], \tag{4.143}$$

$$Res(g) = D^3G + (1-\xi)\left(\frac{\eta}{2}(D^2G) - \xi\frac{\partial(DG)}{\partial\xi}\right) + \xi\left[(F+G)(D^2G) - (DG)^2 - M^2(DG) - \lambda(DG)\right], \tag{4.144}$$

$$Res(\theta) = D^2\Theta + Pr\,(1-\xi)\left(\frac{\eta}{2}(D\Theta) - \xi\frac{\partial\Theta}{\partial\xi}\right) + Pr\xi\,(F+G)(D\Theta), \tag{4.145}$$

$$Res(\phi) = D^2\Phi + Sc\,(1-\xi)\left(\frac{\eta}{2}(D\Phi) - \xi\frac{\partial\Phi}{\partial\xi}\right) + Sc\xi\,(F+G)(D\Phi) - \gamma Sc\xi\Phi. \tag{4.146}$$

While the SRM residual error of the governing partial differential equations (4.9 - 4.12) is defined as;

$$Res(f) = D^2U + (1-\xi)\left(\frac{\eta}{2}(DU) - \xi\frac{\partial U}{\partial\xi}\right) + \xi\left[(F+G)(DU) - (U)^2 - M^2U - \lambda U\right], \tag{4.147}$$

$$Res(g) = D^2V + (1-\xi)\left(\frac{\eta}{2}(DV) - \xi\frac{\partial V}{\partial\xi}\right) + \xi\left[(F+G)(DV) - (V)^2 - M^2V - \lambda V\right], \tag{4.148}$$

$$Res(\theta) = D^2\Theta + Pr\,(1-\xi)\left(\frac{\eta}{2}(D\Theta) - \xi\frac{\partial\Theta}{\partial\xi}\right) + Pr\xi\,(F+G)(D\Theta), \tag{4.149}$$

$$Res(\phi) = D^2\Phi + Sc\,(1-\xi)\left(\frac{\eta}{2}(D\Phi) - \xi\frac{\partial\Phi}{\partial\xi}\right) + Sc\xi\,(F+G)(D\Phi) - \gamma Sc\xi\Phi.. \tag{4.150}$$

In the equations (4.147 - 4.150), $U = F'$ and $V = G'$. Also, U, F, V, G, Θ and Φ are defined as;

$$\frac{U_{r+1}^{n+1} + U_r^{n+1}}{2}, \quad \frac{F_{r+1}^{n+1} + F_r^{n+1}}{2}, \quad \frac{V_{r+1}^{n+1} + V_r^{n+1}}{2}, \quad \frac{G_{r+1}^{n+1} + G_r^{n+1}}{2},$$
$$\frac{\Theta_{r+1}^{n+1} + \Theta_r^{n+1}}{2}, \quad \text{and} \quad \frac{\Phi_{r+1}^{n+1} + \Phi_r^{n+1}}{2}. \tag{4.151}$$

In addition, we define $\frac{\partial U}{\partial\xi}, \frac{\partial V}{\partial\xi}, \frac{\partial\Theta}{\partial\xi}$, and $\frac{\partial\Phi}{\partial\xi}$ as;

$$\frac{U_{r+1}^{n+1} - U_r^{n+1}}{\Delta\xi}, \quad \frac{V_{r+1}^{n+1} - V_r^{n+1}}{\Delta\xi}, \quad \frac{\Theta_{r+1}^{n+1} - \Theta_r^{n+1}}{\Delta\xi}, \quad \text{and} \quad \frac{\Phi_{r+1}^{n+1} - \Phi_r^{n+1}}{\Delta\xi}. \tag{4.152}$$

Table 4.1 displays a comparison between the SPM and SRM approximate numerical solutions of the skin friction coefficients $f''(0,\xi)$ at different values of the local Hartman number M, and local porosity parameter λ when the stretching parameter $c = 0.5$ and $\xi = 0.5$. The comparison between the two results showed an excellent agreement. As can be seen from the table, the influence of the

Hartman number and the porosity parameter on the skin friction $f''(0,\xi)$ is to decrease the skin friction. With high values of M and λ, the skin friction coefficient $f''(0,\xi)$ decreases. The physical reason for this result, is as a consequence of the presence of the transverse magnetic field which causes a Lorenz drag force. This Lorenz drag force retards the velocity field. Thus, as Hartman number increases, the retarding force also increases and hence the velocity boundary layer thickness decreases as well as the shear stress on the sheet. In Table 4.2, an excellent agreement between the SPM and the SRM approximate numerical solutions for the skin friction coefficients $g''(0,\xi)$ is observed as the Hartman number M, local porosity parameter λ, and stretching parameter c are varied for fixed Pr, Sc, and γ when $\xi = 0.5$. The skin friction $g''(0,\xi)$ decreases as the values of Hartman number, local porosity parameter and stretching parameter increases. Tables 4.1 and 4.2 also gives the order of the SPM approximation, the SRM iterations (It) and the SRM grid points N_t used in the $\xi-$direction required to obtain the results presented in Tables 4.1 - 4.2. The tables also give the difference between the SPM and the SRM results. It is seen from the tables that the number of SRM iterations and grid points required to generate the results in Tables 4.1 - 4.2 is four and 10000 respectively. We observe from the difference column in Table 4.1 that for small values of M and λ, the results are consistent to at least nine decimal digits while the consistency reduces to at least eight decimal places as the values of M and λ increase. Similarly, it can be seen from the difference column in Table 4.2 that as M, λ and c increases, the consistency of the result decreases gradually from ten to eight decimal digits. While, for smaller values of M, λ and c considered, the results were consistent to at least nine to ten decimal places.

Table 4.1: *Comparison of the SPM and SRM approximate solutions of $f''(0,\xi)$ at different values of M, λ when $\xi = 0.5$, and $c = 0.5$*

M	λ	Order	SPM	It	N_t (Grid Points)	SRM	Difference (SPM - SRM)
0	0.1	18	-0.8618972983	4	10000	-0.8618972984	0.0000000001
0.1	0.3	19	-0.9127705562	4	10000	-0.9127705563	0.0000000001
0.3	0.5	19	-0.9780724238	4	10000	-0.9780724240	0.0000000002
0.5	0.7	16	-1.0581336442	4	10000	-1.0581336446	0.0000000002
0.7	1.0	17	-1.1709068581	4	10000	-1.1709068588	0.0000000007
1.0	1.3	16	-1.3260786756	4	10000	-1.3260786767	0.0000000011
1.3	1.5	21	-1.4808075196	4	10000	-1.4808075211	0.0000000015
1.5	1.7	22	-1.6023847463	4	10000	-1.6023847481	0.0000000018
1.8	1.9	33	-1.7771858677	4	10000	-1.7771858698	0.0000000021
2.0	2.0	60	-1.8938949413	4	10000	-1.8938949436	0.0000000023

A comparison of the SPM and SRM approximate solutions of different Prandtl numbers Pr, and

Table 4.2: *Comparison of the SPM and SRM approximate solutions of* $g''(0,\xi)$ *at different values of* M, λ, *and* c *when* $\xi = 0.5$, *and* $\gamma = 1$,

M	λ	c	Order	SPM	It	N_t (Grid Points)	SRM	Difference (SPM - SRM)
0	0.1	0.1	18	-0.0652511145	4	10000	-0.0652511145	0.0000000000
0.1	0.3	0.2	16	-0.1484037184	4	10000	-0.1484037184	0.0000000000
0.3	0.5	0.3	20	-0.2530874829	4	10000	-0.2530874829	0.0000000000
0.5	0.7	0.4	16	-0.3827752324	4	10000	-0.3827752325	0.0000000001
0.7	1.0	0.5	15	-0.5501787416	4	10000	-0.5501787419	0.0000000003
1.0	1.3	0.6	15	-0.7694772805	4	10000	-0.7694772811	0.0000000006
1.3	1.5	0.7	21	-1.0210982899	4	10000	-1.0210982909	0.0000000010
1.5	1.7	0.8	29	-1.2781272468	4	10000	-1.2781272482	0.0000000014
1.8	1.9	0.9	78	-1.6082832345	4	10000	-1.6082832365	0.0000000020
2.0	2.0	1.0	117	-1.9162241830	4	10000	-1.9162241854	0.0000000024

Table 4.3: *Comparison of the SPM and SRM approximate solutions of* $\theta'(0,\xi)$ *at different values of* Pr, *when* $\xi = 0.5$, $\lambda = 0.5$, $c = 0.5$, *and* $M = 1$

Pr	Order	SPM	It	N_t (Grid Points)	SRM	Difference (SPM - SRM)
0.7	25	-0.5171492110	3	10000	-0.5171492111	0.0000000001
1.0	25	-0.6311180420	3	10000	-0.6311180421	0.0000000001
1.5	23	-0.7903264184	3	10000	-0.7903264185	0.0000000001
2.0	22	-0.9260048183	3	10000	-0.9260048183	0.0000000000
3.0	21	-1.1555293460	3	10000	-1.1555293460	0.0000000000
4.0	23	-1.3502518090	4	10000	-1.3502518089	-0.0000000001
5.0	21	-1.5224200716	3	10000	-1.5224200715	-0.0000000001
6.0	23	-1.6784308376	3	10000	-1.6784308373	-0.0000000003
7.0	22	-1.8221281144	3	10000	-1.8221281141	-0.0000000003
9.0	24	-2.0819204885	3	10000	-2.0819204881	-0.0000000004
10	21	-2.2010699191	3	10000	-2.2010699187	-0.0000000004

Table 4.4: *Comparison of the SPM and SRM approximate solutions of $\phi'(0,\xi)$ at different values of Sc, and γ when $\xi = 0.5$, $\lambda = 0.5$, and $M = 1$*

Sc	γ	Order	SPM	It	N_t (Grid Points)	SRM	Difference (SPM - SRM)
0.2	0.0	24	-0.2562002019	3	10000	-0.2562002020	0.0000000001
0.6	0.0	25	-0.4743719885	3	10000	-0.4743719886	0.0000000001
0.78	0.0	26	-0.5494170791	3	10000	-0.5494170793	0.0000000002
1.0	0.0	25	-0.6311180420	3	10000	-0.6311180421	0.0000000001
2.62	0.0	24	-1.0734129612	3	10000	-1.0734129612	0.0000000000
0.2	0.2	23	-0.2843369876	3	10000	-0.2843369876	0.0000000000
0.6	0.2	23	-0.5216200266	3	10000	-0.5216200267	0.0000000001
0.78	0.2	24	-0.6028213111	3	10000	-0.6028213112	0.0000000001
1.0	0.2	22	-0.6910771345	3	10000	-0.6910771345	0.0000000000
2.62	0.2	23	-1.1673731301	3	10000	-1.1673731300	-0.0000000001
0.2	0.7	21	-0.3495743591	3	10000	-0.3495743591	0.0000000000
0.6	0.7	19	-0.6313734067	3	10000	-0.6313734068	0.0000000001
0.78	0.7	23	-0.7269495829	3	10000	-0.7269495829	0.0000000000
1.0	0.7	20	-0.8305256075	3	10000	-0.8305256076	0.0000000001
2.62	0.7	22	-1.3864433400	3	10000	-1.3864433401	0.0000000001
0.2	1.0	20	-0.3856527976	3	10000	-0.3856527976	0.0000000000
0.6	1.0	19	-0.6921968130	3	10000	-0.6921968131	0.0000000001
0.78	1.0	20	-0.7957847095	3	10000	-0.7957847096	0.0000000001
1.0	1.0	19	-0.9079079318	3	10000	-0.9079079320	0.0000000002
2.62	1.0	15	-1.5083384624	3	10000	-1.5083384627	0.0000000003

Table 4.5: *Approximate numerical values of the skin friction $f''(0,\xi)$ for various ξ and N_t (Grid Points) computed using the SRM, when $\gamma = 1$,$\lambda = 0.5$, $c = 0.5$ and $M = 1$.*

ξ	N_t (Grid Points)				
	500	1000	2000	5000	10000
0.1	-0.70089793	-0.70089761	-0.70089753	-0.70089751	-0.70089751
0.3	-0.95054474	-0.95054447	-0.95054440	-0.95054438	-0.95054438
0.5	-1.17291983	-1.17291960	-1.17291955	-1.17291953	-1.17291953
0.6	-1.27529489	-1.27529463	-1.27529462	-1.27529461	-1.27529461
0.7	-1.37243796	-1.37243778	-1.37243773	-1.37243771	-1.37243771
0.8	-1.46477045	-1.46477029	-1.46477025	-1.46477024	-1.46477024
0.9	-1.55266818	-1.55266810	-1.55266807	-1.55266806	-1.55266806
0.98	-1.62001003	-1.62001371	-1.62001447	-1.62001462	-1.62001463

Table 4.6: *Approximate numerical values of the skin friction $g''(0,\xi)$ for various ξ and N_t (Grid Points) computed using the SRM, when $\gamma = 1$,$\lambda = 0.5$, $c = 0.5$ and $M = 1$.*

ξ	N_t (Grid Points)				
	500	1000	2000	5000	10000
0.1	-0.34099681	-0.34099670	-0.34099668	-0.34099667	-0.34099667
0.3	-0.45094479	-0.45094469	-0.45094467	-0.45094466	-0.45094466
0.5	-0.55123781	-0.55123772	-0.55123771	-0.55123770	-0.55123770
0.6	-0.59806211	-0.59806203	-0.59806201	-0.59806200	-0.59806200
0.7	-0.64282229	-0.64282222	-0.64282220	-0.64282219	-0.64282219
0.8	-0.68562376	-0.68562369	-0.68562368	-0.68562366	-0.68562366
0.9	-0.72656325	-0.72656319	-0.72656317	-0.72656316	-0.72656316
0.98	-0.75802993	-0.75802992	-0.75802991	-0.75802991	-0.75802991

Table 4.7: *Approximate numerical values of the heat transfer rate $\theta'(0,\xi)$ for various ξ and grid points N_t computed using the SRM, when $Pr = 1.5$, $\gamma = 1$, $\lambda = 0.5$, $c = 0.5$ and $M = 1$.*

ξ	N_t (Grid Points)				
	500	1000	2000	5000	10000
0.1	-0.71206132	-0.71206130	-0.71206129	-0.71206129	-0.71206129
0.3	-0.75256293	-0.75256290	-0.75256289	-0.75256289	-0.75256289
0.5	-0.79032646	-0.79032643	-0.79032642	-0.79032642	-0.79032642
0.6	-0.80785960	-0.80785956	-0.80785955	-0.80785955	-0.80785955
0.7	-0.82416364	-0.82416359	-0.82416358	-0.82416357	-0.82416357
0.8	-0.83869529	-0.83869522	-0.83869520	-0.83869519	-0.83869519
0.9	-0.85001183	-0.85001165	-0.85001161	-0.85001160	-0.85001160
0.98	-0.85183933	-0.85183740	-0.85183693	-0.85183680	-0.85183679

Table 4.8: *Approximate numerical values of the mass transfer rate $\phi'(0,\xi)$ for various ξ and grid points N_t computed using the SRM, when $Sc = 1$, $\gamma = 1$, $\lambda = 0.5$, $c = 0.5$ and $M = 1$.*

ξ	N_t (Grid Points)				
	500	1000	2000	5000	10000
0.1	-0.63542422	-0.63542417	-0.63542416	-0.63542416	-0.63542416
0.3	-0.77418913	-0.77418907	-0.77418906	-0.77418906	-0.77418906
0.5	-0.90790800	-0.90790795	-0.90790793	-0.90790793	-0.90790793
0.6	-0.97288595	-0.97288590	-0.97288588	-0.97288588	-0.97288588
0.7	-1.03664365	-1.03664360	-1.03664358	-1.03664358	-1.03664358
0.8	-1.09923138	-1.09923134	-1.09923132	-1.09923132	-1.09923132
0.9	-1.16074127	-1.16074123	-1.16074122	-1.16074122	-1.16074122
0.98	-1.20932923	-1.20932912	-1.20932910	-1.20932909	-1.20932909

Table 4.9: *Comparison of the SPM and SRM numerical values of the skin friction* $f''(0,\xi)$ *at different values of* ξ *when* $\gamma = 1$, $\lambda = 0.5$, $c = 0.5$ *and* $M = 1$.

ξ	Order	SPM	SPM Time(sec)	SRM	N_t (Grid Points)	It	SRM Time(sec)
0.1	6	-0.70089751	0.011	-0.70089751	5000	3	52.774
0.3	10	-0.95054438	0.033	-0.95054438	5000	3	53.108
0.5	12	-1.17291953	0.044	-1.17291953	5000	3	53.238
0.6	14	-1.27529461	0.064	-1.27529461	5000	4	70.735
0.7	20	-1.37243771	0.113	-1.37243771	5000	4	71.770
0.8	23	-1.46477024	0.186	-1.46477024	5000	4	72.012
0.9	42	-1.55266806	0.549	-1.55266806	5000	4	73.744
0.98	106	-1.62001463	8.364	-1.62001463	10000	4	144.337

Table 4.10: *Comparison of the SPM and SRM numerical values of the skin friction* $g''(0,\xi)$ *at different values of* ξ *when* $\gamma = 1$, $\lambda = 0.5$, $c = 0.5$ *and* $M = 1$.

ξ	Order	SPM	SPM Time(sec)	SRM	N_t (Grid Points)	It	SRM Time(sec)
0.1	6	-0.34099667	0.011	-0.34099667	5000	3	52.774
0.3	8	-0.45094466	0.033	-0.45094466	5000	3	53.108
0.5	11	-0.55123770	0.044	-0.55123770	5000	3	53.238
0.6	14	-0.59806200	0.064	-0.59806200	5000	3	53.257
0.7	18	-0.64282219	0.113	-0.64282219	5000	3	53.385
0.8	35	-0.68562366	0.186	-0.68562366	5000	4	70.735
0.9	44	-0.72656316	0.549	-0.72656316	5000	4	71.770
0.98	84	-0.75802991	8.364	-0.75802991	5000	4	72.012

Table 4.11: *Comparison of the SPM and SRM numerical values of the surface heat transfer rate* $\theta'(0,\xi)$ *at different values of* ξ *when* $Pr = 1.5$, $\gamma = 1$, $\lambda = 0.5$, $c = 0.5$ *and* $M = 1$.

ξ	Order	SPM	SPM Time(sec)	SRM	N_t (Grid Points)	It	SRM Time(sec)
0.1	6	-0.71206129	0.011	-0.71206129	2000	3	21.167
0.3	13	-0.75256289	0.033	-0.75256289	2000	3	21.776
0.5	17	-0.79032642	0.044	-0.79032642	2000	3	21.781
0.6	23	-0.80785955	0.064	-0.80785955	2000	3	21.886
0.7	37	-0.82416357	0.113	-0.82416357	5000	3	21.941
0.8	52	-0.83869519	0.186	-0.83869519	5000	3	21.967
0.9	100	-0.85001160	0.549	-0.85001160	5000	3	22.005
0.98	452	-0.85183679	8.364	-0.85183679	10000	4	144.337

Table 4.12: *Comparison of the SPM and SRM numerical values of the surface mass transfer rate* $\phi'(0,\xi)$ *at different values of* ξ *when* $Sc = 1$, $\gamma = 1$, $\lambda = 0.5$, $c = 0.5$ *and* $M = 1$.

ξ	Order	SPM	SPM Time(sec)	SRM	N_t (Grid Points)	It	SRM Time(sec)
0.1	6	-0.63542416	0.011	-0.63542416	2000	3	22.167
0.3	10	-0.77418906	0.033	-0.77418906	2000	3	21.776
0.5	13	-0.90790793	0.044	-0.90790793	2000	3	21.781
0.6	18	-0.97288588	0.064	-0.97288588	2000	3	21.886
0.7	23	-1.03664358	0.113	-1.03664358	2000	3	21.941
0.8	33	-1.09923132	0.186	-1.09923132	2000	3	21.967
0.9	64	-1.16074122	0.549	-1.16074122	2000	3	22.005
0.98	234	-1.20932909	8.364	-1.20932909	5000	4	70.735

fixed values of M, λ, Sc, γ when $\xi = 0.5$ is shown in Table 4.3. Comparing the two results reveals a good agreement for converged results that are consistent to at least nine decimal digits. The influence of the Prandtl number is seen to reduce the surface heat transfer rate $\theta'(0,\xi)$. The heat transfer rate is reduced by an increase in Pr. The number of grid points N_t used in the $\xi-$ dirction in generating the results in Table 4.3 was 10000. From the difference column, it can be seen that results that are consistent to at least nine decimal digits was achieved with only three to four iterations.

Table 4.4 gives a comparison between the SPM and the SRM result for the surface mass transfer $\phi'(0,\xi)$ for varying values of γ, Sc and constant M, λ, c, Pr for $\xi = 0.5$. Increasing the values of Schmidt number and the destructive chemical reaction $\gamma > 0$ reduces the surface mass rate $\phi'(0,\xi)$. We remark that the number of grid points N_t used in generating the results in Table 4.4 was 10000. Consistent results within nine to ten decimal places was achieved with only four iterations.

The SRM results for the skin frictions $f''(0,\xi)$ and $g''(0,\xi)$, heat transfer rate $\theta'(0,\xi)$, and mass transfer rate $\phi'(0,\xi)$ are presented in Tables 4.5 - 4.8, respectively for various values of grid points (N_t) and selected time ξ. The results presented in these tables was computed using the same number of collocation points N_x and L. Increasing the grid points improves the accuracy of the results until the results match exactly to eight decimal places. In Table 4.5, it can be seen that for small ξ, full convergence within eight decimal digits was achieved with an initial grid points $N_t = 2000$. As ξ increases, more grid points N_t were needed to give the converged results presented in Table 4.5. In table 4.6, full convergence to at least eight decimal digits was reached when N_t was at least 5000 for all values of ξ considered. In Table 4.7, when ξ is small, convergence to at least eight decimal places was attained when N_t was at least 5000. As ξ tends towards 1, the N_t required to achieve full convergence increases. Same trend can be seen in Table 4.8. In Table 4.8, full convergence within

eight decimal places was reached when $N_t = 2000$ for small ξ. The grid points N_t was progressively increased as ξ increases. We note that for all the values of grid points N_t used in Tables 4.5 - 4.8 only four iterations was used to obtain the results.

In Tables 4.9 - 4.12, the comparison between the SPM and SRM numerical results of the reduced skin friction coefficients $(f''(0,\xi), g''(0,\xi))$, the surface heat transfer rate $(\theta'(0,\xi))$, and the surface mass transfer rate $(\phi'(0,\xi))$ at different values of the dimensionless time ξ are given for $M = 1$, $Pr = 1.5$, $c = 0.5$, $\lambda = 0.5$, $Sc = 1$, $\gamma = 1$. The order of the SPM approximation required to obtain the solution to a minimum of eight decimal places can also be seen in the tables. This shows that more terms of the SPM approximation are needed to reach convergence when ξ approaches 1 when ξ is small. The Tables further display the computational times needed to compute the SPM and the SRM solutions. A comparison of the computational times clearly showed that the SPM is much faster than the SRM in the computation of accurate solutions for the governing equations (4.9 - 4.16). This is indicative of the efficiency of the SPM approach in terms of the amount of time it requires the method to give desired results. It is worth noting that the computational speed of the SPM may be explained by the fact that discretization is done only in the η direction, unlike the SRM where discretization is done in both η and ξ directions. Also, using spectral methods to integrate the linearized equations leads to computation time saving because with spectral methods, only few grid points are required to yield accurate results when the solution is smooth. Hence, from the the numerical results, it can be seen that the two methods were in good agreement. In addition, the Table further gives the number of grid points N_t and iterations (It) required to give converged SRM results that match exactly with the SPM results to within eight decimal places. It was observed from that for the time ξ closer to 1, the grid points N_t and iterations required to obtain the results increased.

Figures 4.2 - 4.5 depict the velocity profiles $(f'(\xi,\eta), g'(\xi,\eta))$, the temperature profile $(\theta(\xi,\eta))$, and the concentration profile $(\phi(\xi,\eta))$ for different values of the dimensionless time ξ. We note that an increase in ξ reduces the velocity, temperature and concentration profiles. Similar observations in Figures 4.2 and 4.3 were made in earlier studies by Aurangzaib et al. (2013) while the results in Figure 4.4 are consistent with those reported by Ishak et al. (2006). Figure 4.5 corroborates earlier findings by Aurangzaib et al. (2013) and Dulal and Mondal (2011).

The effect of porosity parameter λ, on the velocity profiles $(f'(\xi,\eta), g'(\xi,\eta))$, the temperature pro-

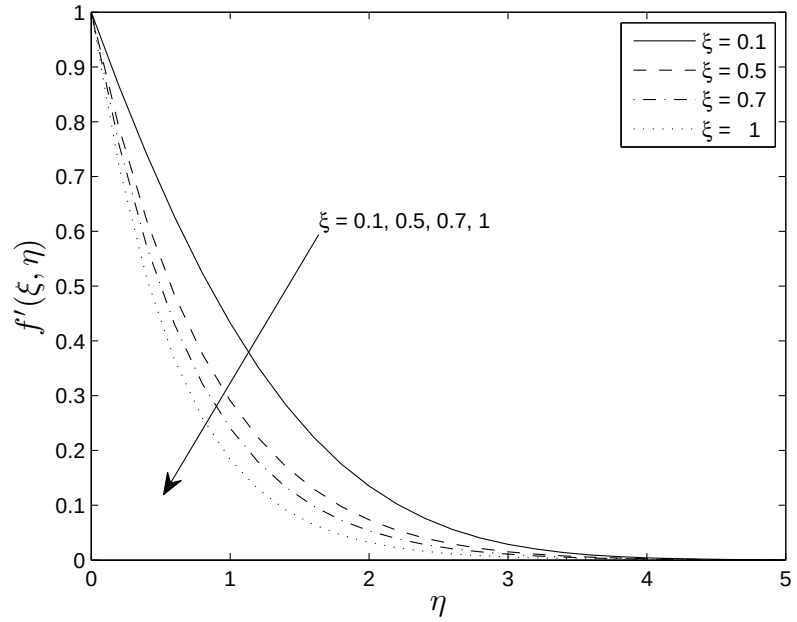

Figure 4.2: *Velocity profile* $f'(\xi,\eta)$ *for different* ξ, *with* $M = 1,\ \gamma = 0.5,\ c = 0.5,\ \lambda = 1,\ N = 100,\ L = 30.$

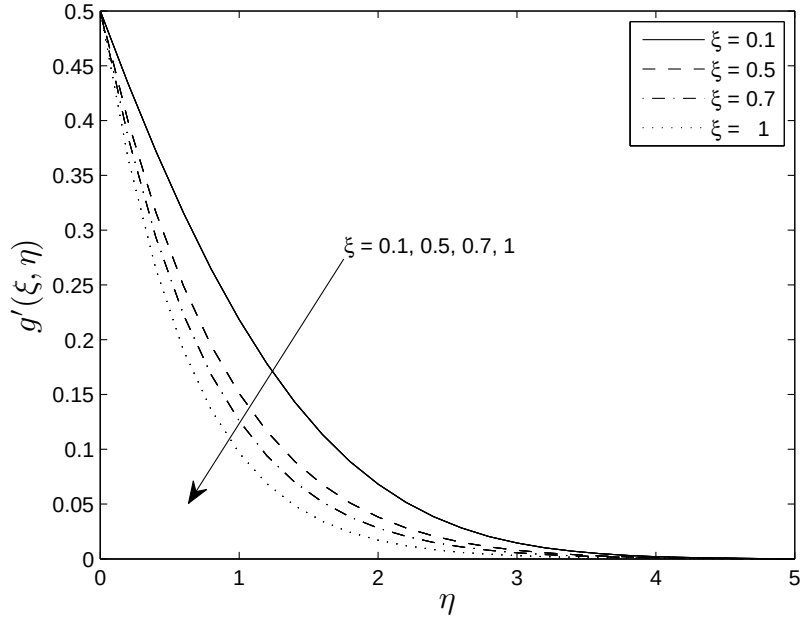

Figure 4.3: *Velocity profile* $g'(\xi,\eta)$ *for different* ξ, *with* $M = 1,\ \gamma = 0.5,\ c = 0.5,\ \lambda = 1,\ N = 100,\ L = 30.$

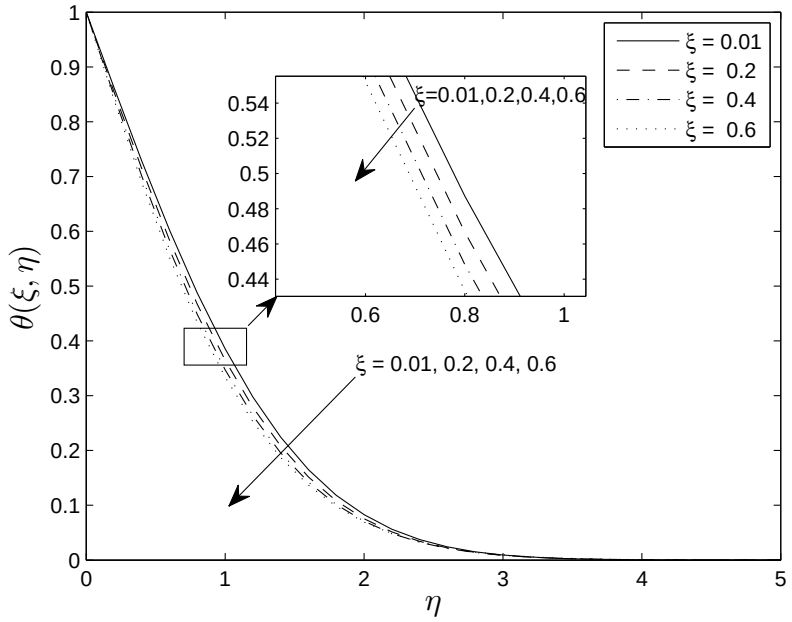

Figure 4.4: *Temperature profile* $\theta(\xi, \eta)$ *for different* ξ, *with* $M = 1,\ \gamma = 1,\ Pr = 1.5,\ c = 0.5,\ \lambda = 1,\ N = 100,\ L = 30$.

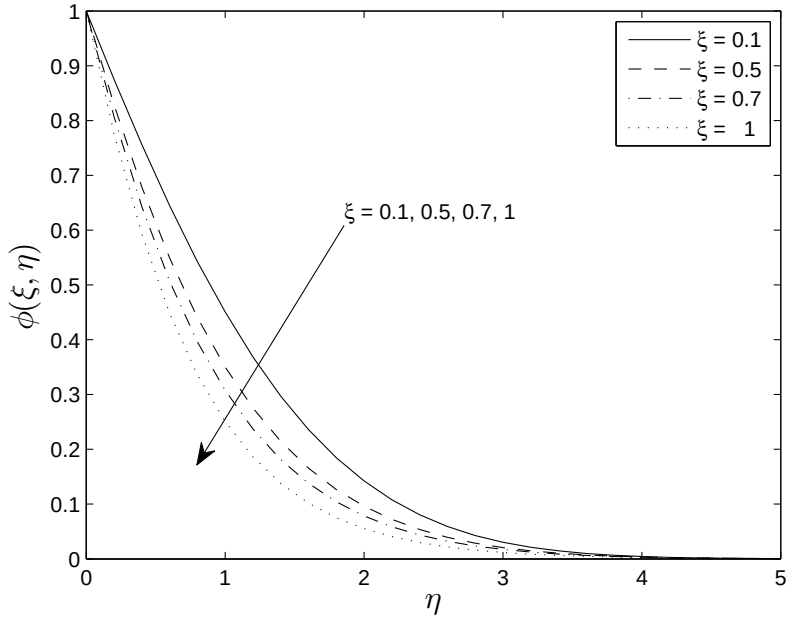

Figure 4.5: *Concentration profile* $\phi(\xi, \eta)$ *for different* ξ, *with* $M = 1,\ \gamma = 0.5,\ c = 0.5,\ \lambda = 1,\ N = 100,\ L = 30$.

file ($\theta(\xi,\eta)$), and the concentration profile ($\phi(\xi,\eta)$) were presented respectively in Figures 4.6 - 4.9. Figures 4.6 and 4.7 show the influence of the porosity parameter λ on the velocity profiles ($f'(\xi,\eta), g'(\xi,\eta)$). It can be seen that an increase in λ considerably reduces the boundary layer thickness. The effect of the porosity parameter is exhibited in Figure 4.8. We note that the dimensionless temperature profile increases with an increase in the porosity parameter. This means that increase in the porosity parameter increases the thermal boundary layer thickness. The impact of the porosity parameter on the concentration profile is displayed in Figure 4.9. The increase in porosity parameter leads to an increase in both the concentration profile and the boundary layer thickness. Similar results in Figures 4.6 - 4.8 have been reported in studies by Hayat et al. (2010) and Olanrewaju et al. (2012). In Figure 4.9 similar observations were made by Hayat et al. (2010).

Figures 4.11 - 4.14 demonstrate the influence of the Hartman number M on velocity distributions ($f'(\xi,\eta), g'(\xi,\eta)$), the temperature distribution ($\theta(\xi,\eta)$), and the concentration distribution ($\phi(\xi,\eta)$) accordingly. Figures 4.10 and 4.11 shows that increasing the values of the Hartman number gives rise to a decrease in the velocity distributions. This affirms the fact that the Hartman number symbolizes the significance of the magnetic field on the fluid flow. This magnetic field results in Lorentz force, which develops in retarding force on the velocity field, leading to an increase in Hartman number and an enhancement in the retarding force as well, thereby causing a decrease in the velocity distributions. In Figure 4.12, the Hartman number increases the temperature distribution. It was observed that the thermal boundary layer increased with an increase in the Hartman number. It was seen in Figure 4.13 that the effect of the Hartman number on the concentration distribution is to increase both the concentration distribution and the boundary layer thickness. These findings are consistent with those of Hayat et al. (2010) and Olanrewaju et al. (2012).

Figures 4.14 - 4.17 were sketched to show the influence of the stretching parameter c on the velocity components ($f'(\xi,\eta), g'(\xi,\eta)$), the temperature component ($\theta(\xi,\eta)$), and the concentration component ($\phi(\xi,\eta)$). In Figure 4.14, the influence of the stretching parameter c on the velocity profile ($f'(\xi,\eta)$) is to cause a negligible decrease in the velocity profile. Increasing the stretching parameter, reduces the velocity profile ($f'(\xi,\eta)$). Figure 4.15 shows that the velocity profile ($g'(\xi,\eta)$) is an increasing function of the stretching parameter. The velocity profile ($g'(\xi,\eta)$) increases when the stretching parameter was increased. The temperature profile for different values of the stretching parameter is displayed in Figure 4.16. With an increase in the stretching parameter, the temperature profile as well as the thermal boundary layer thickness decreases. Figure 4.17 shows the impact of

the stretching parameter on the concentration. The concentration profile decreases with an increase in the stretching parameter. The behavior of the stretching parameter on the velocity profiles , temperature profile and concentration profile accords with earlier observations by Olanrewaju et al. (2012).

The effect of both destructive chemical reaction ($\gamma > 0$) and the generative chemical reaction ($\gamma < 0$) on the concentration profile ($\phi(\xi, \eta)$) is shown in Figures 4.18 and 4.19 respectively. It is obvious that an increase in the destructive chemical reaction parameter amounts to a reduction in the concentration profile while the concentration profile increases with an increase in the generative chemical reaction parameter. Related remarks on the destructive chemical reaction were reported in studies by Hayat et al. (2010) and Olanrewaju et al. (2012) while the present findings on the generative chemical reaction are consistent with those of Hayat et al. (2010).

Figure 4.20 shows the impact of the Prandtl number on the temperature profile. We noted that an increase in the Prandtl number causes the temperature profile to reduce. The behavior of the Prandtl number on the temperature profile $\theta(\xi, \eta)$ correlates with results obtained by Hayat et al. (2010) and Olanrewaju et al. (2012).

Figure 4.21 illustrates the effect of the Schmidt number on the concentration profile ($\phi(\xi, \eta)$). It is seen from the Figure that the concentration profile decreases with the Schmidt number. When the Schmidt number increases, the concentration profile and the boundary layer thickness decreases. This implies that an increase in Schmidt number corresponds to a reduction in the concentration profile. These findings are consistent with those of Hayat et al. (2010) and Olanrewaju et al. (2012).

Figures 4.22 - 4.25 displays the variation of the SRM residual errors in f, g, θ and ϕ respectively against the number of iterations. The results are given for different values of the time ξ. It can be seen that for small value of time ξ, convergence to accurate result to within a specific level below 10^{-10} can be achieved with few iterations of the SRM. We note that the residual error curves for $f(\xi, \eta)$, $g(\xi, \eta)$, $\theta(\xi, \eta)$, $\phi(\xi, \eta)$ levels at a certain level below 10^{-10} for all values of ξ considered.

The residual error in f, g, θ and ϕ is shown in Figures 4.26 - 4.29 respectively, against increasing orders of the SPM approximation at different values of time ξ. We note that the residual errors decreased sharply with an increase in the order of approximation. Also, it can be seen that the residual error curves tend to plateau at more or less a fixed level for the different values of time ξ considered. The interpretation of this results is that the SPM will converge up to a specific saturation level which

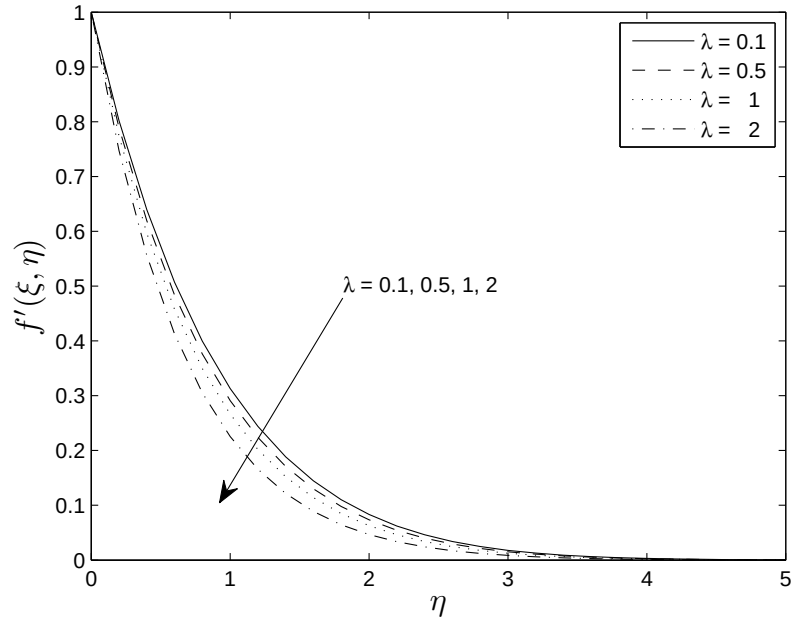

Figure 4.6: *Effect of local porosity parameter* λ *on velocity profile* $f'(\xi,\eta)$ *with* $\xi = 1,\ M = 1,\ \gamma = 0.5,\ c = 0.5,\ N = 100,\ L = 30.$

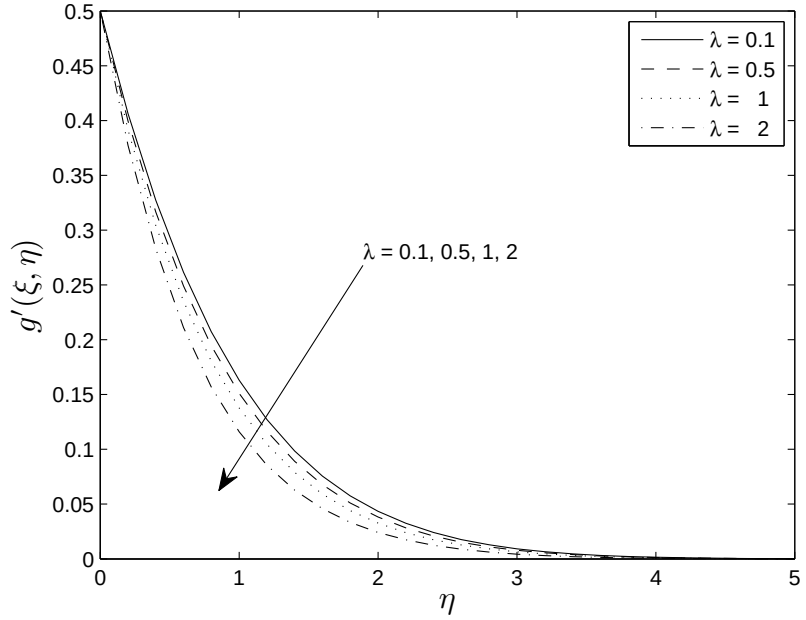

Figure 4.7: *Effect of local porosity parameter* λ *on velocity profile* $g'(\xi,\eta)$ *with* $\xi = 1,\ M = 1,\ \gamma = 0.5,\ c = 0.5,\ N = 100,\ L = 30.$

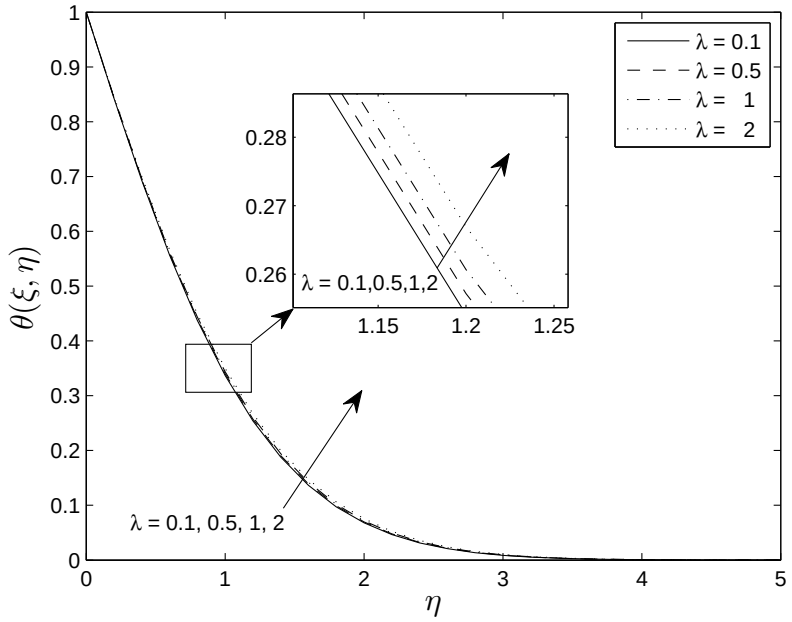

Figure 4.8: *Effect of local porosity parameter* λ *on temperature profile* $\theta(\xi, \eta)$ *with* $\xi = 1,\ M = 1,\ \gamma = 1,\ Pr = 1.5,\ c = 0.5,\ N = 100,\ L = 30.$

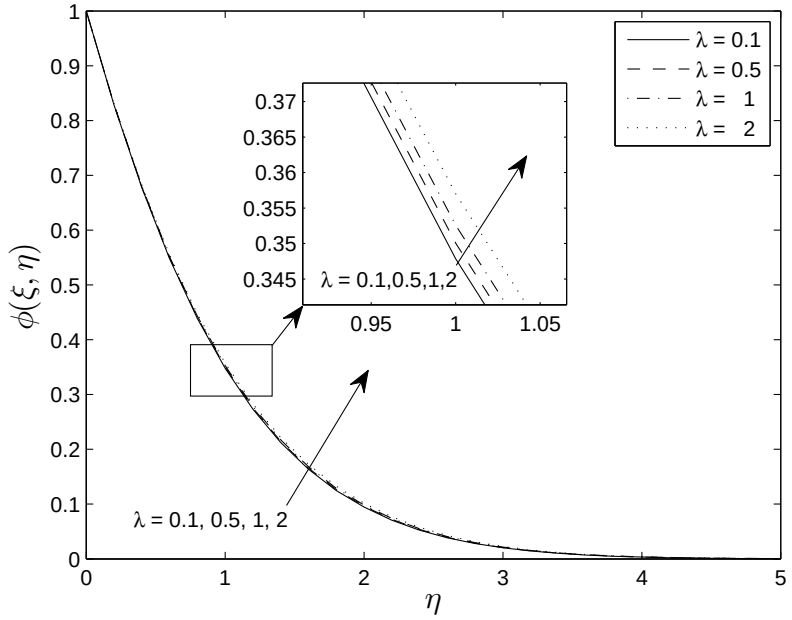

Figure 4.9: *Effect of local porosity parameter* λ *on concentration profile* $\phi(\xi, \eta)$ *with* $\xi = 1,\ M = 1,\ Sc = 1,\ \gamma = 1,\ c = 0.5,\ N = 100,\ L = 30.$

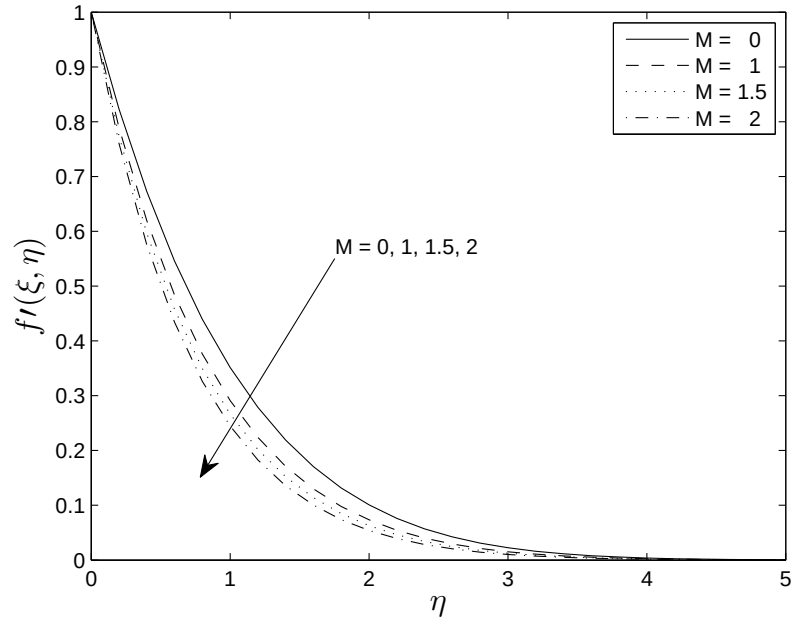

Figure 4.10: *Effect of local Hartman number M on velocity profile $f'(\xi,\eta)$ with* $\xi = 1,\ \lambda = 1,\ \gamma = 0.5,\ c = 0.5,\ N = 100,\ L = 30$.

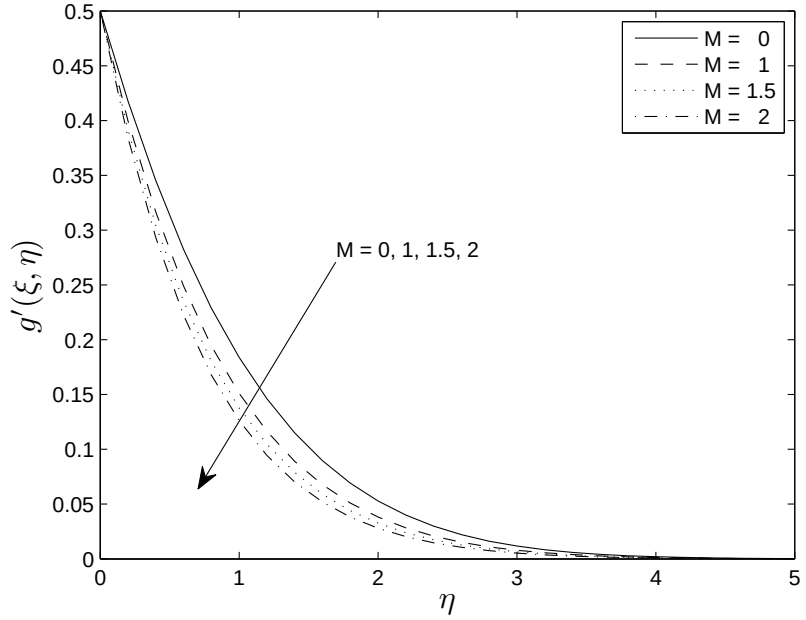

Figure 4.11: *Effect of local Hartman number M on velocity profile $g'(\xi,\eta)$ with* $\xi = 1,\ \lambda = 1,\ \gamma = 0.5,\ c = 0.5,\ N = 100,\ L = 30$.

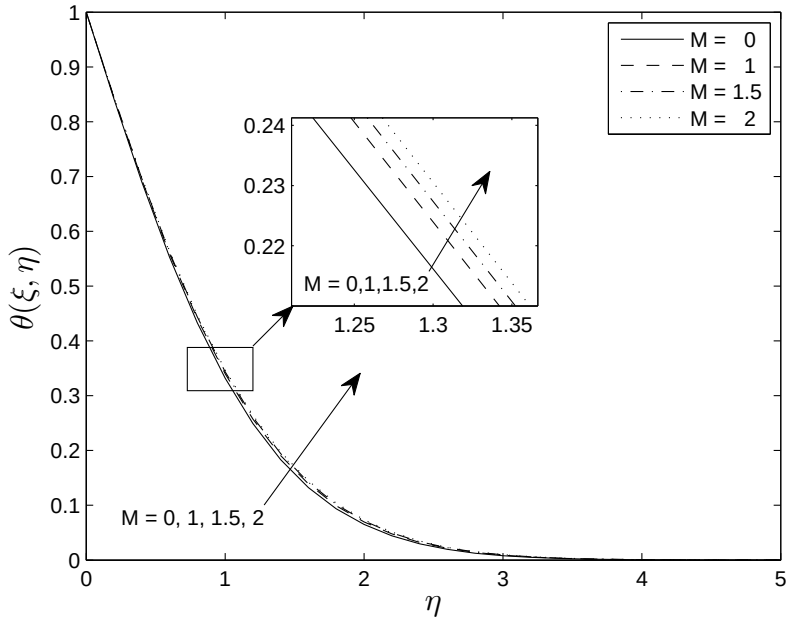

Figure 4.12: *Effect of local Hartman number M on temperature profile $\theta(\xi,\eta)$ with $\xi = 1,\ \lambda = 1,\ \gamma = 0.5,\ Pr = 1.5,\ c = 0.5,\ N = 100,\ L = 30$.*

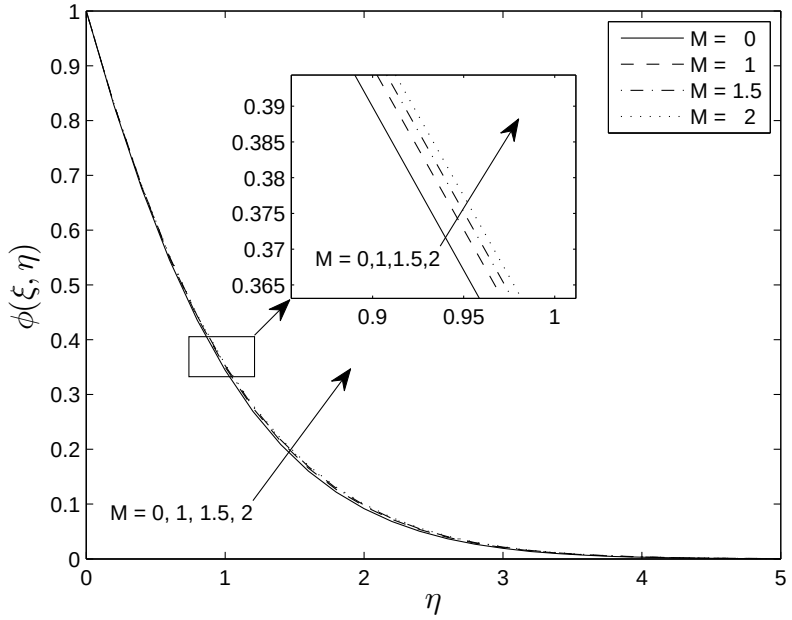

Figure 4.13: *Effect of local Hartman number M on concentration profile $\phi(\xi,\eta)$ with $\xi = 1,\ \lambda = 1,\ Sc = 1,\ \gamma = 0.5,\ c = 0.5,\ N = 100,\ L = 30$.*

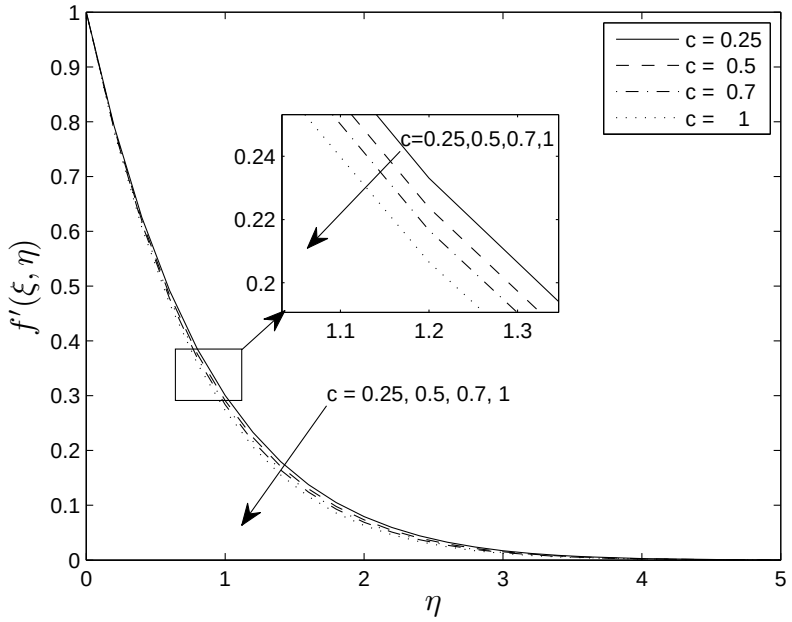

Figure 4.14: *Effect of stretching parameter c on velocity profile* $f'(\xi,\eta)$ *with* $\xi = 1,\ \lambda = 1,\ \gamma = 0.5,\ M = 1,\ N = 100,\ L = 30.$

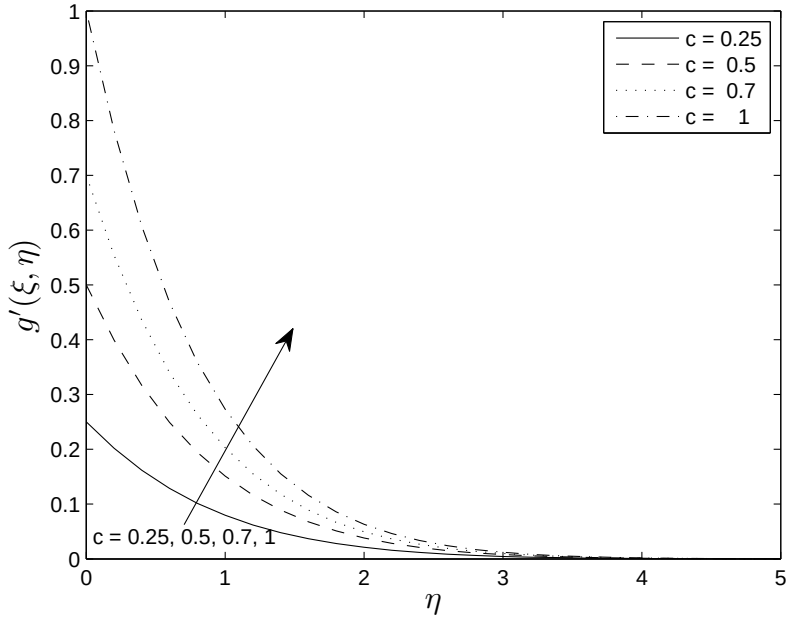

Figure 4.15: *Effect of stretching parameter c on velocity profile* $g'(\xi,\eta)$ *with* $\xi = 1,\ \lambda = 1,\ \gamma = 0.5,\ M = 1,\ N = 100,\ L = 30.$

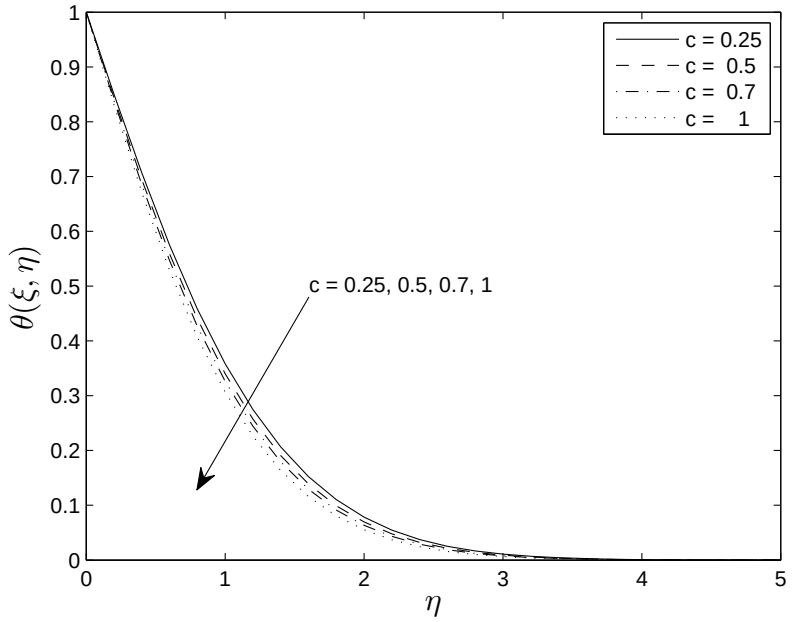

Figure 4.16: *Effect of stretching parameter c on temperature profile* $g'(\xi,\eta)$ *with* $\xi = 1,\ \lambda = 1,\ \gamma = 0.5,\ Pr = 1.5,\ M = 1,\ N = 100,\ L = 30.$

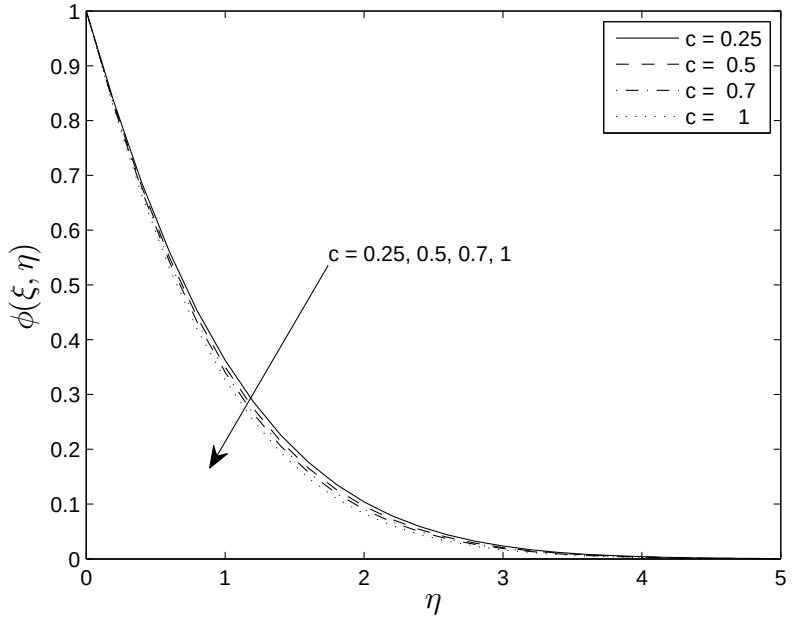

Figure 4.17: *Effect of stretching parameter c on concentration profile* $\phi(\xi,\eta)$ *with* $\xi = 1,\ \lambda = 0.5,\ Sc = 1,\ \gamma = 1,\ M = 1,\ N = 100,\ L = 30.$

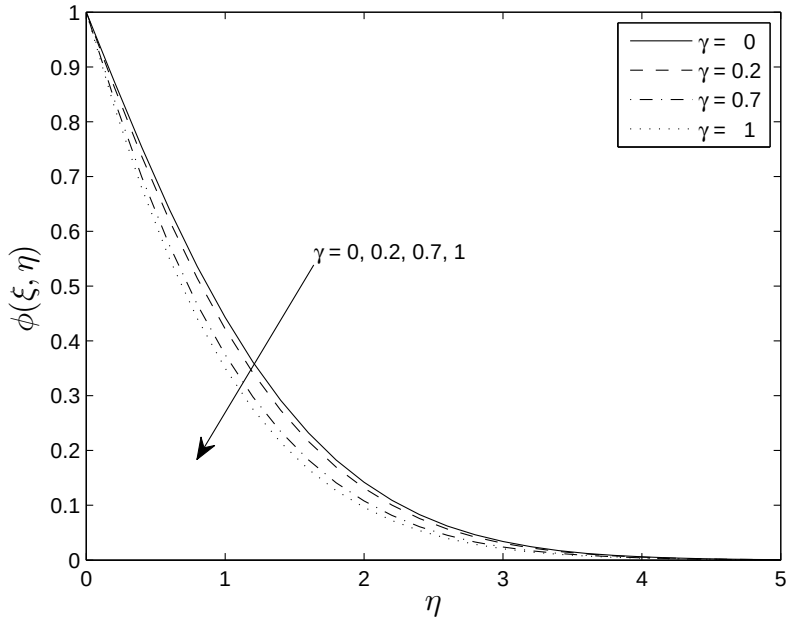

Figure 4.18: *Effect of chemical reaction parameter* $\gamma > 0$ *on concentration profile* $\phi(\xi,\eta)$ *with* $\xi = 1,\ \lambda = 1,\ Sc = 1,\ M = 1,\ c = 0.5,\ N = 100,\ L = 30$

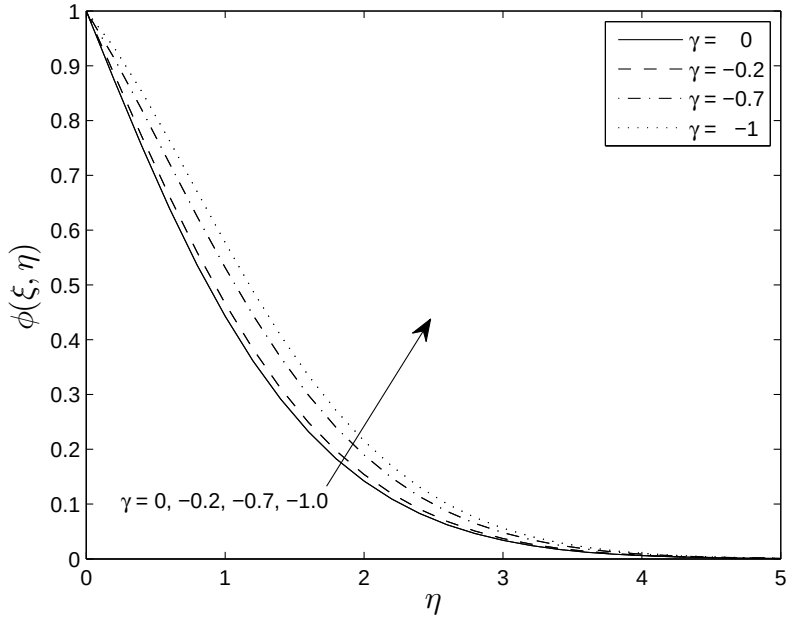

Figure 4.19: *Effect of chemical reaction parameter* $\gamma < 0$ *on concentration profile* $\phi(\xi,\eta)$ *with* $\xi = 1,\ \lambda = 1,\ Sc = 1,\ M = 1,\ c = 0.5,\ N = 100,\ L = 30$.

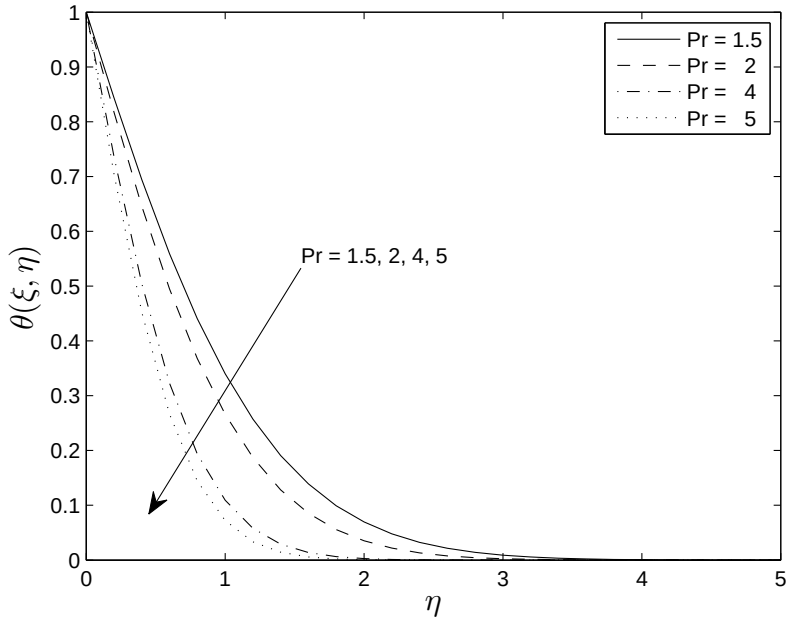

Figure 4.20: *Effect of Prandtl number Pr on temperature profile* $\theta(\xi,\eta)$ *with* $\xi = 1,\ \lambda = 1,\ \gamma = 0.5,\ M = 1,\ c = 0.5,\ N = 100,\ L = 30.$

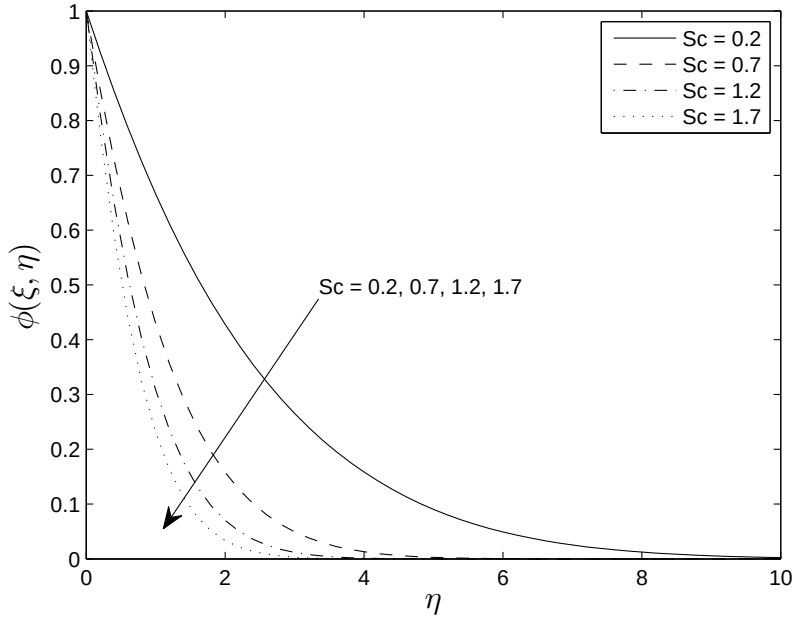

Figure 4.21: *Effect of Schmidt number Sc on concentration profile* $\phi(\xi,\eta)$ *with* $\xi = 1,\ \lambda = 1,\ M = 1,\ \gamma = 0.5,\ c = 0.5,\ N = 100,\ L = 30.$

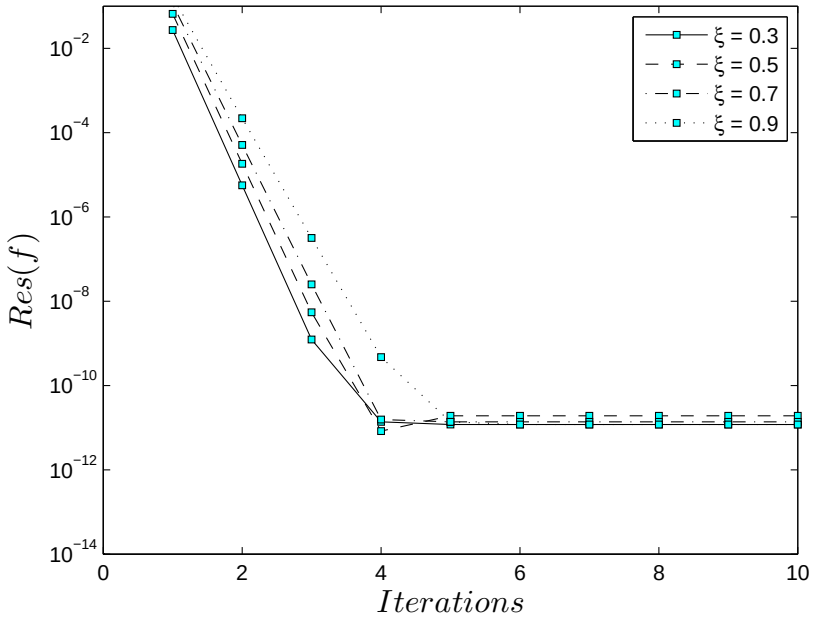

Figure 4.22: *Residual error curve* $Res(f)$ *against SRM iterations when* $\xi = 0.3, 0.5, 0.7, 0.9,\ M = 1,\ \gamma = 1,\ \lambda = 0.5,\ c = 0.5,$ *grid ponts* $N_t = 5000,\ L = 30,\ N_x = 100.$

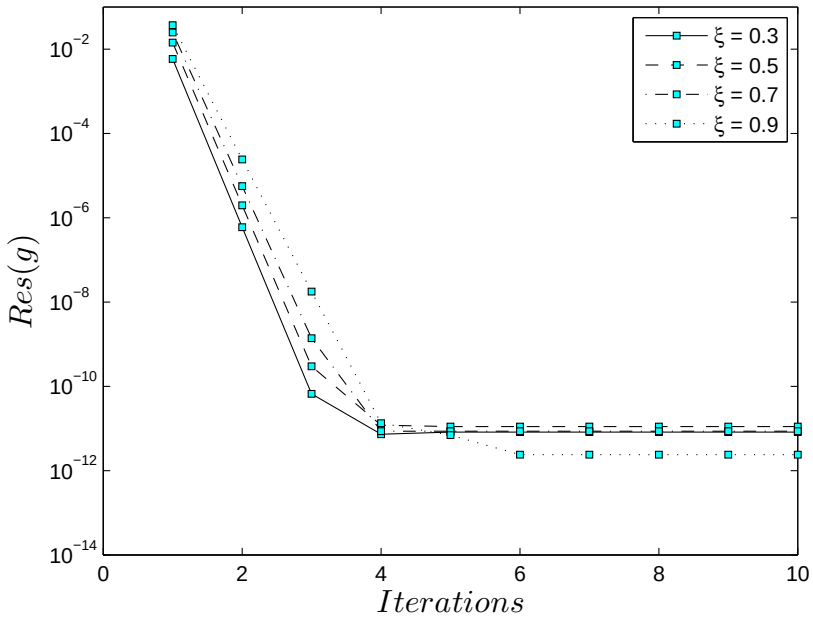

Figure 4.23: *Residual error curve* $Res(g)$ *against SRM iterations when* $\xi = 0.1, 0.3, 0.5, 0.7,\ M = 1,\ \gamma = 1,\ \lambda = 0.5,\ c = 0.5,$ *grid ponts* $N_t = 5000,\ L = 30,\ N_x = 100.$

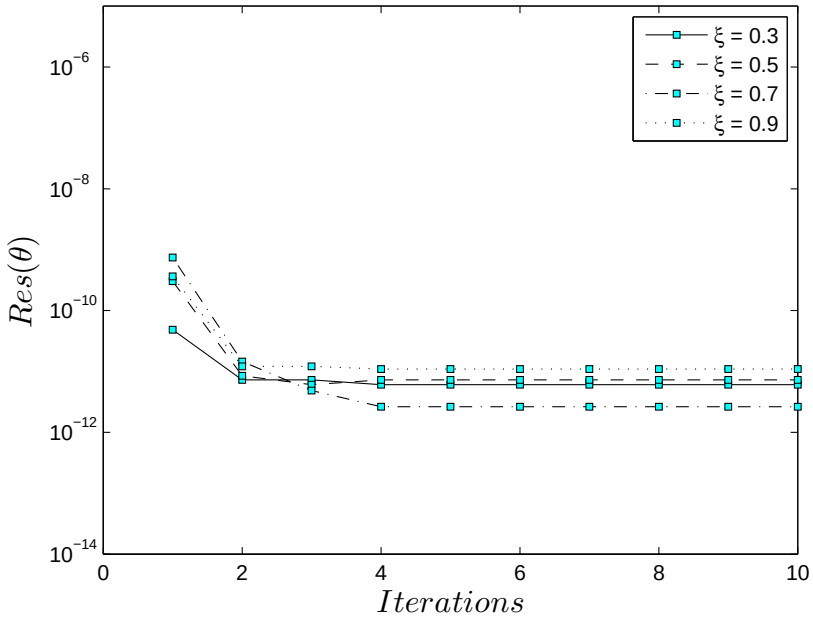

Figure 4.24: *Residual error curve* $Res(\theta)$ *against SRM iterations when* $\xi = 0.3, 0.5, 0.7, 0.9,\ M = 1,\ Pr = 1.5,\ \gamma = 1,\ \lambda = 0.5,\ c = 0.5,$ *grid ponts* $N_t = 5000,\ L = 30,\ N_x = 100.$

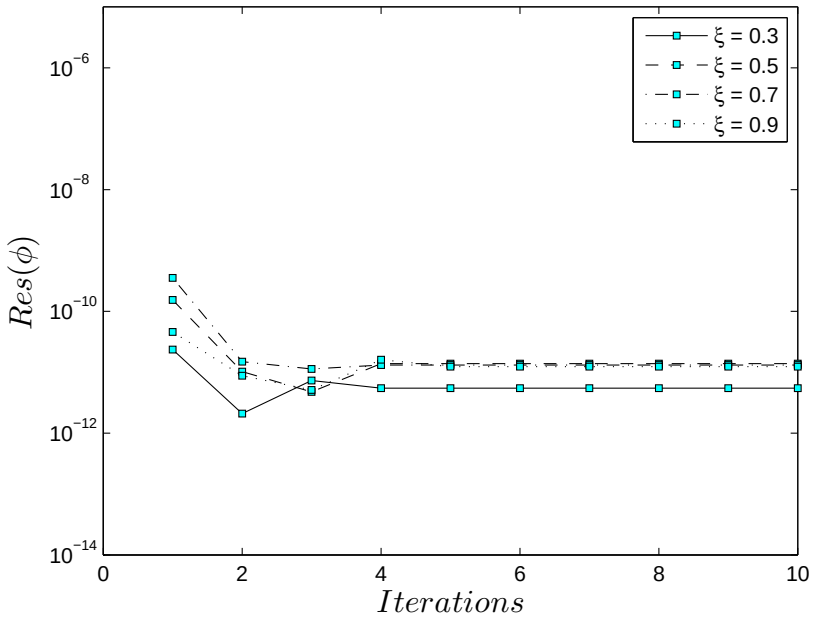

Figure 4.25: *Residual error curve* $Res(\phi)$ *against SRM iterations when* $\xi = 0.1, 0.3, 0.5, 0.7,\ M = 1,\ Sc = 1,\ \gamma = 1,\ \lambda = 0.5,\ c = 0.5,$ *grid ponts* $N_t = 5000,\ L = 30,\ N_x = 100.$

corresponds to the level at which the curve levels off. In the equation for $f(\xi, \eta)$ and $g(\xi, \eta)$, the residual error curve levels off below 10^{-8} for all values of ξ. In the equation for $\theta(\xi, \eta)$, it can be seen that the residual error curve levels off below 10^{-10} and also below 10^{-10} in the equation for $\phi(\eta, \xi)$. Furthermore, it can be noticed that as ξ approaches 1, the plateau was reached at a higher order of the SPM approximation. This observation accord with the results presented in Tables 4.9 - 4.12 where it was observed that when ξ is small, only few order of the SPM approximation are required to give converged results that are accurate up to eight decimal places and more terms of the SPM approximation are needed as ξ approaches 1. This observation is typical of standard perturbation based methods which are known to be accurate when the series expansion is with respect to a small parameter. It is interesting to observe that in the case of the SPM, very accurate results can be obtained even when ξ is close to 1, $\xi \longrightarrow 1$, albeit with a higher order of the SPM approximation.

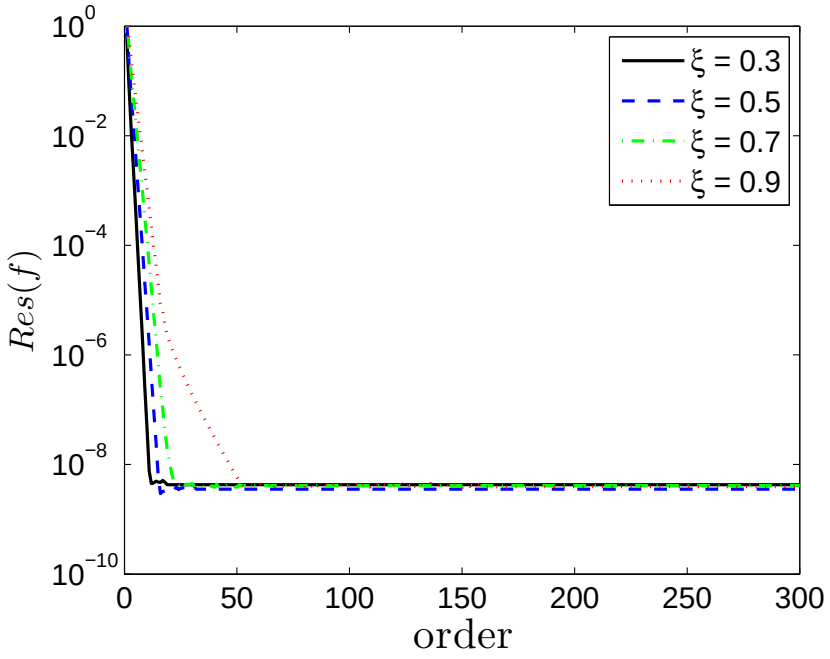

Figure 4.26: *Residual error curve* $Res(f)$ *against increasing SPM approximation order when* $M = 1,\ \gamma = 1,\ \lambda = 0.5,\ c = 0.5,\ N_x = 100.$

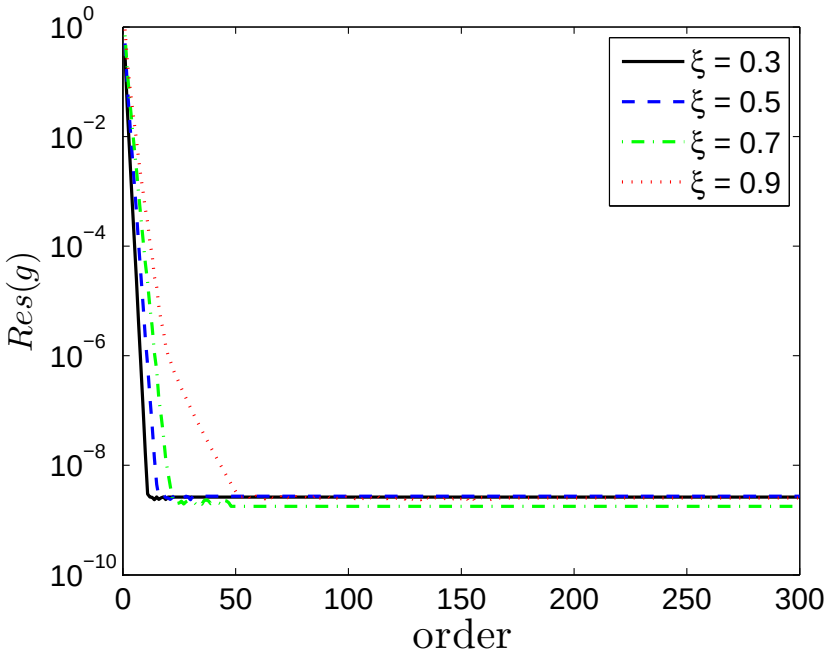

Figure 4.27: *Residual error curve* $Res(g)$ *against increasing SPM approximation order when* $M = 1,\ \gamma = 1,\ \lambda = 0.5,\ c = 0.5,\ L = 30,\ N_x = 100.$

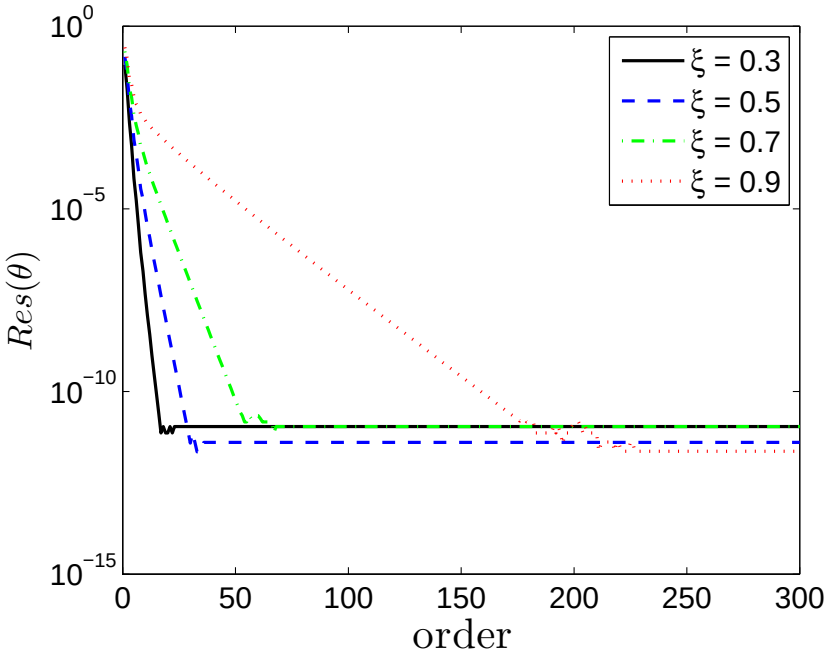

Figure 4.28: *Residual error curve* $Res(\theta)$ *against increasing SPM approximation order when* $M = 1,\ Pr = 1.5,\ \gamma = 1,\ \lambda = 0.5,\ c = 0.5,\ L = 30,\ N_x = 100.$

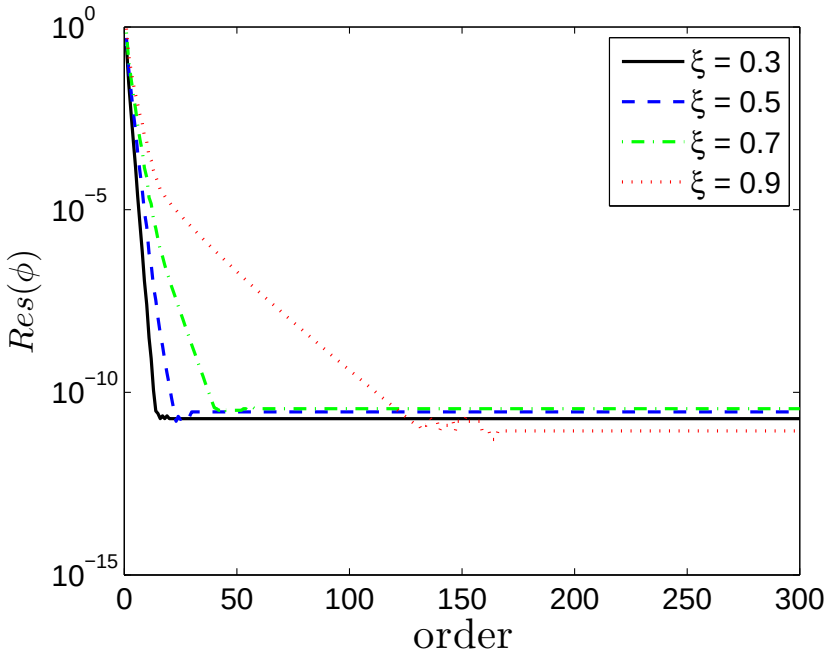

Figure 4.29: *Residual error curve* $Res(\phi)$ *against increasing SPM approximation order when* $M = 1,\ Sc = 1,\ \gamma = 1,\ \lambda = 0.5,\ c = 0.5,\ L = 30,\ N_x = 100.$

5

Conclusion

In this dissertation, a Chebyshev spectral perturbation method based approach for solving nonlinear differential equations in fluid dynamics has been presented. The methods has been used to solve different fluid flow problems. Below, we give a summary of the findings for each of the problem solved in Chapters 2, 3 and 4 respectively.

In Chapter 2, the equations modeling the flow and heat transfer in an incompressible electrically conducting fluid near a stagnation point on a stretching sheet was solved. The flow model considered the effects of heat source/sink and suction/injection in porous media. The purpose of the chapter was to present a spectral perturbation method (SPM) for solving nonlinear ordinary differential equations (ODEs). Approximate numerical solutions for the skin friction coefficient, Nusselt number, velocity profile and temperature profile were generated using the SPM for different flow parameter values. Asymptotic solutions of the skin friction coefficient for large perturbation parameter were also generated. The method proved to be efficient even in the case where the perturbation parameter was large, as the convergence rate was seen to improve with increase in the parameter values. The SPM results were validated using the spectral quasi-linearisation method (SQLM), where a good agreement between the two sets of results was achieved up to eight decimal digits. The results generated were also found to be in agreement with those found in the literature. The study demonstrated that the SPM can be used as an alternative approach to find numerical solutions for complicated expansions encountered in perturbation schemes. With the SPM, higher order approximate solutions are possible to find, where not possible or very difficult to find with the usual analytical perturbation schemes. For problems similar to the one examined in Chapter 2, the SPM can be use. In as much as the SPM is limited to problems with small parameters, accurate numerical solutions are possible as compared

to ordinary perturbation schemes.

In Chapter 3, we considered the application of the perturbation technique coupled with the Chebyshev pseudo-spectral collocation method to the solution of unsteady heat and mass transfer by MHD mixed convection flow over an impulsively stretched vertical surface with chemical reaction effect. Approximate numerical results were generated using the spectral perturbation method for the solution of the skin friction coefficient, heat transfer rate, mass transfer rate, velocity distribution, temperature distribution and concentration distribution at different flow parameter values. The accuracy of the SPM was demonstrated by comparing with results generated using the spectral relaxation (SRM) where a good agreement was achieved between the two set of results up to at least eight decimal places. The computational efficiency of the SPM was confirmed by comparing the computational times of generating the SPM solutions with the computational times of the SRM solutions. It was observed that the SPM is much faster than the SRM. Residual errors were obtained for the SPM and SRM. From the residual errors analysis we observed that in terms of convergence, the SPM converges faster than the SRM but the SRM gives more accurate results than the SPM in terms of accuracy. The study showed that the SPM can be used as an alternative numerical method to the usual perturbation methods to obtain numerical solutions of partial differential equations (PDEs). It was noted that the SPM solves a partial differential equation by applying discretization only in the space direction. This feature combined with integrating using the spectral method results in computation time saving. Unlike standard perturbation methods, the SPM gives higher order approximate solutions which are not possible or very complicated to find with the usual perturbation methods. For problems related to one investigated in Chapter 3, the SPM can be used efficiently. The numerical results presented in this study suggests that the proposed SPM has the potential to be utilized for solving complex nonlinear partial differential equations particularly defined using the Williams and Rhyne (1980) transformation.

In Chapter 4, we have discussed the application of the SPM on larger systems of nonlinear PDEs. The SPM was used to solve the previously reported nonlinear PDEs that models the flow of an unsteady three dimensional MHD flow and mass transfer in a porous medium. The flow model investigated the effects of the embedded parameters in details. Approximate numerical solutions for the skin friction coefficient, surface heat and mass transfer rate were generated using the SPM for different flow parameter values and dimensionless time. The SPM results were validated using SRM, where an excellent agreement between the two sets of results was achieved. The graphical results

obtained were also found to be in agreement with those found in the literature. The investigation also sought to assess the accuracy of the SPM when compared with the SRM. It was noticed from the comparison of the computational times between the SPM and SRM that there is much difference in the computational times of the two methods. The SPM being faster than the SRM. Hence, it was concluded from the observations made that the SPM is much more computationally efficient than the SRM. We noted that for sufficiently large grid points, the SRM yields result that are consistent to at least eight decimal digits. Residual errors were obtained for the SPM and SRM. From the residual error analysis carried out on the SPM and SRM, the SPM was observed to converge faster than the SRM, while, the SRM was observed to be more accurate than the SPM. With the SPM, higher order approximate solutions are possible to find, where not possible or very difficult to find with the usual perturbation schemes. The numerical results presented in Chapter 4 clearly indicate that the SPM can be used efficiently as a practical tool for solving problems similar to the one investigated in Chapter 4. We conclude that the SPM can be used for solving complex nonlinear larger systems of PDEs defined using the Williams and Rhyne (1980) transformation.

In conclusion, the SPM presented in this study adds to a growing body of literature on numerical methods for solving complex nonlinear fluid flow problems. Also, the present study contributes additional evidence that suggests the use of the SPM as a very good numerical approach for solving complex nonlinear ODEs and PDEs defined using the Williams and Rhyne (1980) transformation. On comparing the methods, the SPM was observed to converge faster than SRM and the SQLM but the SRM was noticed to give more accurate result than the SPM. In addition, the SPM was noted to be more computationally efficient than the SQLM, which, in turn, was faster than the SRM. A limitation of the SPM is that the SPM is limited to ODEs problems involving small or large parameters and nonlinear PDEs defined using the Williams and Rhyne (1980) transformation. In future investigations, it would be interesting to extend the range of validity of the SPM by combining the SPM with methods such as the Pade approximant that can improve the convergence rate of the SPM even as ξ becomes larger in order to widen the scope of problems that can be solved using the SPM.

Bibliography

Ahmad, B. (2006). A quasilinearization method for a class of integro-differential equations with mixed nonlinearities. *Nonlinear Analysis: Real World Applications 7*(5), 997–1004.

Ahmad, B., A. Alsaedi, and B. Alghamdi (2008). Generalized quasilinearization method for a forced duffing equation with three-point nonlinear boundary conditions. *Mathematical Inequalities and Applications 11*(1), 163.

Ahmad, B., J. J. Nieto, and N. Shahzad (2001). The Bellman–Kalaba–Lakshmikantham quasilinearization method for neumann problems. *Journal of Mathematical Analysis and Applications 257*(2), 356–363.

Ahmad, B., J. J. Nieto, and N. Shahzad (2002). Generalized quasilinearization method for mixed boundary value problems. *Applied Mathematics and Computation 133*(2), 423–429.

Aksoy, Y. and M. Pakdemirli (2010). New perturbation–iteration solutions for Bratu-type equations. *Computers & Mathematics with Applications 59*(8), 2802–2808.

Al-sudais, N. S. (2012). Thermal radiation effects on MHD fluid flow near stagnation point of linear stretching sheet with variable thermal conductivity. *International Mathematical Forum 7*(51), 2525–2544.

Alam, M. S., M. M. Rahman, and M. A. Sattar (2007). Similarity solutions for hydromagnetic free convective heat and mass transfer flow along a semi-infinite permeable inclined flat plate with heat generation and thermophoresis. *Nonlinear Analysis: Modelling and Control 12*(4), 433–445.

Ali, A. and A. Mehmood (2008). Homotopy analysis of unsteady boundary layer flow adjacent to permeable stretching surface in a porous medium. *Communications in nonlinear science and Numerical Simulation 13*(2), 340–349.

Ali, F. M., R. Nazar, N. M. Arifin, and I. Pop (2011). MHD mixed convection boundary layer flow toward a stagnation point on a vertical surface with induced magnetic field. *Journal of Heat Transfer 133*(6), 022502–1.

Ali, K. and M. Ashraf (2012). Thermal reversal in MHD stagnation point flow towards a stretching sheet with induced magnetic field and viscous dissipation effects. *World Applied Sciences Journal 16*(11), 1615–1625.

Ali, K., M. Ashraf, S. Ahmad, and K. Batool (2012). Viscous dissipation and radiation effects in MHD stagnation point flow towards a stretching sheet with induced magnetic field. *World Applied Sciences Journal 16*(11), 1638–1648.

Ampadu, E. (2007). Implementation of some finite difference methods for the pricing of derivatives using c++ programming. *MSc Thesis, Worcester Polytechnic Institute*.

Asaithambi, A. (2004). A second-order finite-difference method for the Falkner–Skan equation. *Applied Mathematics and Computation 156*(3), 779–786.

Aurangzaib, A. R. M., N. F. Mohammad, and S. Shafie (2013). Unsteady MHD mixed convection flow with heat and mass transfer over a vertical plate in a micropolar fluid-saturated porous medium. *Journal of Applied Science and Engineering 16*(2), 141–150.

Babolian, E., M. Bromilow, R. England, and M. Saravi (2007). A modification of pseudo-spectral method for solving a linear ODEs with singularity. *Applied Mathematics and Computation 188*(2), 1260–1266.

Belgacem, F. B. and M. Grundmann (1998). Approximation of the wave and electromagnetic diffusion equations by spectral method. *SIAM Journal on Scientific Computing 20*(1), 13–32.

Bellman, R. (1966). *Perturbation techniques in mathematics, physics, and engineering.* Holt, Rinehart and Winston, New York, NY, USA.

Bellman, R. E. and R. Kalaba (1965). Quasilinearization and Nonlinear Boundary-Value Problems. Elsevier, New York, NY, USA.

Bourke, W. (1988). Spectral methods in global climate and weather prediction models. In *Physically-Based Modelling and Simulation of Climate and Climatic Change*, pp. 169–220. Springer.

Bruno, C. (2004). Spectral methods for partial differential equations. *A Mathematical Journal 6*(4), 1–32.

Canuto, C., M. Y. Hussaini, A. Quarteroni, and T. A. Zang (1988). *Spectral Methods in Fluid Dynamics*. Springer-Verlag, Berlin, Germany.

Canuto, C., M. Y. Hussaini, A. Quarteroni, and T. A. Zang (2007). *Evolution to complex geometries and applications to fluid dynamics*. Springer-Verlag, Berlin, Germany.

Cebeci, T. and P. Bradshaw (1984). *Physical and Computational Aspects of Convective Heat Transfer*, Volume 1. Springer, New York, NY, USA.

Chamkha, A. J. and S. M. M. El-Kabeir (2013). Unsteady heat and mass transfer by MHD mixed convection flow over an impulsively stretched vertical surface with chemical reaction and soret and dufour effects. *Chemical Engineering Communications 200*(9), 1220–1236.

Cheng, J., S. J. Liao, and I. Pop (2005). Analytic series solution for unsteady mixed convection boundary layer flow near the stagnation point on a vertical surface in a porous medium. *Transport in porous media 61*(3), 365–379.

Cole, J. D. and J. D. Cole (1968). *Perturbation methods in applied mathematics*, Volume 260. Blaisdell Waltham, Mass.

Cueto-Felgueroso, L. and R. Juanes (2009). Adaptive rational spectral methods for the linear stability analysis of nonlinear fourth-order problems. *Journal of Computational Physics 228*(17), 6536–6552.

Demaret, P. and M. O. Deville (1991). Chebyshev collocation solutions of the Navier-Stokes equations using multi-domain decomposition and finite element preconditioning. *Journal of Computational Physics 95*(2), 359–386.

Dlamini, P. G., S. S. Motsa, and M. Khumalo (2013). On the comparison between compact finite difference and pseudospectral approaches for solving similarity boundary layer problems. *Mathematical Problems in Engineering*. Volume 2013, Article ID 746489, 15 pages, doi:10.1155/2013/746489.

Don, W. S. and A. Solomonoff (1995). Accuracy and speed in computing the chebyshev collocation derivative. *SIAM Journal on Scientific Computing 16*(6), 1253–1268.

Duffy, D. J. (2006). *Finite Difference methods in financial engineering: a Partial Differential Equation approach*. John Wiley & Sons, New York, NY, USA.

Dulal, P. and H. Mondal (2011). Effects of soret dufour, chemical reaction and thermal radiation on MHD non-Darcy unsteady mixed convective heat and mass transfer over a stretching sheet. *Communications in Nonlinear Science and Numerical Simulation 16*(4), 1942–1958.

Durran, D. R. (1999). *Numerical Methods for Wave Equations in Geophysical Fluid Dynamics*, Volume 32. Springer-Verlag, Berlin.

Ekström, E. and J. Tysk (2011). Boundary conditions for the single-factor term structure equation. *The Annals of Applied Probability 21*(1), 332–350.

El-Gebeily, M. and D. ORegan (2006). A generalized quasilinearization method for second-order nonlinear differential equations with nonlinear boundary conditions. *Journal of Computational and Applied Mathematics 192*(2), 270–281.

EL-Kabeir, S. M. M. and A. M. Rashad (2012). Melting effect on unsteady heat and mass transfer by MHD mixed convection flow over an impulsively stretched vertical surface in a quiescent fluid. *Applied Mathematical Sciences 6*(106), 5293–5303.

Elbarbary, E. M. E. and N. S. Elgazery (2004a). Chebyshev finite difference method for the effect of variable viscosity on magneto-micropolar fluid flow with radiation. *International Communications in Heat and Mass Transfer 31*(3), 409–419.

Elbarbary, E. M. E. and N. S. Elgazery (2004b). Chebyshev finite difference method for the effects of variable viscosity and variable thermal conductivity on heat transfer from moving surfaces with radiation. *International Journal of Thermal Sciences 43*(9), 889–899.

Elgazery, N. S. (2009). The effects of chemical reaction, hall and ion-slip currents on MHD flow with temperature dependent viscosity and thermal diffusivity. *Communications in Nonlinear Science and Numerical Simulation 14*(4), 1267–1283.

Ferziger, J. H. and M. Perić (1996). *Computational methods for fluid dynamics*, Volume 3. Springer, Berlin.

Finlayson, B. A. and L. E. Scriven (1966). The method of weighted residuals - a review. *Applied Mechanics Reviews 19*(9), 735–748.

Gheorghiu, C. I. (2007). Spectral methods for differential problems. *Casa Cartii de Stiinta Publishing House, Cluj-Napoca*. http://www.ictp.acad.ro, (25 June 2014).

Grandclément, P. and J. Novak (2009). Spectral methods for numerical relativity. *Living Reviews in Relativity 12*(1), 107 pages.

Hale, N. P. (2006). A sixth-order extension to the matlab bvp4c software of J. Kierzenka and L. Shampine. *MSc Thesis, Imperial College, London*.

Hayat, T., M. Qasim, and Z. Abbas (2010). Homotopy solution for the unsteady three-dimensional MHD flow and mass transfer in a porous space. *Communications in Nonlinear Science and Numerical Simulation 15*(9), 2375–2387.

Hesthaven, J. S., S. Gottlieb, and D. Gottlieb (2007). *Spectral methods for time-dependent problems*, Volume 21. Cambridge University Press, New York, NY, USA.

Hiemenz, K. K. (1911). Die Grenzschicht an einem in den gleichformingen Flussigkeitsstrom eingetauchten graden Kreiszylinder. *Dinglers Polytechnic Journal 326*, 321–324.

Hinch, E. J. (1991). *Perturbation methods*. Cambridge University Press, New York, NY, USA.

Holmes, M. H. (1995). *Introduction to perturbation methods*. Springer-Verlag, New York, NY, USA.

Hu, H. (2008). Perturbation method for periodic solutions of nonlinear jerk equations. *Physics letters A 372*(23), 4205–4209.

Hunter, J. K. (2004). Asymptotic analysis and singular perturbation theory. *Department of Mathematics, University of California at Davis*.

Hussaini, M. Y., C. L. Streett, and T. A. Zang (1984). Spectral methods for partial differential equations. *II. s. ARMY RESEARCH OFFICE*, 883.

Hussaini, M. Y. and T. A. Zang (1987). Spectral methods in fluid dynamics. *Annual Review of Fluid Mechanics 19*(1), 339–367.

Ibrahim, W., B. Shankar, and M. M. Nandeppanavar (2013). MHD stagnation point flow and heat transfer due to nanofluid towards a stretching sheet. *International Journal of Heat and Mass Transfer 56*(1), 1–9.

Ishak, A., K. Jafar, R. Nazar, and I. Pop (2009). MHD stagnation point flow towards a stretching sheet. *Physica A: Statistical Mechanics and its Applications 388*(17), 3377–3383.

Ishak, A., R. Nazar, and I. Pop (2006). Unsteady mixed convection boundary layer flow due to a stretching vertical surface. *Arabian Journal for Science & Engineering (Springer Science & Business Media BV) 31*(2), 165–182.

Jiang, J. and A. S. Vatsala (1998). The quasilinearization method in the system of reaction diffusion equations. *Applied Mathematics and Computation 97*(2), 223–235.

Juang, H. M. H. and M. Kanamitsu (1994). The NMC nested regional spectral model. *Monthly Weather Review 122*(1), 3–26.

Kahn, P. B. and Y. Zarmi (2004). Weakly nonlinear oscillations: A perturbative approach. *American Journal of Physics 72*(4), 538–552.

Kameswaran, P. K., Z. G. Makukula, P. Sibanda, S. S. Motsa, and P. V. S. N. Murthy (2014). A new algorithm for internal heat generation in nanofluid flow due to a stretching sheet in a porous medium. *International Journal of Numerical Methods for Heat & Fluid Flow 24*(5), 1020–1043.

Kameswaran, P. K., P. Sibanda, and S. S. Motsa (2013). A spectral relaxation method for thermal dispersion and radiation effects in a nanofluid flow. *Boundary Value Problems*. **2013**:242, doi:10.1186/1687-2770-2013-242.

Kato, T. (1958). Perturbation theory for nullity, deficiency and other quantities of linear operators. *Journal d'Analyse Mathématique 6*(1), 261–322.

Kato, T. (1982). *A short introduction to perturbation theory for linear operators*. Springer, Berlin, Heidelberg, New York, NY, USA.

Kato, T. (1995). *Perturbation theory for linear operators*, Volume 132. Springer, Berlin, Heidelberg, New York, NY, USA.

Keller, H. B. and H. Cebeci (1971). Accurate numerical methods for boundary layer flows i. two dimensional laminar flows. In *Proceedings of the second international conference on numerical methods in fluid dynamics*, pp. 92–100. Springer.

Keller, J. B. and S. Kogelman (1970). Asymptotic solutions of initial value problems for nonlinear partial differential equations. *SIAM Journal on Applied Mathematics 18*(4), 748–758.

Kevorkian, J. (1987). Perturbation techniques for oscillatory systems with slowly varying coefficients. *SIAM Review 29*(3), 391–461.

Kevorkian, J. and J. D. Cole (1981). *Perturbation methods in applied mathematics*. Springer, New York, NY, USA.

Kikani, J. (1989). Application of boundary element method to streamline generation and pressure transient testing. *PhD Thesis, Stanford University*.

Korostyshevskiy, V. R. and T. Wanner (2007). A hermite spectral method for the computation of homoclinic orbits and associated functionals. *Journal of Computational and Applied Mathematics 206*(2), 986–1006.

Krivec, R. and V. B. Mandelzweig (2001). Numerical investigation of quasilinearization method in quantum mechanics. *Computer Physics Communications 138*(1), 69–79.

Kumari, M. and G. Nath (2009). Analytical solution of unsteady three-dimensional MHD boundary layer flow and heat transfer due to impulsively stretched plane surface. *Communications in Nonlinear Science and Numerical Simulation 14*(8), 3339–3350.

Kumari, M. and G. Nath (2010). Unsteady MHD mixed convection flow over an impulsively stretched permeable vertical surface in a quiescent fluid. *International Journal of Non-Linear Mechanics 45*(3), 310–319.

Lakshmikantham, V. (1994). An extension of the method of quasilinearization. *Journal of Optimization Theory and Applications 82*(2), 315–321.

Lakshmikantham, V. (1996). Further improvement of generalized quasilinearization method. *Nonlinear Analysis: Theory, Methods & Applications 27*(2), 223–227.

Lakshmikantham, V., S. Leela, and S. Sivasundaram (1995). Extensions of the method of quasilinearization. *Journal of Optimization Theory and Applications 87*(2), 379–401.

Lakshmikantham, V., N. Shahzad, and J. J. Nieto (1996). Methods of generalized quasilinearization for periodic boundary value problems. *Nonlinear Analysis: Theory, Methods & Applications 27*(2), 143–151.

Lee, E. S. (1966). Quasi-linearization, non-linear boundary value problems and optimization. *Chemical Engineering Science 21*(2), 183–194.

Leveque, R. J. (1998). Finite difference methods for differential equations. *Draft version for use in AMath 585*(6).

Liao, S. (2003a). *Beyond perturbation: introduction to the homotopy analysis method*. CRC press.

Liao, S. (2006a). An analytic solution of unsteady boundary-layer flows caused by an impulsively stretching plate. *Communications in Nonlinear Science and Numerical Simulation 11*(3), 326–339.

Liao, S. (2006b). Series solutions of unsteady boundary-layer flows over a stretching flat plate. *Studies in Applied Mathematics 117*(3), 239–263.

Liao, S. J. (2002). An analytic approximation of the drag coefficient for the viscous flow past a sphere. *International Journal of Non-Linear Mechanics 37*(1), 1–18.

Liao, S. J. (2003b). An analytic approximate technique for free oscillations of positively damped systems with algebraically decaying amplitude. *International Journal of Non-Linear Mechanics 38*(8), 1173–1183.

Macaraeg, M. G. and C. L. Streett (1986). Improvements in spectral collocation discretization through a multiple domain technique. *Applied Numerical Mathematics 2*, 95–108.

Mahapatra, T. R., S. K. Nandy, and A. S. Gupta (2010). Dual solution of MHD stagnation-point flow towards a stretching surface. *Engineering 2*(4), 299–305.

Makukula, Z. G., S. S. Motsa, and S. Shateyi (2014). Numerical analysis for the Synthesis of Biodiesel using spectral relaxation method. *Mathematical Problems in Engineering*. Volume 2014, Article ID 601374, 6 pages, doi:10.1155/2013/601374.

Maleknejad, K. and E. Najafi (2011). Numerical solution of nonlinear volterra integral equations using the idea of quasilinearization. *Communications in Nonlinear Science and Numerical Simulation 16*(1), 93–100.

Mandelzweig, V. B. (1999). Quasilinearization method and its verification on exactly solvable models in quantum mechanics. *Journal of Mathematical Physics 40*(12), 6266–6291.

Mandelzweig, V. B. and F. Tabakin (2001). Quasilinearization approach to nonlinear problems in physics with application to nonlinear odes. *Computer Physics Communications 141*(2), 268–281.

Mantzaris, N. V., P. Daoutidis, and F. Srienc (2001). Numerical solution of multi-variable cell population balance models. ii. spectral methods. *Computers & Chemical Engineering 25*(11), 1441–1462.

Mehmood, A., A. Ali, and T. Shah (2008). Heat transfer analysis of unsteady boundary layer flow by homotopy analysis method. *Communications in Nonlinear Science and Numerical Simulation 13*(5), 902–912.

Moczo, P. (1998). *Introduction to Modeling Seismic Wave Propagation by the Finite-Difference Methods*. Disaster Prevention Research Institute, Kyoto University.

Moczo, P., J. Kristek, and L. Halada (2004). *The finite-difference method for seismologists*. Comenius University.

Mohamed, M. K. A., R. N. M. Z. Salleh, and A. Ishak (2013). Numerical investigation of stagnation point flow over a stretching sheet with convective boundary conditions. *Boundary Value Problems*. **2013**:4, doi:10.1186/1687-2770-2013-4.

Motsa, S. S. (2013). A new spectral local linearization method for nonlinear boundary layer flow problems. *Journal of Applied Mathematics*. Volume 2013, Article ID 423628, 15 pages, doi:10.1155/2013/423628.

Motsa, S. S. (2014). A new spectral relaxation method for similarity variable nonlinear boundary layer flow systems. *Chemical Engineering Communications 201*(2), 241–256.

Motsa, S. S., P. Dlamini, and M. Khumalo (2013). A new multistage spectral relaxation method for solving chaotic initial value systems. *Nonlinear Dynamics 72*(1-2), 265–283.

Motsa, S. S., P. G. Dlamini, and M. Khumalo (2012). Solving hyperchaotic systems using the spectral relaxation method. *Abstract and Applied Analysis*. Volume 2012, Article ID 203461, 18 pages, doi:10.1155/2012/203461.

Motsa, S. S., P. G. Dlamini, and M. Khumalo (2014). Spectral relaxation method and spectral quasilinearization method for solving unsteady boundary layer flow problems. *Advances in Mathematical Physics*. Volume 2014, Article ID 341964, 12 pages, doi:10.1155/2014/341964.

Motsa, S. S. and Z. G. Makukula (2013). On spectral relaxation method approach for steady von Kármán flow of a Reiner-Rivlin fluid with Joule heating, viscous dissipation and suction/injection. *Central European Journal of Physics 11*(3), 363–374.

Motsa, S. S., Z. G. Makukula, and S. Shateyi (2013). Spectral local linearisation approach for natural convection boundary layer flow. *Mathematical Problems in Engineering*. Volume 2013, Article ID 765013, 7 pages, doi:10.1155/2013/765013.

Motsa, S. S. and P. Sibanda (2013a). On extending the quasilinearization method to higher order convergent hybrid schemes using the spectral homotopy analysis method. *Journal of Applied Mathematics*. Volume 2013, Article ID 879195, 9 pages, doi:10.1155/2013/879195.

Motsa, S. S. and P. Sibanda (2013b). Some modifications of the quasilinearization method with higher-order convergence for solving nonlinear bvps. *Numerical Algorithms 63*(3), 399–417.

Nadeem, S., A. Hussain, and M. Khan (2010). HAM solutions for boundary layer flow in the region of the stagnation point towards a stretching sheet. *Communications in Nonlinear Science and Numerical Simulation 15*(3), 475–481.

Nandy, S. K. (2013). Analytical solution of MHD stagnation-point flow and heat transfer of casson fluid over a stretching sheet with partial slip. *ISRN Thermodynamics 2013*, 9.

Nayfeh, A. H. (1973). *Perturbation methods*. John Wiley & Sons, New York, NY, USA.

Nayfeh, A. H. (2011). *Introduction to perturbation techniques*. John Wiley & Sons, Great Britain.

Nazar, R., N. Amin, and I. Pop (2004a). Unsteady boundary layer flow due to a stretching surface in a rotating fluid. *Mechanics Research Communications 31*(1), 121–128.

Nazar, R., N. Amin, and I. Pop (2004b). Unsteady mixed convection boundary layer flow near the stagnation point on a vertical surface in a porous medium. *International journal of heat and mass transfer 47*(12), 2681–2688.

Nieto, J. (1997). Generalized quasilinearization method for a second order ordinary differential equation with dirichlet boundary conditions. *Proceedings of the American Mathematical Society 125*(9), 2599–2604.

Ogundare, B. S. (2009). On the pseudo-spectral method of solving linear ordinary differential equations. *Journal of Mathematics and Statistics 5*(2), 136–140.

Olanrewaju, P. O., M. A. Olanrewaju, and D. A. Ajadi (2012). Unsteady three-dimensional MHD flow and mass transfer in a porous space in the presence of thermal radiation. *International Research Journal of Petroleum and Gas Exploration Research 2*(2), 044–051. http://www.interesjournals.org/JPGER.

Ostrovsky, L. and K. Gorshkov (2000). Perturbation theories for nonlinear waves. In *Nonlinear Science at the Dawn of the 21st Century*, pp. 47–65. Springer.

Pal, D. and B. Talukdar (2010). Perturbation analysis of unsteady magnetohydrodynamic convective heat and mass transfer in a boundary layer slip flow past a vertical permeable plate with thermal radiation and chemical reaction. *Communications in Nonlinear Science and Numerical Simulation 15*(7), 1813–1830.

Pandit, S. G. (1997). Quadratically converging iterative schemes for nonlinear volterra integral. *Journal of Applied Mathematics and Stochastic Analysis 1*(2), 169–178.

Patera, A. T. (1984). A spectral element method for fluid dynamics: laminar flow in a channel expansion. *Journal of Computational Physics 54*(3), 468–488.

Peiró, J. and S. Sherwin (2005). Finite difference, finite element and finite volume methods for partial differential equations. In *Handbook of Materials Modeling*, pp. 2415–2446. Springer.

Pop, S. R., T. Grosan, and I. Pop (2004). Radiation effects on the flow near the stagnation point of a stretching sheet. *Technische Mechanik 25*(2), 100–106.

Prasad, K. V., M. S. Abel, and S. K. Khan (2000). Momentum and heat transfer in visco-elastic fluid flow in a porous medium over a non-isothermal stretching sheet. *International Journal of Numerical Methods for Heat & Fluid Flow 10*(8), 786–801.

Qi, D. and Z. Hong-Qing (2009). Analytic solution for magnetohydrodynamic stagnation point flow towards a stretching sheet. *Chinese Physics Letters 26*(10), 104701.

Ramesh, G. K., B. J. Gireesha, and C. S. Bagewadi (2014). Stagnation point flow of a MHD dusty fluid towards a stretching sheet with radiation. *Afrika Matematika 25*(1), 237–249.

Ramos, J. I. (2007). Piecewise-quasilinearization techniques for singularly perturbed volterra integro-differential equations. *Applied Mathematics and Computation 188*(2), 1221–1233.

Rasekh, A., M. Farzaneh-Gord, and S. R. Varedi (2013). Analytical solution for magnetohydrodynamic stagnation point flow and heat transfer over a permeable stretching sheet with chemical reaction. *Journal of Theoretical and Applied Mechanics 51*(3), 675–686.

Raspo, I. (2003). A direct spectral domain decomposition method for the computation of rotating flows in a t-shape geometry. *Computers & fluids 32*(3), 431–456.

Roslinda, N., N. Amin, D. Filip, and I. Pop (2004). Unsteady boundary layer flow in the region of the stagnation point on a stretching sheet. *International Journal of Engineering Science 42*(11), 1241–1253.

Sajid, M., I. Ahmad, T. Hayat, and M. Ayub (2008). Series solution for unsteady axisymmetric flow and heat transfer over a radially stretching sheet. *Communications in Nonlinear Science and Numerical Simulation 13*(10), 2193–2202.

Sajid, M., I. Ahmad, T. Hayat, and M. Ayub (2009). Unsteady flow and heat transfer of a second grade fluid over a stretching sheet. *Communications in Nonlinear Science and Numerical Simulation 14*(1), 96–108.

Salem, A. M. and R. Fathy (2012). Effects of variable properties on MHD heat and mass transfer flow near a stagnation point towards a stretching sheet in a porous medium with thermal radiation. *Chinese Physics B 21*(5), 054701.

Saravi, M., F. Ashrafi, and S. R. Mirrajei (2009). Numerical solution of linear ordinary differential equations in quantum chemistry by clenshaw method. *World Academy of Science, Engineering and Technology 49*, 1051–1054.

Segami, A., K. Kurihara, H. Nakamura, M. Ueno, and I. Takano (1989). Operational mesoscale weather prediction with japan spectral model. *Meteorological Society of Japan, Journal 67*, 907–924.

Seshadri, R., N. Sreeshylan, and G. Nath (2002). Unsteady mixed convection flow in the stagnation region of a heated vertical plate due to impulsive motion. *International journal of heat and mass transfer 45*(6), 1345–1352.

Shan, X. and D. Montgomery (1994). Magnetohydrodynamic stabilization through rotation. *Physical Review Letters 73*(12), 1624–1627.

Shan, X., D. Montgomery, and H. Chen (1991). Nonlinear magnetohydrodynamics by galerkin-method computation. *Physical Review A 44*(10), 6800.

Sharma, P. R. and G. Singh (2009). Effects of variable thermal conductivity and heat source/sink on MHD flow near a stagnation point on a linearly stretching sheet. *Journal of Applied fluid mechanics 2*(1), 13–21.

Shateyi, S. (2013). A new numerical approach to MHD flow of a Maxwell fluid past a vertical stretching sheet in the presence of thermophoresis and chemical reaction. *Boundary Value Problems*. **2013**:196, doi:10.1186/1687-2770-2013-196.

Shateyi, S. and O. D. Makinde (2013). Hydromagnetic stagnation-point flow towards a radially stretching convectively heated disk. *Mathematical Problems in Engineering*. Volume 2013, Article ID 616947, 8 pages, doi:10.1155/2013/616947.

Shateyi, S. and G. T. Marewo (2013). A new numerical approach of MHD flow with heat and mass transfer for the UCM fluid over a stretching surface in the presence of thermal radiation. *Mathematical Problems in Engineering*. Volume 2013, Article ID 670205, 8 pages, doi:10.1155/2013/670205.

Shateyi, S. and J. Prakash (2014). A new numerical approach for MHD laminar boundary layer flow and heat transfer of nanofluids over a moving surface in the presence of thermal radiation. *Boundary Value Problems*. **2014**:2, doi:10.1186/1687-2770-2014-2.

Sibanda, P., S. S. Motsa, J. M. Ngnotchouye, and G. T. Marewo (2014). A spectral relaxation approach for unsteady boundary-layer flow and heat transfer of a nanofluid over a permeable stretching/shrinking sheet. *Advances in Mathematical Physics*. Volume 2014, Article ID 564942, 10 pages, doi:10.1155/2014/564942.

Simmonds, J. G. and J. E. Mann (1985). *A first look at perturbation theory.* Robert E. Krieger Publishing Company, Inc. Malabar, Florida, USA.

Skinner, L. A. (2011). *Singular Perturbation Theory.* Springer, New York, NY, USA.

Smith, D. R. (1985). *Singular-perturbation theory: an introduction with applications.* Cambridge University Press, New York, NY, USA.

Suna, L., M. Zhoub, and G. Wangb (2010). Generalized quasilinearization method for nonlinear boundary value problems with integral boundary conditions. *Electronic Journal of Qualalitative Theory of Differential Equations 66*, 1–14.

Takhar, H. S., A. J. Chamkha, and G. Nath (2001). Unsteady three-dimensional MHD-boundary-layer flow due to the impulsive motion of a stretching surface. *Acta Mechanica 146*(1-2), 59–71.

Takhar, H. S., A. Mehmood, A. Ali, and T. Shah (2008). Unsteady three-dimensional MHD boundary-layer flow due to the impulsive motion of a stretching surface (acta mech. 146, 59–71, 2001). *Acta Mechanica 199*(1-4), 241–249.

Tandjiria, V. (1999). Development of finite difference method applied to consolidation analysis of embankments. *Dimensi Teknik Sipil 1*(2), 73–80.

Trefethen, L. N. (2000). *Spectral methods in MATLAB*, Volume 10. SIAM.

Trefethen, L. N. and M. R. Trummer (1987). An instability phenomenon in spectral methods. *SIAM Journal on Numerical Analysis 24*(5), 1008–1023.

Vatsala, A. S. and J. Yang (2006). Generalized quasilinearization method for reaction diffusion systems. *Nonlinear Studies 13*(1), 53–72.

Wang, H. F. and M. P. Anderson (1995). *Introduction to groundwater modeling: finite difference and finite element methods*. Academic Press.

Williams, J. C. and T. B. Rhyne (1980). Boundary layer development on a wedge impulsively set into motion. *SIAM Journal on Applied Mathematics 38*(2), 215–224.

Witelski, T. and M. Bowen (2009). Singular perturbation theory. *Scholarpedia 4*(4), 3951. doi:10.4249/scholarpedia.3951.

Xu, H. and S. J. Liao (2005). Series solutions of unsteady magnetohydrodynamic flows of non-newtonian fluids caused by an impulsively stretching plate. *Journal of Non-Newtonian Fluid Mechanics 129*(1), 46–55.

Xu, H., S. J. Liao, and I. Pop (2006). Series solutions of unsteady boundary layer flow of a micropolar fluid near the forward stagnation point of a plane surface. *Acta Mechanica 184*(1-4), 87–101.

Xu, H., S. J. Liao, and I. Pop (2007). Series solutions of unsteady three-dimensional MHD flow and heat transfer in the boundary layer over an impulsively stretching plate. *European Journal of Mechanics-B/Fluids 26*(1), 15–27.

Yang, J. and A. S. Vatsala (2005). Numerical investigation of generalized quasilinearization method for reaction diffusion systems. *Computers & Mathematics with Applications 50*(3), 587–598.

Yian, L. Y., A. Ishak, and I. Pop (2011). MHD stagnation point flow with suction towards a shrinking sheet. *Sains Malaysiana 40*(10), 1179–1186.